

POLITECNICO DI TORINO

Corso di Laurea Magistrale in Ingegneria per l'Ambiente e per il Territorio



Up-scaling laboratory set-ups for water flow and solute transport in
unsaturated soils: from column tests to laboratory lysimeter

Relatore

Prof.ssa Tiziana Tosco

Co-relatori

Prof. Rajandrea Sethi

Prof. Roberto Revelli

Dott.ssa Monica Granetto

Candidato

Luca Vetere

A.A. 2020/2021

Abstract

Tracer tests in laboratory columns have been widely used, both in saturated and unsaturated conditions, to study water and contaminant infiltration and movement in soil. In this thesis, carried out with the Groundwater Engineering Research Group at Politecnico di Torino, water flow and tracer tests have been performed at three different laboratory scales (small and intermediate column, and laboratory lysimeter). In the small scale, saturated and unsaturated tests have been performed while, with the intermediate column and the lysimeter, only unsaturated tests have been done. The main aim was to investigate the differences between the scales in terms of operating conditions, dispersivity value and hydraulic conductivity. Furthermore, with a particular focus, the set-up and data of the lysimeter have been studied. The results obtained from the experiments have been modelled with HYDRUS-1D software. They show that there is no substantial variation in the hydraulic conductivity values between the scales while a very little variation can be observed on the dispersivity value, as it increases as the column length increases. Interesting data have been obtained also from the lysimeter's tensiometers, which have shown an unexpected behaviour in the first part of the sand column. This phenomenon is probably caused by a non-homogeneous flux in the first part of the column, but further studies could be performed to deeper investigate this behaviour. In addition, from the lysimeter tests, some practical considerations can be highlighted. Anomalous dispersivity values have been detected at the lysimeter's exit. It is very likely that, since the lysimeter's exit hole is smaller than its section, stagnant water, which would cause dilution and subsequently dispersivity increase, is present at the bottom of the vessel. Few suggestions on how to solve this practical problem are also presented in the thesis. Furthermore, the influence of the suction probes in the lysimeter has been evaluated. The results shown that, with the suction probes activated, the water content and the average water velocity decrease respectively around 2 and 5%. While no influence has been detected on the dispersivity value. To conclude, the lysimeter proved to be a very useful device for studying the vadose zone. In comparison to the other scales, its high precision sensors allow to study with a great detail the phenomena occurring within the unsaturated zone. This thesis can be considered a good starting point, from which new studies, regarding infiltration of contaminants and water flow in the vadose layer, can be undertaken.

Contents

List of Figures	i
List of Tables	iv
List of Acronyms and Symbols	v
1 Introduction	1
2 Literature background	4
2.1 Water flow and solute transport in saturated porous media	4
2.2 Water flow and solute transport in unsaturated porous media	7
2.3 Laboratory tests	13
3 Materials and Methods	17
3.1 Materials	17
3.1.1 Small scale test setup	19
3.1.2 Intermediate scale test setup	19
3.1.3 Lysimeter	21
3.2 Methods	22
3.2.1 Small scale tests	23
3.2.2 Intermediate scale tests	24
3.2.3 Lysimeter tests	25
3.3 Data processing and modelling	27
3.3.1 HYDRUS modelling for small scale tests	28
3.3.2 HYDRUS modelling for intermediate scale tests	30
3.3.3 HYDRUS modelling for lysimeter scale tests	31
4 Results and discussion	33
4.1 Small scale results	33
4.2 Intermediate scale results	40
4.3 Lysimeter results	43
4.3.1 Flow tests	43
4.3.2 Tracer tests	45
4.4 Comparison between scales	54

5	Conclusions	59
	References	61
A	Appendix A	66
B	Appendix B	68
C	Appendix C	71
	Acknowledgements	72

List of Figures

1.1	Example of a field lysimeter. Image retrieved from Eijkelkamp (2017)	2
2.1	Different mechanisms occurring to a contaminant plume during a continuous injection. a) only advective transport; b) advective and dispersive transport; c) advective and dispersive transport of a solute affected by retardation; d) advective and dispersive transport of a solute affected by biodegradation. Source: modified image from Sethi & Di Molfetta (2019)	7
2.2	Example of soil water retention curve for sand.	8
2.3	a) Hysteresis curve of $\psi(\theta)$; b) hysteresis curve of $\psi(K)$; Source: modified image from Freeze & Cherry (1979)	9
2.4	Examples of main and scanning curves, both in wetting and drying conditions. Source: modified image from Huang et. al (2005)	10
2.5	$K(\theta)$ relationship of different types of soil. From left to right the two lines are representing the sand, loam and clay. Source: modified image from Landsberg et al. (2011).	12
2.6	Infiltration in unsaturated soil. a) Runoff for infiltration excess. b) Runoff for saturation excess. Source: modified image from Tarboton (2003)	12
2.7	Typical BTCs of column test with a continuous injection. <i>Green</i> : curve for a tracer (subject only to advection-dispersion). <i>Blue</i> : curve of a solute subjected also to retardation, other than advection-dispersion. <i>Red</i> : curve of a solute subjected also to biodegradation, other than advection-dispersion.	14
2.8	Typical profiles of normalized concentrations during tracer tests at different fixed times.	15
2.9	Schemes of typical field lysimeters. A: box lysimeter. B: weighing lysimeter. Irrigation controlled lysimeter C: Source: modified image from Soltysiak & Rakoczy (2019)	16
3.1	Sketch of the two plastic columns and the lysimeter. The suction probes of the lysimeter are also represented.	17
3.2	Spectrophotometer carousel with bromophenol blue samples.	18
3.3	Absorbance's spectra of a 12.5 mg/l BPB solution at different pH values.	18
3.4	Small scale tests set-up. 1: column; 2: in-flow; 3: out-flow; 4: 4-channels peristaltic pump; 5: solution for the test; 6: C_0 tank; 7: spectrophotometer; 8: waste tank.	19
3.5	Intermediate scale tests set-up. 1: main column; 2: pre-filter layers; 3: in-flow; 4: outflow; 5: outflow collection tank; 6: solution for the test; 7: tensiometers.	20
3.6	Scheme of a UGT lysimeter. Source: modified image from UGT (2019a).	21
4.1	Small scale, saturated test: test data and fitting result, at the three different flow rates. Time = 0 is considered at the start of BPB injection.	33
4.2	Small scale, saturated test: HYDRUS fitting curves as a function of the pore volume.	34
4.3	Small scale, unsaturated test: test data and fitting result, at the three different flow rates. Time = 0 is considered at the start of BPB injection.	35

4.4	Small scale, unsaturated test (forced extraction): HYDRUS fitting curves as a function of the pore volume.	36
4.5	Small scale, free-drainage test: test data and fitting result, at the three different flow rates. Time = 0 is considered at the start of BPB injection.	37
4.6	Small scale, free-drainage test: HYDRUS fitting curves as a function of the pore volume.	37
4.7	Small scale: BTCs comparison from HYDRUS fitting at the three different flow rates. In each graph the saturated, unsaturated and free-drainage results at the same flow rate are displayed. Time = 0 is considered at the start of BPB injection.	39
4.8	Small scale: experimental data and linear interpolations of dispersivity as a function of the effective velocity, at minimum (blue), intermediate (orange) and maximum (grey) flow rate.	39
4.9	Small scale: experimental data of dispersivity as a function of the water content, at minimum (blue), intermediate (orange) and maximum (grey) flow rate.	40
4.10	Intermediate scale, unsaturated free-drainage test: test data and fitting result, at the three different flow rates. Time = 0 is considered at the start of BPB injection. . . .	41
4.11	Intermediate scale, free-drainage test: HYDRUS fitting curves as a function of the pore volume.	41
4.12	Intermediate scale, unsaturated free-drainage test: tensiometers data + the failed test. Tensiometers depths: tens1: 10cm; tens2: 15cm; tens3: 20cm.	43
4.13	Lysimeter scale, flow test: water content data from the four sensors. Injection start at time = 0 hours; injection end at time = 5 hours.	44
4.14	Lysimeter scale, tracer test at minimum flow rate. BTCs at the five different depths.	46
4.15	Lysimeter scale, tracer test at the intermediate flow rate. BTCs at the five different depths.	46
4.16	Lysimeter scale, tracer test at maximum flow rate. BTCs at the five different depths.	48
4.17	Lysimeter scale, maximum flow rate tracer test without suction probe's extraction compared with the same test with the suction probes activated.	50
4.18	Lysimeter scale, water content vs soil water tension data from two cycles of wetting + drying at the minimum flow rate.	51
4.19	Lysimeter scale, water content vs soil water tension data from two cycles of wetting + drying at the intermediate flow rate.	51
4.20	Lysimeter scale, water content vs soil water tension data from two cycles of wetting + drying at the maximum flow rate.	52
4.21	Tensiometers' data vs water content of the second extra test, compared to the ones obtained previously.	53
4.22	Lysimeter scale, maximum flow rate tracer tests with the two different sampling methods. Sampling depth: column's exit (70 cm).	54

4.23	Comparison of tracer tests at the three different scales. Tests at minimum, intermediate and maximum flow rate. Lysimeter's value referring to the second depth (25 cm). . .	55
4.24	Experimental data of dispersivity as a function of the column's length. In red the outlier referred to the lysimeter's bottom.	56
4.25	Experimental data of dispersivity as a function of the column's length to diameter ratio (D/L). In red the outlier referred to the lysimeter's bottom.	57
A.1	Granulometric curve of DORSILIT nr. 8 sand. Source: modified image from Quartsande (2020a)	66
A.2	Granulometric curve of DORSILIT nr. 7 sand. Source: modified image from Quartsande (2020b)	67
B.1	Lysimeter scale, tracer test: water content data from the four sensors.	68
B.2	Lysimeter scale, tracer test: water content data from the four sensors.	68
B.3	Lysimeter scale, tracer test: water content data from the four sensors.	69
B.4	Lysimeter scale, first extra tracer test (without suction probe extraction): water content data from the four sensors.	69
B.5	Lysimeter scale, second extra tracer test (point sampling, without suction probe extraction): water content data from the four sensors.	70
C.1	Lysimeter scale, water content vs soil water tension data from six cycles of wetting + drying, with all the three different flow rates.	71

List of Tables

4.1	Small scale: results of HYDRUS fitting for the three saturated tracer tests, in terms of saturated water content (θ_s), longitudinal dispersivity (α_L) and R^2	34
4.2	Small scale: results of HYDRUS fitting for the three unsaturated tracer tests, in terms of water content (θ), saturated hydraulic conductivity (K_s), hydraulic conductivity (K), longitudinal dispersivity (α_L) and R^2 . *Average values along the column at the end of the test.	36
4.3	Small scale: results of HYDRUS fitting for the three unsaturated free-drainage tracer tests, in terms of water content (θ), saturated hydraulic conductivity (K_s), hydraulic conductivity (K), longitudinal dispersivity (α_L) and R^2 . *Average values along the column at the end of the test.	38
4.4	Intermediate scale: results of HYDRUS fitting for the three unsaturated free-drainage tracer tests, in terms of water content (θ), saturated hydraulic conductivity (K_s), hydraulic conductivity (K), longitudinal dispersivity (α_L) and R^2 . *Average values along the column at the end of the test.	42
4.5	Lysimeter scale: average water content $\theta(-)$ read by the four sensors, during the tap water injection.	44
4.6	Lysimeter scale, flow tests: results of HYDRUS estimation of the parameters θ_s and K_s	45
4.7	Lysimeter scale, tracer tests: results of HYDRUS estimation of α_L . **: the value did not converge.	48
4.8	Lysimeter scale: average water content $\theta(-)$ read by the four sensors, during the BPB solution injection.	49
4.9	Values of specific discharge rate for each scale, at the three different flow rates. . . .	54
4.10	Values of specific discharge rate for each scale, at the three different flow rates. Lysimeter's value referring to the second depth (25 cm).	55
A.1	DORSILIT nr. 8 sand characteristics. Data retried from Quartzsande (2020a)	66
A.2	DORSILIT nr. 7 sand characteristics. Data retried from Quartzsande (2020b)	67

List of Acronyms and symbols

Acronyms

BC: boundary condition
BPB: bromophenol blue
BTC: breakthrough curve
DIW: de-ionized water
EC: electrical conductivity
IC: initial condition
PV: pore volume

Symbols

A : absorbance, [-]
 A_0 : initial absorbance, [-]
 C : concentration, $[\text{ML}^{-3}]$
 C_0 : initial concentration, $[\text{ML}^{-3}]$
 D_L : hydrodynamic dispersivity, $[\text{L}^2\text{T}^{-1}]$
 D_C : cinematic diffusion coefficient, $[\text{L}^2\text{T}^{-1}]$
 D_0 : molecular diffusion coefficient, $[\text{L}^2\text{T}^{-1}]$
 G : sink term, $[\text{T}^{-1}]$
 h : hydraulic head, [-]
 i : hydraulic gradient, [-]
 j_A : advective mass flow, $[\text{ML}^{-2}\text{T}^{-1}]$
 j_I : hydrodynamic dispersion mass flow, $[\text{ML}^{-2}\text{T}^{-1}]$
 K : hydraulic conductivity, $[\text{LT}^{-1}]$
 k_d : half-saturation constant, $[\text{ML}^{-3}]$
 k_d : soil-water partition coefficient, $[\text{M}^{-1}\text{L}^{-3}]$
 K_s : saturated hydraulic conductivity, $[\text{LT}^{-1}]$
 m : empirical soil water retention parameter, [-]
 n : empirical soil water retention parameter, [-]
 l : tortuosity, [-]
 L : column length, [L]
 q : specific discharge, $[\text{LT}^{-1}]$
 Q : discharge, $[\text{L}^3\text{T}^{-1}]$
 R : retardation coefficient, [-]
 R^2 : R-squared value, [-]
 S : degree of saturation, [-]
 S_e : effective saturation, [-]
 $t_{1/2}$: half biological life, [T]
 v_c : solute velocity, $[\text{LT}^{-1}]$
 v_e : effective velocity, $[\text{LT}^{-1}]$
 w : rain intensity, $[\text{LT}^{-1}]$
 α : empirical soil water retention parameter, $[\text{L}^{-1}]$
 α_L : longitudinal dispersivity, [L]
 α_T : transversal dispersivity, [L]
 ϵ : relative dielectric constant, [-]
 θ : volumetric soil water content, [-]
 θ_r : residual volumetric soil water content, [-]
 θ_s : saturated volumetric soil water content, [-]
 λ : natural degradation coefficient, $[\text{T}^{-1}]$
 μ : microorganism growth rate, $[\text{T}^{-1}]$
 μ_{max} : maximum microorganism growth rate, $[\text{T}^{-1}]$
 ρ_b : bulk density, $[\text{ML}^{-3}]$
 τ_w : tortuosity in liquid phase, [-]
 ϕ : porosity, [-]
 ϕ_e : effective porosity, [-]
 ψ : pressure head, [L]
 ψ_a : air-entry pressure head, [L]

1 Introduction

Climate change and population growth are two of the main challenges that today's world is facing.

Climate change is advancing unabated, carrying with it water-related critical issues. As the temperature raises, there will be a substantial reduction of the fresh water resources. Other impacts will regard the increase of floods and droughts, both in term of frequency and magnitude. Water scarcity and growing deserts, will strongly negatively influence the agricultural fields and the crop yields, too.

The demand for food and therefore, land and water for agriculture, is increasing with a rate which has never been seen before. Nowadays, the globe's population almost reached the 8 billion units and the United Nations forecast says that by the end of the century there will be more than 10 billion people in the world (United Nations, 2019). If in one hand, the climate change will produce a limited availability of land and water for agriculture, on the other hand, the population growth means an increasing demand for food. This two conflicting aspects bring the necessity of raising productivity in fields already exploited for agricultural purposes.

For the above mentioned aspects, studying the soil, infiltration, evapotranspiration, groundwater recharge and all the other related phenomena, is becoming more important than ever.

Tests in laboratory columns have been widely used, both in saturated and unsaturated conditions, to study, among others, infiltration and contaminant movement in soil (Dontsova et al., 2006), agricultural soil and herbicide applications (Masipan et al., 2016; Granetto, 2018) and groundwater contamination (Sugita & Nakane, 2007). If experiments under saturated conditions are used for studying processes occurring below the water table, unsaturated tests regard the zone in which the water content is less than soil porosity. In other terms, the unsaturated zone, also referred as vadose zone, is the area between the soil surface and the water table in which solutes and contaminants are transported, attenuated and transformed by liquid and gaseous phases (Nielsen et al., 1986). Since the vadose zone can be considered as a link between the soil surface and the groundwater level, it plays an important role in many hydrological mechanisms such as, infiltration, evaporation and groundwater recharge.

The first studies regarding the unsaturated zone have been carried out in the 19th century (Dalton, 1802; Lawes et al., 1882). These researches mainly focused on the infiltration through porous media, in terms of water velocity and amount of percolation. In the 20th century, studies regarding solute transport and flow mechanisms started to be published (Burgess, 1921; Fireman, 1944). Other than the laboratory soil columns, lysimeters are specific devices used for studying percolation of water and contaminants through the unsaturated zone (Howell et al., 1991). Lysimeters are composed of a rigid shield, usually cylindrical, which can be filled with soil in which water and contaminants can pass through. In figure 1.1, an example of field lysimeter is shown. During the years, lysimeters have been widely used also for agricultural studies and water consumption of crops and plants. Nowadays, lysimeters are also used for hydrological and water quality researches. However, the majority of the lysimeter are placed in field and packed with local soil for outdoor applications. Very few studies, concerning laboratory lysimeters, have been published.

This thesis has been carried out with the Groundwater Engineering Research Group at Politecnico di Torino. It investigates the scale effect on water flow and solute transport, with a particular focus on the set-up and the results of a laboratory lysimeter. In particular, water flow and tracer tests have been performed at three different scales: a small column, an intermediate column and a laboratory lysimeter. The small and intermediate scales are composed by a plastic transparent



Figure 1.1. Example of a field lysimeter. Image retrieved from Eijkelkamp (2017)

column, packed with sand, in which water and solutes can pass through and then be collected at the column's exit. The laboratory lysimeter, produced by Umwelt-Geräte-Technik GmbH (UGT), has four sampling points at different depths and a column exit in which is possible to extract water. In addition, in the lysimeter, many sensors are inserted, among others they retrieve data of soil-water tension, electrical conductivity and moisture content. In the small scale, both saturated and unsaturated tests have been performed while, with the intermediate column and the lysimeter, only unsaturated tests have been realized.

For the tracer tests, bromophenol blue has been used as a tracer. It is a widely used dye, whose purple color enables both visual and quantitative tracing. By modelling the test results with the HYDRUS-1D software, the soil water and solute transport parameters have been estimated.

The main aim of the thesis is to evaluate the effect of the scale on water flow and solute transport parameters (i.e. hydraulic conductivity and longitudinal dispersivity). Furthermore, a substantial portion of the work has been focused on finding a suitable set-up for the lysimeter, investigating problems and identifying possible improvements which can be implemented to enhance further experiments.

The thesis, after this first section in which a general introduction on the main themes and the work have been already presented, is developed in four main chapters.

In the second chapter, a literature background is presented. After a first part, in which general soil-water concepts are explained, the theoretical concepts behind water flow and solute transport, under both saturated and unsaturated conditions, are illustrated. In the last part of the section, a brief review of laboratory experiments, with columns and lysimeters, is presented.

The third chapter describes the materials and methods used in this thesis. It deeply explains the set-ups in the three scales, all the differences and similarities. In this section, a detailed exposition of the methods and protocols used for each test is also shown. At the end of the chapter, it is explained in details the data analysis and the HYDRUS-1D modelling.

In the fourth section, all the results are presented and widely discussed. They are divided into four main sub-chapters: small scale, intermediate scale and lysimeter results, and a last part in which a comparison between the scales is addressed.

Finally, in the fifth and last chapter, the final conclusions of this work are drawn.

2 Literature background

Water flowing through a porous medium is a complex topic in which many processes and mechanisms take place. A first main distinction can be done about the conditions of the soil in which the water (or a solute) is passing through: the soil can either be in saturated or in unsaturated conditions. The first condition is valid when the soil voids are fully saturated with a liquid phase. The saturated condition is defined when the water content θ [-] is equal to the porosity ϕ [-], while unsaturated conditions are when $\theta < \phi$ (Chow et al., 1988). These two quantities are expressed with the following equivalences:

$$\phi = \frac{\text{volume of voids}}{\text{total volume}} \quad (2.1)$$

$$\theta = \frac{\text{volume of liquid phase}}{\text{total volume}} \quad (2.2)$$

Sometimes, it is possible to refer to the amount of water present in the soil with another parameter called degree of saturation S [-], this parameter is defined as follows (Tarboton, 2003):

$$S = \frac{\theta}{\phi} \quad (2.3)$$

The S value is 1 for saturated conditions and, it lies between 0 and 1 for unsaturated soil.

If we look at a macroscopic scale, water passing through a porous medium is governed by the Darcy's equation. The Darcy's law states that the water flux q [LT^{-1}] (also called *specific discharge*) is proportional to the hydraulic conductivity of the soil K [LT^{-1}] and the hydraulic gradient $i = dh/dl$ [-] (Freeze & Cherry, 1979):

$$q = \frac{Q}{A} = -K \frac{dh}{dl} = -Ki \quad (2.4)$$

where: Q is the flow rate [L^3T^{-1}] and A is the cross-sectional area [L^2].

Hydraulic conductivity K is a parameter representing the quantity of water that can pass through a porous medium. It is a very important parameter both for saturated and unsaturated conditions. K depends on the pore-size distribution of the solid matrix, the roughness, the interconnection between the pores and on other soil parameters such as tortuosity. As it will be explained in the following chapters, in unsaturated soil it is strongly dependent also on the soil water content.

In the following chapters, mechanisms and processes occurring in soil under, saturated and unsaturated conditions, will be described.

2.1 Water flow and solute transport in saturated porous media

Water flow and solute transport in porous media is a complex field in which very different processes are contributing.

The processes can be divided into hydrological, chemical-physical and biological mechanisms (Sethi & Di Molfetta, 2019). Among the hydrological processes, advection is the main one. It consists in the solute transport with a velocity equal to the average effective velocity of the water passing through the medium and with the same direction of the water flux. The effective velocity can be expressed as follows:

$$v_e = \frac{q}{\phi_e} = \frac{Ki}{\phi_e} \quad (2.5)$$

Where ϕ_e is the effective porosity [-], K is the hydraulic conductivity [LT^{-1}] and i is the hydraulic gradient [-].

Moreover, called C [ML^{-3}] the concentration, the mass flow along the flow direction axis, considering only the advection process, will be:

$$j_A = v_e \phi_e C \quad (2.6)$$

Within the hydrological processes, there are also other type of processes regarding the dispersion of the solute plume, these processes are called molecular diffusion and cinematic dispersion. The former one is related to the Brownian motion of the solute molecules: collisions between different molecules make that the main motion direction goes from higher to lower solute concentration. While, the latter one is due to the heterogeneity of the flow velocity in the porous medium. In fact, the velocity distribution within each pore channel is not uniform, the pores do not have all the same dimension and therefore the water passing through does not have the same velocity and lastly, the velocity has transverse component due to the flow pathways tortousity (Marion, 2008). These two processes are characterized by similar expressions where the mass flow is proportional to a coefficient and to the derivative of the concentration along the flow axis. Because of this similarity, it is possible to introduce a single expression, called hydrodynamic dispersion, including both processes. This transport mechanism, along the longitudinal direction, can be expressed as follows:

$$j_I = -D_L \frac{\partial C}{\partial x} \quad (2.7)$$

Where D_L [L^2T^{-1}] is the coefficient comprehensive of both dispersion and diffusion coefficients. It is called hydrodynamic dispersivity coefficient, and it refers to the water flow direction axis. It can be expressed as follows:

$$D_L = D_0 + D_C = D_0 + \alpha_L v_e \quad (2.8)$$

In the equation 2.8, D_0 and D_C represent respectively the molecular diffusion and the cinematic dispersion coefficients [L^2T^{-1}], and α_L [L] is the longitudinal dispersivity. Depending on the velocity of the water, one of the two coefficients expressed before can be considered negligible. For very low flow rates, the molecular diffusion is the main cause of plume mixing, while for higher velocities, the typical velocities in groundwater systems, the cinematic dispersion is predominant and therefore the molecular diffusion can be considered negligible (Sethi & Di Molfetta, 2019). Hence, the 2.8 can be re-written as follows:

$$D_L \approx D_C = \alpha_L v_e \quad (2.9)$$

The equations for the two transversal directions are the same, but the α_T (transversal dispersivity) is from 20 to 5 times smaller than the longitudinal dispersivity.

α_L depends on the scale of the phenomenon, the higher the extension of the propagation, the greater the dispersivity. Typical α values in sandy laboratory column, under homogeneous and saturated conditions, lay between 0.1 – 2 cm (Namitha & Ravikumar, 2018). Some authors, like Silliman et. al (1987) and Huang et. al (1995), clearly show that the path length has an important role in the dispersivity value, as the last one increases if the scale is increasing.

All the processes considered until now regard the solute movement with the average water flow or the plume expansion, typical mechanisms characterizing the conservative solutes. However, other processes (e.g. solute retardation and reaction) occur in saturated soil if a non-conservative solute is passing through.

Retardation is a phenomenon in which the solute movement is slowed down because the interaction between the porous medium and the solute itself (Cvetkovic et al., 2006). The sorption can be

caused from different reasons: absorption, adsorption and ion exchange. The solute sorption is a reversible process in which the plume only slows down but it does not react. A quantification of this process comes from the retardation parameter R [-], which depends on both soil and solute characteristics and it can be quantified with the following expression (Sethi & Di Molfetta, 2019):

$$R = \frac{v_e}{v_c} \quad (2.10)$$

where v_e is the effective water velocity and v_c is the solute velocity. If the solute is characterized by a linear adsorption, the R coefficient can be expressed as follows (Sethi & Di Molfetta, 2019):

$$R = 1 + \frac{\rho_b}{n_e} K_d \quad (2.11)$$

in which, ρ_b is the bulk density of the soil [ML^{-3}] and K_d is the solid-liquid partition coefficient [M^{-1}L^3].

There are many reaction mechanisms, among others there are the biodegradation, hydrolysis, redox reactions and volatilization (Cvetkovic et al., 2006). In general, the reaction processes generate a reduction of the contaminant concentration, even if in some particular cases the concentration could increase (Cvetkovic et al., 2006). The biodegradation usually can be expressed with the Monod's model (Sethi & Di Molfetta, 2019):

$$\frac{dC}{dt} = -\mu(C)C = -\mu_{max} \frac{C}{K_C + C} \quad (2.12)$$

where the C is the solute concentration, μ is the microorganisms growth rate [T^{-1}], μ_{max} is the maximum microorganisms growth rate [T^{-1}] and K_C is the half saturation constant [ML^{-3}]. All the parameters present in this biodegradation model are difficult to be estimated, therefore a easier first order kinetic model is usually adopted (Sethi & Di Molfetta, 2019):

$$\frac{dC}{dt} = -\mu C \quad (2.13)$$

If putting altogether, and considering a one dimensional problem, all the mechanisms can be summarized into a single equation, the differential equation of mass transport (Sethi & Di Molfetta, 2019):

$$D_L \frac{\partial^2 C}{\partial x^2} - v_e \frac{\partial C}{\partial x} - \lambda C = R \frac{\partial C}{\partial t} \quad (2.14)$$

where λ [T^{-1}] is the natural degradation coefficient, which depends on the half-biological life $t_{1/2}$ [T]:

$$\lambda = \frac{0.693}{t_{1/2}} \quad (2.15)$$

For conservative solutes (e.g. dyes) $R = 1$ and $\lambda = 0$, therefore the 2.14 becomes as follows:

$$D_L \frac{\partial^2 C}{\partial x^2} - v_e \frac{\partial C}{\partial x} = \frac{\partial C}{\partial t} \quad (2.16)$$

All the processes explained above are schematically represented in figure 2.1.

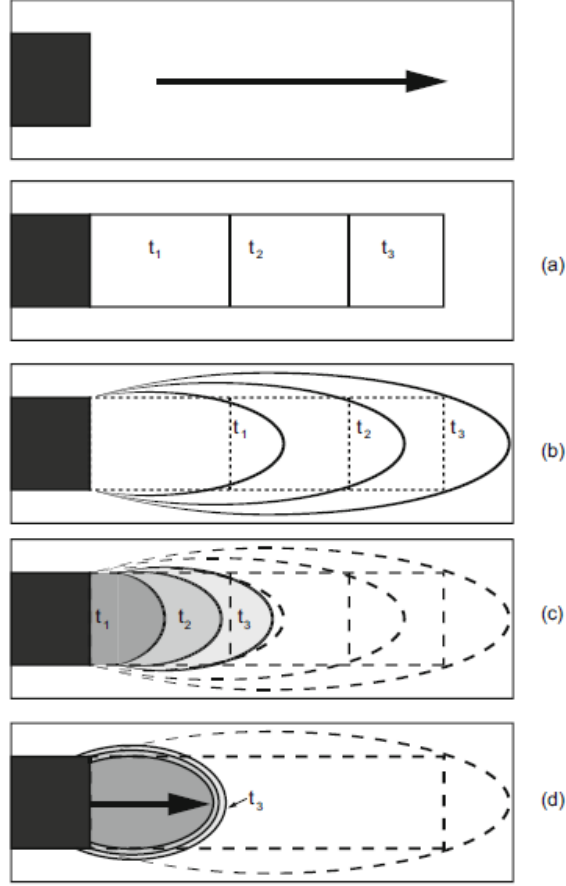


Figure 2.1. Different mechanisms occurring to a contaminant plume during a continuous injection. a) only advective transport; b) advective and dispersive transport; c) advective and dispersive transport of a solute affected by retardation; d) advective and dispersive transport of a solute affected by biodegradation. Source: modified image from Sethi & Di Molfetta (2019)

2.2 Water flow and solute transport in unsaturated porous media

Unsaturated conditions can be involved in many fields, such as agriculture and hydrology. Phenomena like rain water infiltration, irrigation, groundwater recharge and evaporation usually occur under unsaturated conditions (Nielsen et al., 1986).

An important parameter to consider under unsaturated conditions is the residual water content θ_r [-]. It is defined as the water that cannot be expelled by the soil mainly due to disconnected pores (Van Genuchten & Pachepsky, 2011). Because of this consideration, the water content lays in the range between the residual water content and the porosity: $\theta_r < \theta < \phi$. Therefore, also the saturation can be redefined by considering the θ_r value. This saturation value is called effective saturation S_e [-] and it is defined as follows (Kartha & Srivastava, 2008):

$$S_e = \frac{\theta - \theta_r}{\phi - \theta_r} \quad (2.17)$$

Since under unsaturated conditions the soil voids are not fully saturated by water, the matrix is composed by three phases: solid, liquid and gaseous phase. The simpler case of unsaturated soil is when there is a saturated zone with above an unsaturated layer (or vadose zone). In this case, if

we think at the hydraulic head $h = \psi + z$, where z [-] is the elevation and ψ [-] the pressure head, for definition the water table is where the pressure head is equal to zero ($\psi=0$) and then $h = z$. Saturated conditions occur below the water table, and since the h relationship must be valid, in this zone the pressure head will be positive ($\psi > 0$) and above the water table (vadose zone) the pressure head must be negative ($\psi < 0$) (Tarboton, 2003). This consideration brings to another definition of unsaturated zone: it is the part of the soil in which the soil water pressure is negative. In other words, in the vadose zone the water is "trapped" in the soil voids because of surface-tension forces. In unsaturated conditions, the negative pressure head inside the matrix can be expressed also with the term suction head.

Since the suction head that a pore is able to sustain is proportional to the ratio between the external surface of the pore channel and the cross-sectional area, theoretically the bigger is the pore, the lower is the tension head that the pore is able to tolerate. Due to this phenomenon, if the moisture content increases only the smaller pores are able to retain water and it follows the water content dependency on the suction head (Tarboton, 2003). This relationship is represented by the soil-water retention function, which is a characteristic of each soil. A typical soil water retention curve is reported in figure 2.2. From the graph, it is possible to observe that when the water content approaches the saturated value (i.e. $\theta = \phi$), the suction head tends to 0. When the saturated conditions are reached and the water content cannot increase, the curve arrives at an inflection point. This point is a characteristic point of each soil water retention curve and it represents the air-entry tension (ψ_a), which is the pressure value at which a notable volume of air starts to fill the soil pores.

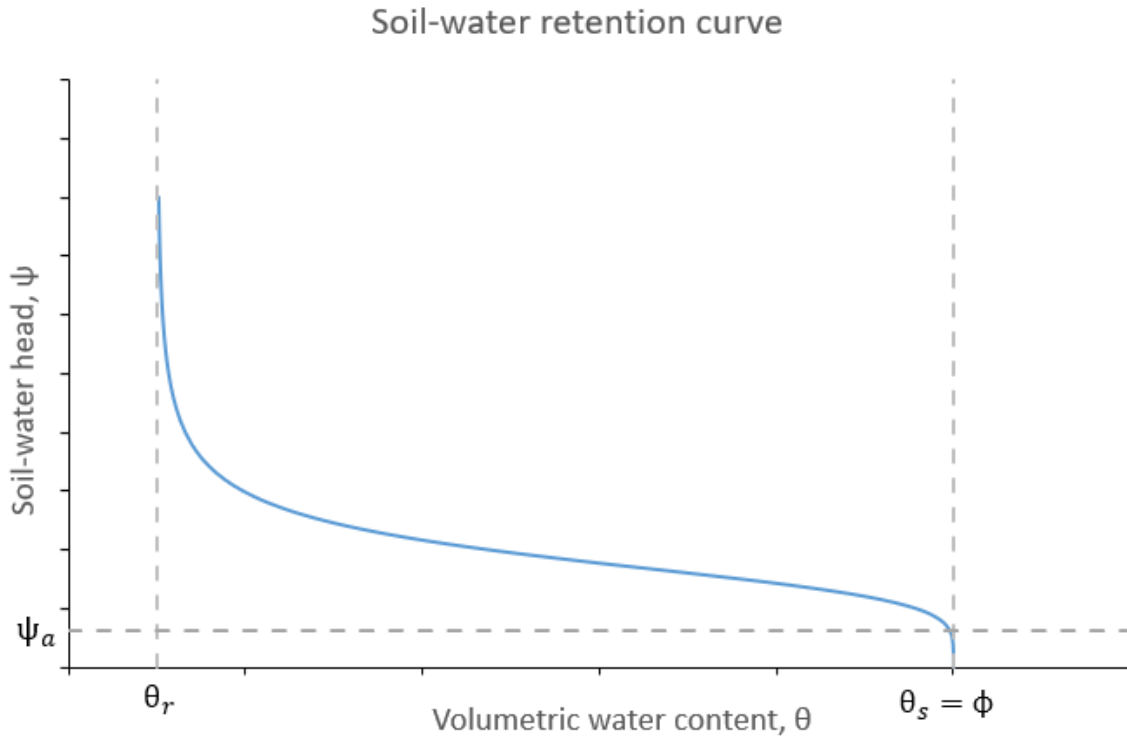


Figure 2.2. Example of soil water retention curve for sand.

All the aspects described above are influencing the hydraulic conductivity of unsaturated systems. As the water content decreases, and the suction head increases, the water finds more difficult to move because the paths are smaller and fewer (Tarboton, 2003). Therefore, the hydraulic conductivity in vadose zone is highly dependent on the soil water content value. From numerous experiments,

it has been observed that the relationship between suction head and water content $\psi(\theta)$ and the one between suction head the hydraulic conductivity $\psi(K)$ can be represented by hysteretic curves (Tindall et al., 1999). These hysteretic relationships are represented in figure 2.3.

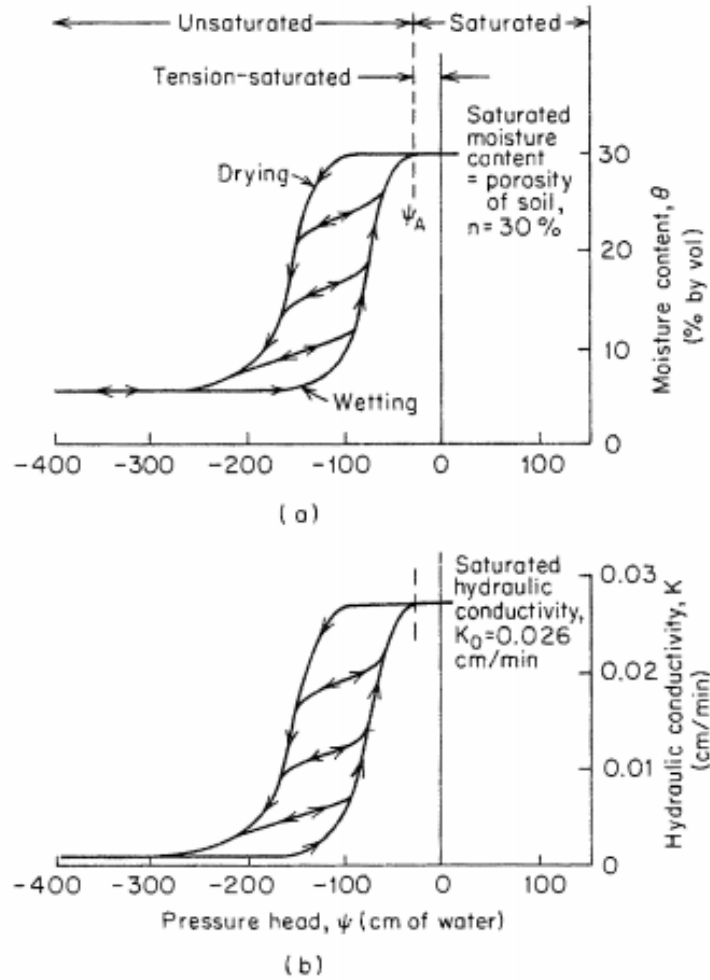


Figure 2.3. a) Hysteresis curve of $\psi(\theta)$; b) hysteresis curve of $\psi(K)$; Source: modified image from Freeze & Cherry (1979)

From the graphs in figure 2.3, it is possible to observe that the ψ and K values do not follow the same path during the wetting and the drying phases, resulting in a hysteretic behaviour. The combination of many processes causes the hysteresis, among others variation in pore diameter, entrapped air and swelling/sinking mechanisms (Hillel, 1980). This hysteretic relationship influences many processes occurring in the vadose zone (Canone et al., 2008; Li, 2005). In particular, hydraulic conductivity and water velocity change according to the degree of saturation, which is directly involved in the hysteresis. Therefore, the water content variations affect the transportation of water, solutes and air, from the surface to the groundwater (Russo et al., 1898). Furthermore, since the water content profile has a direct relationship with the aeration, it influences also chemical and microbial processes (Lehmann et al., 1998).

If we focus on the $\psi(\theta)$ relationship, the soil water retention curves, both wetting and drying, can be considered the *main wetting* and the *main drying* curves. As presented by Basile et al. (2003), these two curves can be obtained experimentally by slowly wetting (from dry soil to saturation) and

slowly drying (from saturation to dry conditions) the soil. Beside these two curves, which represent a sort of limit condition, there are many others which occur in a dynamic change of soil water content (Huang et. al, 2005). These curves, divided into primary, secondary, etc., lay in between the two main curves and they represent the so called *scanning curves*. A clear representation of this concept is schematized in figure 2.4.

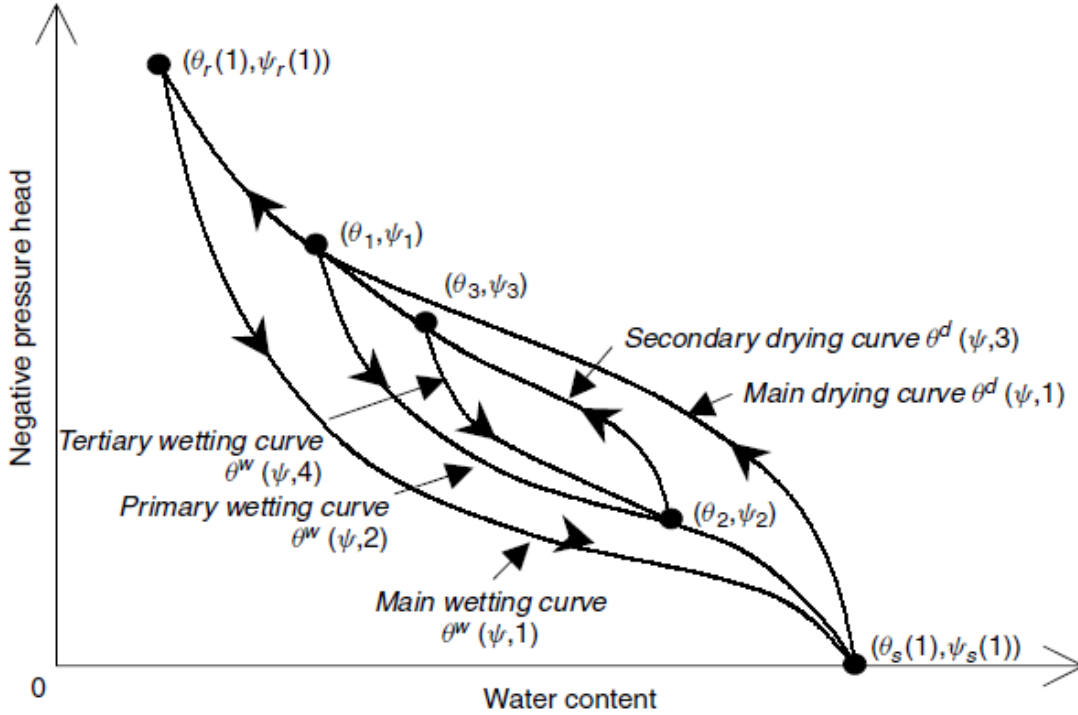


Figure 2.4. Examples of main and scanning curves, both in wetting and drying conditions. Source: modified image from Huang et. al (2005)

Many studies have been developed with the aim of finding a model to describe the hysteresis of $\psi(\theta)$ (Mualem & Dagan, 1975; Topp, 1969; Kutilenk & Nielsen, 1994; Huang et. al, 2005). However, this relationship is still extremely difficult to be implemented in mathematical methods.

Despite the dependency of the hydraulic conductivity on the water content, in unsaturated conditions, it is still valid the Darcy's equation 2.4. From the Darcy's and the continuity (conservation of mass) equations derives the mathematical expression for the vertical water movement through an unsaturated soil. This fundamental equation is known as Richard's equation (Richards, 1931):

$$\frac{\partial \theta}{\partial t} = \frac{\partial}{\partial x} \left[K \left(\frac{\partial h}{\partial x} + \cos \alpha \right) \right] - G \quad (2.18)$$

where h is the water pressure head [L], t is the time, x is the spatial coordinate of the flow direction, G is the sink term [T^{-1}] and α represents the angle between the flux direction and the vertical axis, since in this thesis all the tests have been performed with vertical downwards flow $\alpha = 0^\circ$.

Among others, Van Genuchten (1980) proposed a mathematical empirical function for the soil water

characteristic curve, it can be expressed as follows:

$$\theta(h) = \begin{cases} \theta_r + \frac{\theta_s - \theta_r}{[1 + |\alpha h|^n]^m} & h < 0/\alpha \\ \theta_s & h \geq 0/\alpha \end{cases} \quad (2.19)$$

Where θ_r and θ_s are respectively the residual and the saturated soil water content. α [L^{-1}] and n [-] are empirical soil water retention function parameters. m is a dependent parameter obtainable as follows:

$$m = 1 - 1/n, \quad n > 1 \quad (2.20)$$

If this equation is combined with a pore size distribution model, which relates the soil water retention and hydraulic characteristic curve, it can be obtained a relation for the prediction of the hydraulic conductivity of unsaturated soils. Mualem (1976) is one of the most used pore size distribution models. It can be expressed with the following relationship:

$$K(S_e) = K_s \frac{S_e^l \left\{ \int_0^{S_e} \left[\frac{1}{h(S_e)} \right] dS_e \right\}^2}{\left\{ \int_0^1 \left[\frac{1}{h(S_e)} \right] dS_e \right\}^2} \quad (2.21)$$

Where K_s is the hydraulic conductivity in saturated conditions and l [-] is the tortuosity parameter, considered 0.5 for many soils (Mualem, 1976).

By combining the equations 2.19 and 2.21, the Van Genuchten-Mualem equation can be obtained (Van Genuchten, 1980):

$$K(h) = K_s S_e^l [1 - (1 - S_e^{1/m})^m]^2 \quad (2.22)$$

In the equations 2.22, the parameters m , l and S_e are all lower than 1, therefore it can be deduced that in unsaturated conditions ($\theta < \theta_s$), the hydraulic conductivity $K(\theta)$ will be less than the hydraulic conductivity in saturated conditions K_s . The relationship between hydraulic conductivity and water content is shown in figure 2.5, in which it is clear that as the water content increases also the K value increases.

Water infiltration in soil is a typical phenomenon that occurs in unsaturated conditions, and therefore it is influenced by all the processes and laws described previously in this chapter. In figure 2.6, it is schematized the process of water infiltration in unsaturated soil. When soil is perturbed from its hydrostatic conditions, by the rain or irrigation, the water content increases in the top layer and a gradient Δh is generated between the top of the soil and the bottom layers. Because of this gradient, the water starts to flow downwards and the water content starts to increase also in the bottom layers. At this moment, depending on the rain intensity w [LT^{-1}], two different phenomena can happen:

- If $w > K_s$ (figure 2.6(a)).

Water content increases faster in the top layer rather than in the deeper ones. At a certain time, the top layer reaches the saturation (*ponding time*). From the ponding time on (t_3 in figure 2.6(a)), the wetting front propagates downwards until it reaches the piezometric surface and the infiltration stops. The runoff begins as the ponding time is reached.

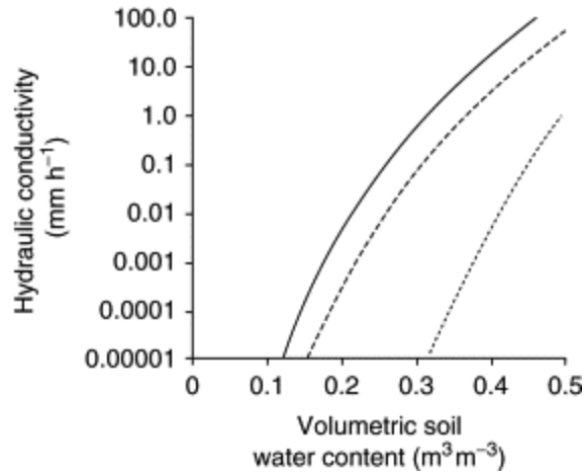


Figure 2.5. $K(\theta)$ relationship of different types of soil. From left to right the two lines are representing the sand, loam and clay. Source: modified image from Landsberg et al. (2011).

- If $w < K_s$ (figure 2.6(b)).

As the water content increases in the top layer, the infiltration process is faster than the top soil saturation. Water starts to reach the piezometric surface before the top layer comes to saturation. The piezometric surface starts to rise up until reaching the top layer. When it happens, the runoff begins.

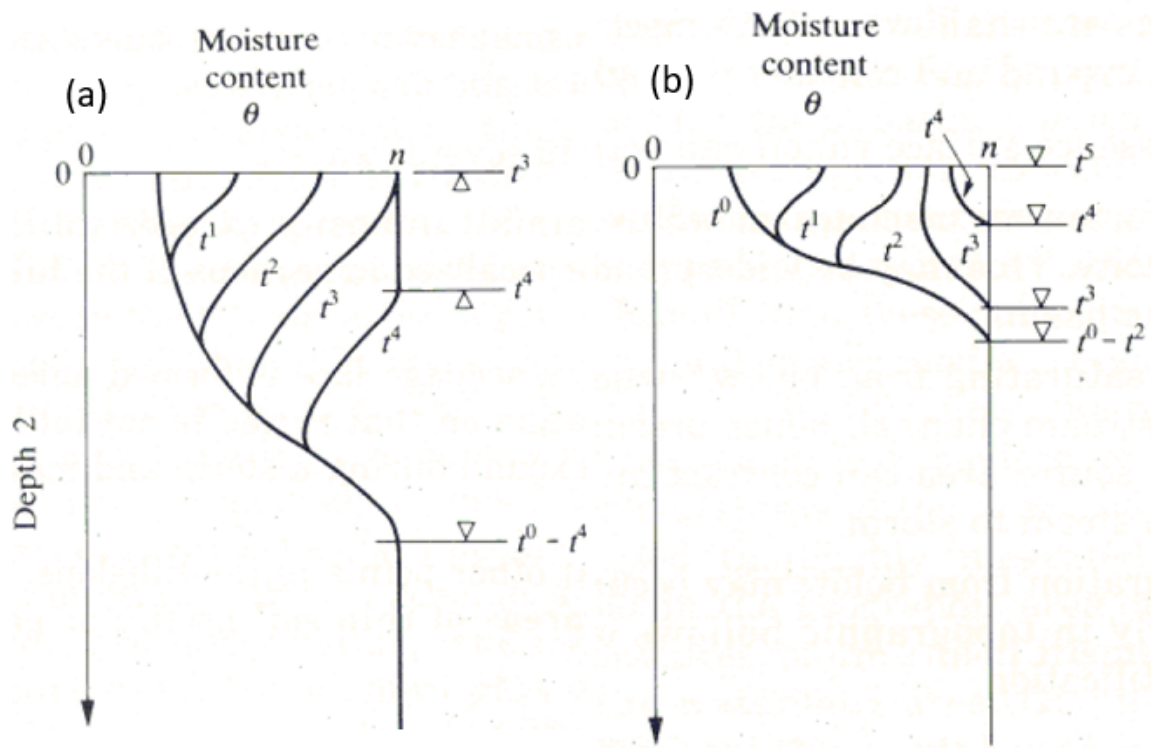


Figure 2.6. Infiltration in unsaturated soil. a) Runoff for infiltration excess. b) Runoff for saturation excess. Source: modified image from Tarboton (2003)

Many mathematical models have been developed to represent the infiltration process, such as *Green-Ampt model* (Rawls et al., 1983), *Horton model* (Clausnitzer et al., 1998), *Philip model* (Smiles & Knight, 1976). The mathematical representation of these models goes beyond the purposes of this thesis and therefore they will not be addressed here.

The solute transport in unsaturated soils is characterized by the same processes of the transport in saturated conditions (equation 3.2). The only differences under unsaturated conditions are the presence of a third phase (gaseous phase) and the water content which is lower than the saturated one. The first aspect regards mainly the volatile compounds which are transferred from the aqueous phase to the gaseous one and in the last one they undergo similar mechanisms (i.e. advective and dispersive processes) that occur in liquid phase (Costanza-Robinson & Brusseau, 2002). The solute used for this thesis is a non-volatile compound and therefore here it will not go deeper into the details of the gaseous transport in unsaturated soil.

In addition, water content affects the solute transport because it directly influences the velocity of the water passing through the porous medium. As the water content decreases, the pathways for the water become smaller in number and more tortuous and therefore, the section available for the water to pass through decreases and, at equal flow rate, the water (or the solute) goes faster.

2.3 Laboratory tests

Laboratory tests on soil columns are the most used way to study hydrological properties and water and contaminant transport models (Lewis & Sjöström, 2010a). A laboratory column can be seen as a block in which water can flow, usually downwards. The shell of the column (of very various dimensions) is usually made of an impermeable material (e.g. plastic or glass) and it is filled with soil. Inside the column there could be inserted some instruments to control parameters like water content, pH, etc. There are many types of test that can be performed in a soil column, a first main distinction can be done between saturated and unsaturated tests. As explained in the previous chapters, saturated conditions are when the water content is equal to the porosity $\theta = \phi$, it means that all the pores interconnected are filled by water. Conversely, unsaturated soils are characterized by a water content that is lower than the porosity: $\theta < \phi$, in this condition also the gaseous phase is present. The first type of tests is mainly performed in order to study properties and contaminant transport in groundwater systems, while the latter ones are executed to evaluate infiltration from rainy events or irrigation, fate of contaminant in unsaturated zones, etc.

Another distinction can be done on the base of the type of soil that fills the column, which can be packed or monolithic. In packed soil columns, which is the case of this thesis work, soil is put inside the column and packed as homogeneously as possible, in order to avoid layers' stratification or heterogeneity which can create preferential flow pathways. The packed soil columns are very useful for general studies of solute and contaminant transport and they are very common because their replicability. On the other hand, monolithic soil columns are closer representations to the soil conditions in actual fields. The soil samples used for monolithic columns are taken directly from the interested field. This type of test is done for very specific application and to replicate the natural heterogeneity, such as root cavities, macropores, etc. (Akhtar et al., 2003).

Tracer tests are used to study the soil water characteristics and the fate of contaminants. For definition, a tracer is a solute that does not undergo biodegradation and adsorption processes, therefore it moves through the porous medium at the same velocity of the water flow. Dyes (e.g. fluorescein, rhodamine, bromophenol blue) are typical tracers, with their colours, they allow, other

than the quantitative evaluation, also a visual qualitative evaluation. Other type of tracers can be salts like NaCl or KBr.

Soil water characteristic parameters (such as porosity, hydraulic conductivity, water content) can be estimated by modelling the results obtained from tracer tests. In these tests, a tracer (with a certain concentration C_0) is injected, usually at the top of the column, instantaneously or for a certain duration. The concentration of the tracer in the water at the exit of the column (or at another fixed distance) is then evaluated. The normalized concentrations (C/C_0) are usually then plotted in a graph called breakthrough curve (BTC), typical BTCs are represented in figure 2.7, in which can be also observed the differences between solutes that undergo only dispersion (tracers) or also adsorption and biodegradation.

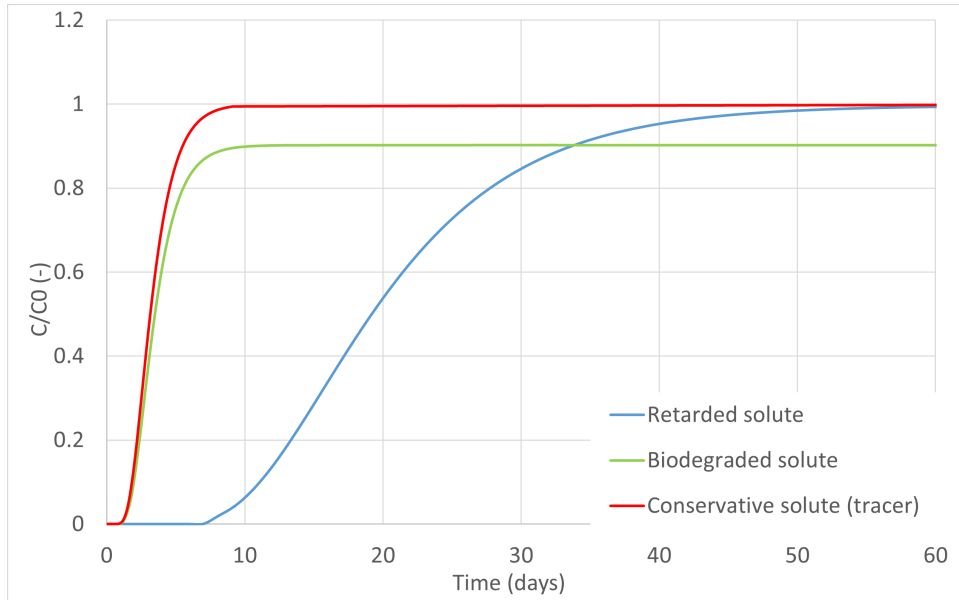


Figure 2.7. Typical BTCs of column test with a continuous injection. Green: curve for a tracer (subject only to advection-dispersion). Blue: curve of a solute subjected also to retardation, other than advection-dispersion. Red: curve of a solute subjected also to biodegradation, other than advection-dispersion.

Rarely, it is also possible to find graphs C/C_0 vs distance, in which profiles of concentration are drawn at fixed times (figure 2.8).

By modelling the BTCs with software (e.g. HYDRUS-1D), it can be obtained, among other parameters, the longitudinal dispersivity value α_L . As mentioned by Rai & Ojha (2007), the α_L value is a very important parameter for the simulation of solute transport through both saturated and unsaturated soils. The dispersivity is strongly related to the extension of the scale (Sethi & Di Molfetta, 2019). For example, in saturated aquifer systems, because their very variable extensions, this dependency is very visible. In addition, some researches states that the dispersivity value is sensibly lower in saturated conditions than in unsaturated ones and that this difference it is approximately an order of magnitude (Bunsri et al., 2008; Hutchison et al., 2003; Toride et al., 2003). Moreover, Bromly et al. (2007) have found that in laboratory columns the dispersivity is related with both the column diameter and length, as the α_L increases as either the diameter or length increases, even if the diameter variability has a greater effect on the dispersivity rather than the length. Conversely, other studies refer that in the laboratory scale the extension does not play a key factor for the dispersivity value. In particular Saravanan et al. (2015) states that the perfect

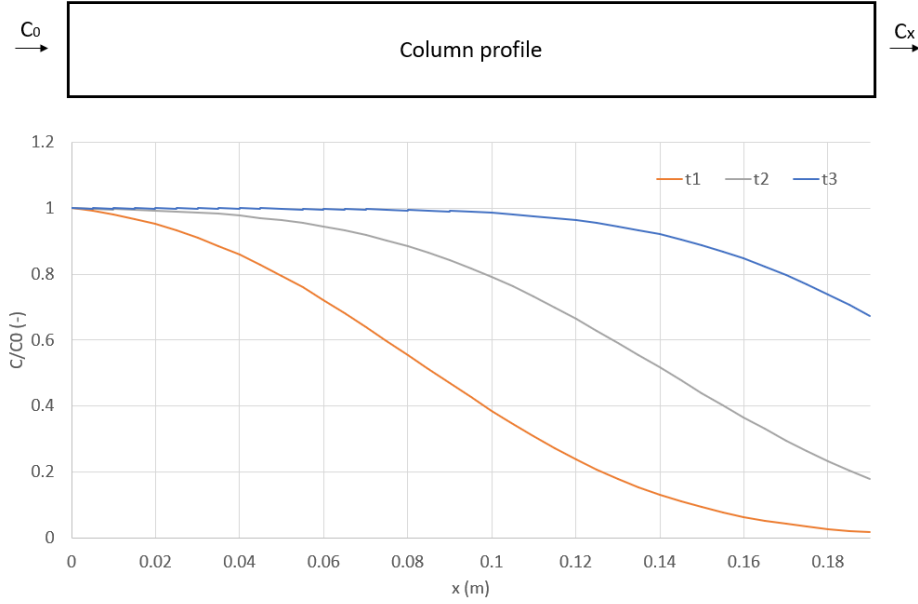


Figure 2.8. Typical profiles of normalized concentrations during tracer tests at different fixed times.

diameter to length ratio for unsaturated columns and lysimeters lays between $1/4$ and $1/20$, in this range the dispersivity should not resent the scale effect. Similar considerations have been done by Bergström (2000) which report, for unsaturated laboratory column, an optimal diameter to length ratio of $1/4$.

The scale effect is something to be considered when performing and comparing laboratory tests made at different scales. Laboratory test can be performed with columns of very different sizes (Lewis & Sjöstrom, 2010a). In literature, some authors reported very small columns with a diameter of 1 cm and a length of 1.4 cm , like the one shown by Voegelin et al. (2003), on the other hand, others like Mali et al. (2007) have presented a large column of $2x2x5\text{ m}$. Usually, within the large columns, we can classify the lysimeters.

Lysimeters are devices used mainly in agriculture, hydrology and water-quality research. Hillel et al. (2004) define lysimeters as "devices for measuring the percolation of water through soils and for determining the soluble constituents removed in drainage". In other words, lysimeters are rigid devices (e.g. tanks, containers) that can be filled with soil and water is allowed to flow from the top to the bottom, with same principles of laboratory columns.

Lysimeters permit the calculation of water balance, which can be easily express with the following formula (Hillel et al., 2004):

$$W_i = W_{i-1} + P_i + I_i - D_i - ET_i \quad (2.23)$$

where:

- W_i (mm): is volume of water inside the lysimeter per unit area, at time i ;
- W_{i-1} (mm): is volume of water inside the lysimeter per unit area, at time $i - 1$;
- P_i (mm): is the precipitation during the time from $i - 1$ to i ;

- I_i (mm): is the irrigation during the time from $i - 1$ to i ;
- D_i (mm): is the lysimeter discharge during the time from $i - 1$ to i ;
- ET_i (mm): is the evapotranspiration during the time from $i - 1$ to i .

Usually the most advanced lysimeters are also equipped with sensors and probes inside the column at different depths for parameter evaluation, such as moisture content, pH, electrical conductivity (EC), etc.

Lysimeters were born to in Europe in the seventeenth century for agricultural purposes, they were used in fact to study water consumption of crops. After years of improvement and development, nowadays lysimeters are also widely used among others, for hydrology and water quality research. Even if the majority of the lysimeters is used in natural outdoor environment, lysimeters can also be employed in laboratory, greenhouse or environment chamber (Führ et al., 1998). The easiest field lysimeters are just cylindrical tanks filled with local soil and placed in field, the system is made in order to allow you to collect drainage water from the bottom of the column. In literature, there are many examples of field lysimeter's applications, for example Zupanc et al. (2012) used a lysimeter placed in a supply pumping station to calculate water balance, Peruski et al. (2018) presented experiments with a lysimeter to study the mobility of aqueous and colloidal species and Brown et al. (2000) with five different lysimeters directly placed in field studied the leaching of pesticides in soil. Sketches of typical field lysimeters are represented in figure 2.9.

On the other hand very few studies of laboratory lysimeters have been published, an example of it is the research made by Sugita & Nakane (2007) about the combine effects of rainfall patterns and porous media properties on nitrate leaching.

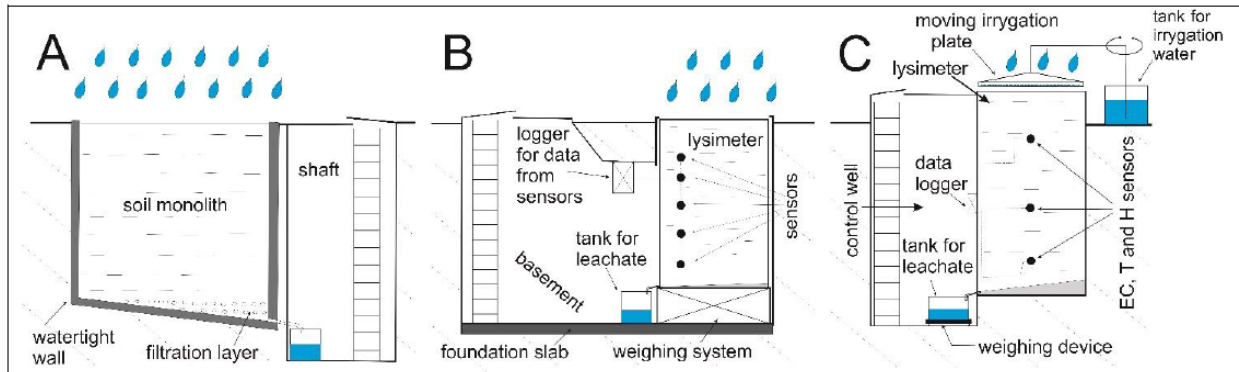


Figure 2.9. Schemes of typical field lysimeters. A: box lysimeter. B: weighing lysimeter. Irrigation controlled lysimeter C: Source: modified image from Soltysiak & Rakoczy (2019)

3 Materials and Methods

The tests performed in this thesis can be divided into three different scales: small, intermediate and lysimeter scale. In this chapter, the materials (different set-ups and configurations) will be described, as well the methods and protocols adopted during the tests at the different scales. In addition, the data processing and the modelling parts will be also explained.

3.1 Materials

The three different scale set-ups all consist in a main column filled with sand and a pump system which creates a vertical downwards water flow. A qualitative comparison of the three column dimensions can be done by looking at the sketch in figure 3.1.

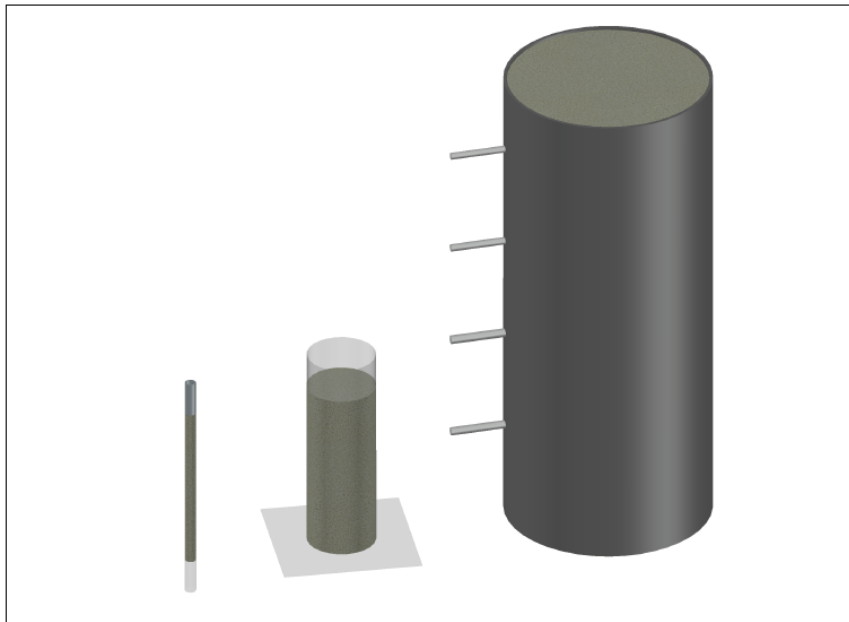


Figure 3.1. Sketch of the two plastic columns and the lysimeter. The suction probes of the lysimeter are also represented.

All the test's samples have been analysed with a UV-Vis spectrophotometer. A spectrophotometer analyses the absorbance of a sample in a cell by using a UV and a visible lamp. By looking at specific wavelengths and comparing the outflow's absorbance with the C_0 's one, it is possible to calculate the outflow concentration of a tracer in terms of C/C_0 . This is possible because of the linearity between the absorbance and the concentration, as expressed by Cannon & Butterworth (1953). Therefore, for every measurement, the ratio C/C_0 can be obtained by calculating the A/A_0 value; where A is the absorbance of the sample and A_0 is the absorbance of the solution injected into the column (initial absorbance). Depending on the test and on the type of column, the sampling process has been performed manually or, when possible, the column exit was directly connected with the spectrophotometer for an automated sample analysis. In figure 3.2, the spectrophotometer carousel is represented. In automated analysis, the carousel is able to rotate and measure one cell at the time.

All the tracer tests have been performed by using a bromophenol blue (BPB) solution. BPB



Figure 3.2. Spectrophotometer carousel with bromophenol blue samples.

(3, 3', 5, 5'-tetrabromophenolsulfonphthalein) is a widely used dye. It is characterized by a yellow colour in the acid form ($pH < 3.5$), while for pH greater than 5, it is characterized by a purple colour, which allows a qualitative visual tracing (Shokrollahi & Zare, 2016). BPB solutions can be also quantitatively analyzed by using a spectrophotometer and monitoring the wavelength around 590 nm , value in which the BPB absorbance spectrum has a peak (Simonenko et al., 2015).

In figure 3.3, the spectra of a 12 mg/l BPB solution, at different pH values, are displayed.

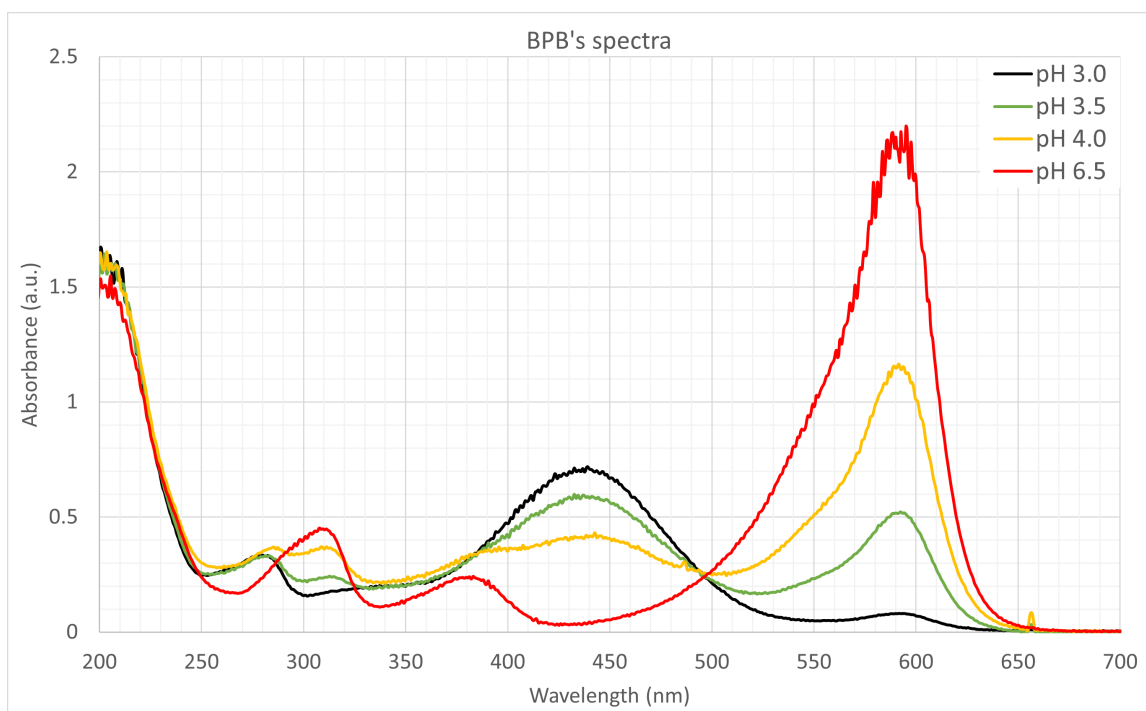


Figure 3.3. Absorbance's spectra of a 12.5 mg/l BPB solution at different pH values.

3.1.1 Small scale test setup

The small scale set-up consist of a main plastic column connected with a 4-channels peristaltic pump and with the UV-Vis spectrophotometer. The set-up is shown in figure 3.4.



Figure 3.4. Small scale tests set-up. 1: column; 2: in-flow; 3: out-flow; 4: 4-channels peristaltic pump; 5: solution for the test; 6: C_0 tank; 7: spectrophotometer; 8: waste tank.

In order to compare the results between the different scales, the length of the column has been set to 24 cm, which approximately corresponds to the depth of the lysimeter's second suction probe. It has been packed with a 24 cm layer of DORSILIT nr. 8 sand, whose characteristics are detailed in table A.1 and figure A.1, in Appendix A. As it is possible to see from figure 3.4, the vertical downwards flow is generated by a 4-channels peristaltic pump. Before going into the waste tank, the outlet and the C_0 pipes are passing through a flow-cell placed in the spectrophotometer's carousel for absorbance measurements.

3.1.2 Intermediate scale test setup

The intermediate scale set-up consists in a main plastic column of 100 mm diameter. The image in figure 3.5 represents the experimental set-up.

In order to have comparable results, the column has been packed with a 23 cm layer of DORSILIT nr. 8 sand, already used in the small scale tests. In addition, a pre-filter layer of DORSILIT nr. 7 sand (approximately 2 cm) has been placed at the top and the bottom of the main layer. Since the

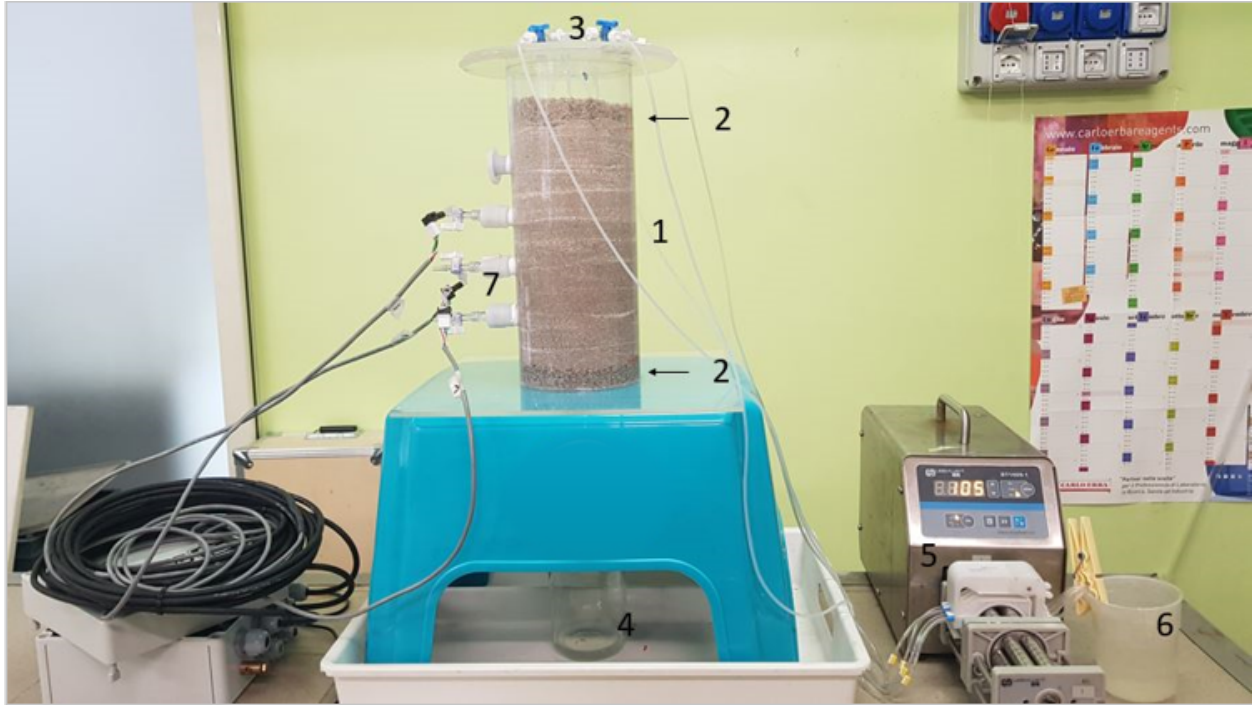


Figure 3.5. Intermediate scale tests set-up. 1: main column; 2: pre-filter layers; 3: in-flow; 4: outflow; 5: outflow collection tank; 6: solution for the test; 7: tensiometers.

dimension of the column could not guarantee a homogeneous flow in the first part of the column, these layers of coarse sand are meant to help the uniformization of the inflow and outflow. The characteristics of this sand are detailed in in table A.2 and figure A.2, in Appendix A.

The free-drainage at the bottom of the column consisted in a 16 mm hole. Between the hole and the bottom sand layer, an additional filter has been placed in order to avoid sand coming out from the outlet. As it is possible to see from figure 3.5, the inflow was coming out from 8 different dripping tubes uniformly distributed on the column section. A peristaltic pump was pumping de-ionized water (DIW) or BPB solution with 4 different channels and just before the top of the column the 4 pipes were splitted into the 8 final dripping tube.

Three tensiometers have been placed into the column at different depth: 10, 15 and 20 below the sand surface (respectively referred as: tensiometer 3, 2 and 1). A tensiometer is a device for the determination of the matrix potential which is a measure of the tension exercised by the soil matrix on the water. It consists of a porous cup (usually made of ceramic) connected to an air-tight sealed tube, which is filled with water. The tensiometer, which is inserted into the soil, is able to exchange water (through the porous cup) with the volume of the sand surrounding it, until reaching a state of equilibrium. If the soil is dry, water will flow from the tensiometer to the soil, creating a negative pressure inside the tensiometer until this negative pressure is equal to the pressure of the surrounding soil. When the soil is wetting again, the negative pressure of the soil tends to decrease and therefore, water will flow inside the tensiometer going to decrease the negative tension inside of it. Usually a manometer or a pressure transducer is connected to the tensiometer to measure the tension inside of it. In this case a pressure transducer, which measures automatically, is connected with the three tensiometers.

3.1.3 Lysimeter

The laboratory lysimeter used for the tests is produced by Umwelt-Geräte-Technik GmbH (UGT) and its scheme is represented in figure 3.6.

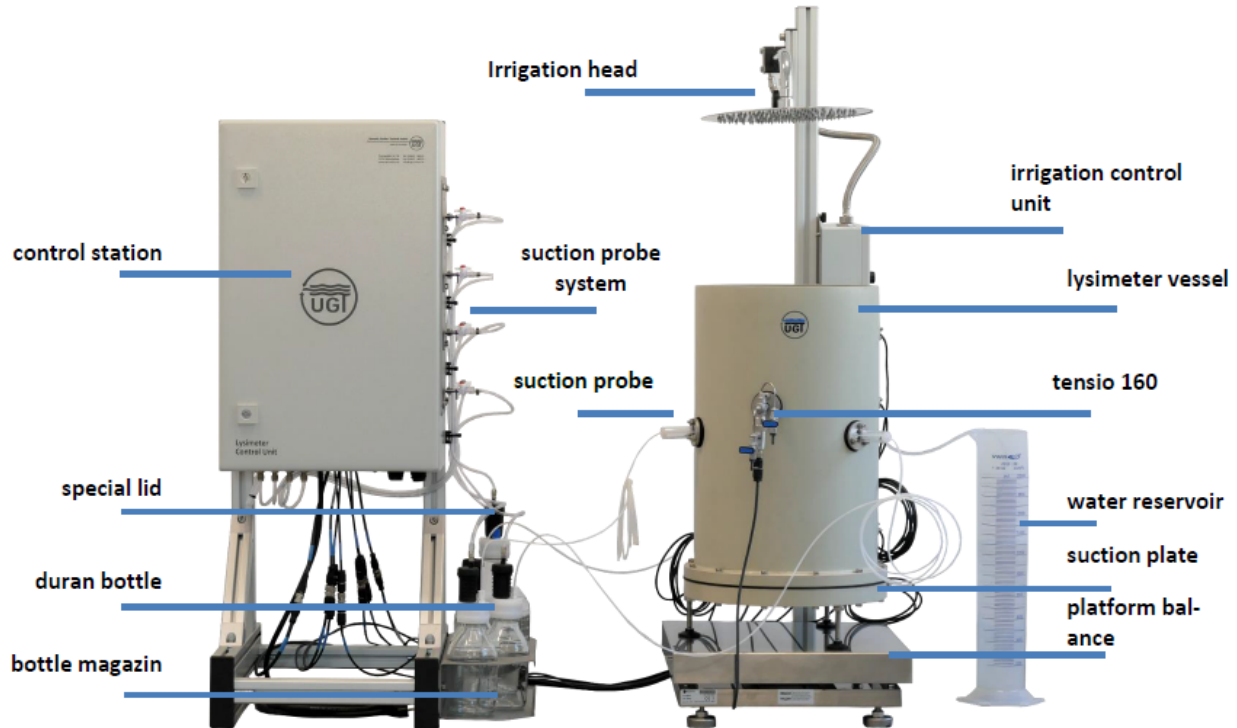


Figure 3.6. Scheme of a UGT lysimeter. Source: modified image from UGT (2019a).

The core of the system is represented by the cylindrical vessel of a total length of 70 cm. It has been filled with DORSILIT nr. 8 sand, as it has been done for the other scale columns. In order to create more similar conditions with the intermediate scale and to have a layer able to homogenize the incoming flow, a 2 cm – layer of pre-filter DORSILIT nr. 8 sand has been placed on the top of the column. The whole column is placed on a platform balance which is able to retrieve weight values of the entire system. The water flow is controlled by the irrigation system, consisting of an irrigation plate and an irrigation control which allows you to choose the flow rate for the test. In the main column, a series of soil hydrological sensors are placed. In addition, four tension-controlled suction probes, four tensiometers, two pH electrodes and two redox electrodes are present. All the sensors and the weighing system are connected to the lysimeter control station which logs and stores the data. A tipping counter has also been added at the lower exit of the column. The tipping counter measures the quantity of the leachate coming out from the column. The outflow tank and the tipping counter are connected to the support rod behind the vessel so that the water exiting the cylinder will not weight on the weighing system anymore.

In the set-up used for the tests four sensors have been placed in the column at different depths: 10, 25, 40 and 55 cm below the top surface. Each of these sensors are able to measure together volumetric water content, EC and temperature in soils. The main advantage to have a single sensor measuring the three parameters placed in a single vessel, instead of having three different sensors, other than saving money and time during installation, is to reduce the water flow disturbance. For water content, the measuring system is made of two antennae able to measure a volume of

approximately 500 *ml*. By sending a signal of constant frequency (120 *MHz*) and by reading the phase difference of the signal running back and forth, the antennae are able to estimate the dielectric constant ϵ of the surrounding soil-water matrix. The dielectric constant value is strongly related to the soil moisture: values of $\epsilon = 2 - 5$ are representing a dry soil, while the value in distilled water is 80 (UGT, 2019b). The water content is then determined by the Topp/Davis empirical equation, which represents the relationship between θ and ϵ (Topp et al., 1980):

$$\epsilon = 3.03 + 9.30(\theta) + 164.00(\theta)^2 - 76.70(\theta)^3 \quad (3.1)$$

The water content sensors are measuring in a range between 0 and 100% of volumetric water content, with an accuracy of $\pm 2\%$ and a resolution equal 0.1% of volumetric water content.

The EC measurements are performed by using a different circuit than the one used for the ϵ value. The conductivity measure is done by sending a signal with a frequency in the *kHz* range while the ϵ measure is temporary stopped (UGT, 2019b).

The four tensiometers have been placed at a depth of 10, 25, 40 and 55 *cm*. The tensiometers have been calibrated before the installation and they are connected to the data logger in which the pressure measurements are stored.

The four suction probes are placed at 10, 25, 40 and 55 *cm* under the topsoil surface. A suction probe consists of a porous ceramic cup inserted into the ground for water extraction. The cups are connected with to storage bottles were the water extracting is going. In order to have a uniform suction pressure, the bottles are connected to a vacuum system which maintains a constant negative pressure inside of them. The probes are then extracting with constant suction pressure and every time the negative pressure drops below a pre-set value, the vacuum pump is activated to restore that value.

3.2 Methods

The tests run in laboratory have been mainly water flow and solute tracer tests. The tests have been run into three different scales: small scale (column diameter: 16 *mm*), intermediate scale (column diameter: 100 *mm*) and lysimeter scale (column diameter: 300 *mm*). For a better comparison of the test results between the different scales, the flow rates have been chosen in order to have the same specific discharge (q) in all the scales. Three different flow rates have been selected, corresponding to the minimum, an intermediate and the maximum flow rate given by the irrigation control system of the lysimeter. The three values are reported here below:

- Minimum velocity: $q_{min} \approx 2.0 \cdot 10^{-5} \text{ m/s}$;
- Intermediate velocity: $q_{int} \approx 3.5 \cdot 10^{-5} \text{ m/s}$;
- Maximum velocity: $q_{max} \approx 4.3 \cdot 10^{-5} \text{ m/s}$;

Because pumps' limits, the real q values vary a bit from the ones listed above and they are not exactly the same for all the scales.

By processing the data of the solute tracer tests, soil water and solute transport parameters have been estimated. Then by making a comparison between the three different scales, it was possible to evaluate if there is a scale effect for the lysimeter test or not. Furthermore, with the lysimeter, water flow tests have also been performed in order to have a better estimation of the soil water parameters and to run more tests to find potential practical problems.

3.2.1 Small scale tests

With the small scale three different type of tests have been performed: saturated, unsaturated and free drainage tracer tests. As mentioned before, each test has been repeated three times with different flow rates corresponding to the specific discharges expressed above. The three flow rates, corresponding respectively to q_{min} , q_{int} and q_{max} , are reported here:

- $Q_{min} = 0.24 \text{ ml/min}$;
- $Q_{int} = 0.45 \text{ ml/min}$;
- $Q_{max} = 0.60 \text{ ml/min}$;

For each flow rate, the column has been packed with 74 g of sand in saturated conditions. In order to avoid sand to infiltrate and clog the inlet and outlet tubes, two filters have been placed: one on the bottom and the other on the top of the sand column. After verifying the sealing of the column and that no air entered during the packing procedure, the tracer test could finally start. For the saturated test, two pipes were connected to the pump: the inlet tube and a tube supplying from the C_0 tank. While the former one was going into into the top of the column, the latter one was directly going towards the spectrophotometer for absorbance measures. The outlet pipe was in-line connected with the spectrophotometer. The absorbance values were detected from the spectrophotometer which was performing the measures with a frequency of a reading every 30 seconds.

The protocol used for saturated tests is as follows:

1. DIW injection for approximately 1 pore volume (PV);
2. Tracer injection (BPB) for 2/4 PV;
3. Flushing (DIW injection) for 2 PV, except for the slowest flow rate test in which the test was stopped after the second step.

A pore volume (PV) is defined as the volume of interconnected pores and in this case, it refers to a time, precisely the hypothetical time to fill once all the pores in the packed column. Experimentally, it is considered as the time elapsed between the start of dye's injection and the arrival at the column outlet of the solution with a concentration equal to $C_0/2$.

After the end of the saturated test, without unpacking the column and without changing the flow rate, it has been proceeded to the unsaturated test. For the unsaturated tests, the set-up was almost the same as before. In order to guarantee a constant water flow within the column and a consequent constant water content inside of it, the only difference is that the outlet pipe has been connected to the pump to extract water from the bottom of the column with the same incoming flow rate.

The procedure for the unsaturated test is as follows:

1. The outlet tube was disconnected, and the column was let desaturating by gravity for approximately 24 hours;
2. In the meanwhile, the water expelled was collected and weighted for further data analysis;

3. After the 24-hours desaturation, the pump was turned on again and DIW was injected from the top of the column;
4. Finally, when the water started to exit the column, also the outlet pipe has been connected with the pump. The time elapsed between the pump restart and the arrival of the water was timed for further data analysis;
5. DIW has been injected for approximately 1 PV;
6. Tracer injection (BPB) for 3.5/4.5 PV;
7. Flushing (DIW injection) for 3/5 PV.

As for the saturated tests, both the outlet tube and the C_0 's one was directly going into the spectrophotometer, which was taking a measure every 30 seconds.

On the other hand, for the free drainage test no pipe was connected to the exit of the column, hence for this test no tube was linked directly with the spectrophotometer. The column outlet was collected with test tubes and further manually examined with the spectrophotometer. Each sample was collecting for 4 minutes, so that the absorbance value measured afterwards was an average of the absorbances within those 4 minutes (for the lower flow rate test the sampling frequency was 6 minutes instead of 4). Furthermore, several samples of C_0 have been taken during the test, in order to have a C_0 average value.

The protocol used for the free drainage tests is the following one:

1. After the unsaturated test, the outlet tube was disconnected, and the column was let desaturating by gravity for approximately 24 hours;
2. After the 24-hours desaturation, the pump was turned on again and DIW was injected from the top of the column;
3. When the water started to exit the column the first falcon was put down the column and the test started;
4. DIW has been injected for approximately 1 PV;
5. Tracer injection (BPB) for 2/3 PV;
6. Flushing (DIW injection) for 3/4 PV.

This entire procedure (saturated + unsaturated + free drainage test) have been repeated three times with the three different flow rates mentioned above. After each cycle of tests, the column was in unsaturated conditions, therefore it was necessary to unpack and repack it again to have saturated conditions and start again from the beginning.

3.2.2 Intermediate scale tests

Since the intermediate column was difficult to keep in saturated conditions, it has been chosen not to perform the saturated tracer tests. Unsaturated tests, with water extraction at the bottom of the column, have been tried but the outlet pipe was not able to extract as much water was entering,

resulting in an increasing water content inside the column during the test. Therefore, also the unsaturated tests with the outflow pumping extraction have not been performed.

Consequently, only free-drainage unsaturated tests have been performed (set-up shown in figure 3.5). As mentioned before, three tests have been performed with a different flow rate corresponding respectively to q_{min} , q_{int} and q_{max} :

- $Q_{min} = 9 \text{ ml/min}$;
- $Q_{int} = 16.5 \text{ ml/min}$;
- $Q_{max} = 20 \text{ ml/min}$;

The protocol used for tests was as follows:

1. Before the first test started and between each test, the column has been let desaturating for 24 hours;
2. DIW has been injected for approximately 1 PV;
3. Tracer injection (BPB) for 1.5/2 PV;
4. Flushing (DIW injection) for approximately 3 PV.

During the tests, samples of water coming out from the column have been taken. Each sample was collecting the outflow for 3 minutes for the intermediate and maximum flow rate and 4 minutes for the minimum one. Each sample has been examined manually with the spectrophotometer after the test. Furthermore, to have an average A_0 , some samples of C_0 have been taken throughout the whole test and analysed with the spectrophotometer. During the whole test, the three tensiometers were performing measurements every minute and sending the data to a computer were they were collected.

3.2.3 Lysimeter tests

As for the intermediate scale, with the lysimeter, only free-drainage unsaturated tests have been performed. Three cycles of flow + tracer test have been performed at the three different flow rates: 5, 9 and 11 l/h.

The flow tests consisted only in flushing water through the column and monitoring the bottom boundary flux and the column parameters with the data logger. During the tracer tests, samples have been taken from the suction probes and from the column exit. The sampling from the suction probes has been done by opening the suction cup (therefore producing the loss of vacuum inside the bottle for the sampling time), then weighing the bottle, pouring the bottle content inside a numbered test tube and reconnecting the empty bottle to the vacuum system to restore the negative pressure inside of it. While, for the sampling at the exit of the column, it has been placed a small tank right below the exit of the column. By using a syringe, samples were withdrawn from the cup, which was emptied and then placed again right below the tipping counter.

Because the big volumes of water that had to be used, tap water has been utilize instead of DIW. Since the tracer tests have been performed by analysing BPB at 590 nm and the ions dissolved into the tap water are invisible at that wavelength, this choice does not affect the spectroscopy results.

Below here, the protocol used each cycle of test is described:

- flow test:
 1. Tap water injection for 5 *hours*;
 2. The column was let desaturating for at least 24 *hours* and all the test data was retrieved from the lysimeter data logger;
- tracer test:
 1. Tap water injection for approximately 1 – 2 *PV*;
 2. BPB injection for approximately 3 *PV*;
 3. Flushing with tap water for 3 – 4 *PV*;
 4. The column was then let desaturating for 24 hours and all the test data were retrieved from the lysimeter data logger.

As mentioned before, the sampling has been done in the four different suction cup and at the column exit. The sampling frequency was different for each test and it was varying also within the same test. It has been sampled with higher frequency before the reaching of the plateau in the breakthrough curve (around 5 minutes between each sample for each sampling port), while for the rest of the test the sampling frequency was between 7 and 10 minutes for each sampling port.

All the samples have been put into numbered test tubes and further examined with the spectrophotometer. During the whole test, samples of BPB (before entering the lysimeter) have been taken, these samples further examined with the spectrophotometer represent the C_0 concentration. All this process has been repeated three times, one for each flow rate.

Two additional solute tracer tests has been performed. The first extra test has been executed in order to evaluate the possible influence that the suction probe extractions have on the water flow and solute transport. While the second one aimed at deeper investigating the tensiometers' data, with an evaluation of the correct functioning of them, and it has been also evaluated if the type of sampling technique from the column's exit could have affected the results in terms of longitudinal dispersivity. The two tests have been performed with the same conditions of the lysimeter tracer test at the maximum flow rate (11 l/h).

For the first extra test, all the suction probes have been disconnected in order that they could not extract water from the column. Therefore, it has been sampled only from the bottom cup situated at the column free-drainage exit. The results of this tests, in terms of BTCs (at the column exit) and water content, have been compared with the results of the test with the suction probes working.

The test has been performed as follows:

1. flushing with tap water until the water content of the previous test at maximum flow rate (at the BPB injection time) was reached;
2. BPB injection for the same duration of the previous maximum flow rate test (2 *h*);
3. tap water flushing for the same duration of the previous maximum flow rate test (2.5 *h*).

Also the second extra test has been performed without the suction probe extraction. As it will be explained in the results' section, from the tensiometers' data can be observed a very different behaviour between the first two tensiometers and the deepest two. In order to evaluate if this difference has to be attributed to errors in the devices or this behaviour really occurs within the

column, the tensiometers 2 and 3 (respectively 25 and 40 cm below the soil surface) have been swapped before the test.

Furthermore, the influence of the sampling technique, on the dispersivity value, has been evaluated by changing the way in which the samples have been withdrawn at the lysimeter's exit. During this test, between two consecutive samples, the cup was not let at the column's exit the whole time as it happened in the other tests, but it was placed in that position only for few seconds, just enough to have some sufficient liquid for the spectroscopic analysis. Each sample was then withdrawn with a syringe and placed on a numbered test tube. This can be considered a point sampling method, which avoids the sample's dilution caused by stagnant liquid inside the cup.

The test has been performed as follows:

1. swap between tensiometer 2 and 3;
2. flushing with tap water until the water content of the previous test at maximum flow rate (at the BPB injection time) was reached;
3. BPB injection for the same duration of the previous maximum flow rate test ($2 h$);
4. tap water flushing for the same duration of the previous maximum flow rate test ($2.5 h$)

3.3 Data processing and modelling

The data obtained from the tests have been processed in order to create the related BTCs, i.e. plots in which C/C_0 is represented as a function of time. The BTCs have been modelled with HYDRUS-1D software. HYDRUS-1D is a software for the simulation of water, heat and solute movement in 1-D and variably-saturated conditions (Simunek et al., 2013), which makes this software very suitable for the work's purposes.

The modelling part aims to estimate water flow and solute transport parameters, depending on the test type, as described below:

- saturated test: saturated soil water content (e.i. porosity) θ_s [-] and longitudinal dispersivity α_L [L];
- unsaturated test: volumetric water content θ [-], saturated hydraulic conductivity K_s [L/T], hydraulic conductivity K [L/T] and longitudinal dispersivity α_L [L];
- free-drainage test: volumetric water content θ [-], saturated hydraulic conductivity K_s [L/T], hydraulic conductivity K [L/T] and longitudinal dispersivity α_L [L].

Since the values of θ and K are not fixed during an unsaturated test, but they vary with the hydraulic head (h) and with θ itself (equations 2.19 and 2.22), these values found with the modelling are average values along the column's profile.

For the estimation of the water flow parameters (θ_s , θ e K), HYDRUS numerically solves the Richards's equation 2.18.

As expressed in the previous chapter, $\theta(h)$ and $K(h)$ are non-linear functions and they can be expressed with several numerical models (Clapp & Hornberger, 1978). In this case the Van Genuchten model (equations 2.19 and 2.22) has been selected.

The value of θ_r used is 0.05, it is the suggested value by HYDRUS for sand. The empirical values n and α have been obtained from the soil water retention curve realized from the tensiometers calibration, they are respectively 2.68 and 14.5.

The solute transport parameter (D_L) has been estimated from the relative concentrations (C/C_0) of the BTCs by using the advection-dispersion equation described below:

$$\frac{\partial \theta C}{\partial t} = \frac{\partial}{\partial x} \left(\theta D \frac{\partial C}{\partial x} \right) - \frac{\partial q C}{\partial x} \quad (3.2)$$

in which, D_L [L^2T^{-1}] is the hydrodynamic dispersion and q [LT^{-1}] represents the flux. The longitudinal dispersivity parameter (α_L) is obtained by reversing the following equation:

$$\theta D = \alpha_L |q| + \theta D_w \tau_w \quad (3.3)$$

where D_w [L^2T^{-1}] represents the molecular diffusion in water and τ_w [-] is the tortuosity in the liquid phase. The tortuosity term is obtained from the *Moldup*'s equation, with the following formula:

$$\tau_w = 0.66 \left(\frac{\theta}{\theta_s} \right)^{8/3} \quad (3.4)$$

In HYDRUS, the temporal derivatives are discretized by means of finite differences with the Crank-Nicholson scheme while, the spatial discretization is performed with the Galerkin method of the finite elements (Simunek et al., 2013).

3.3.1 HYDRUS modelling for small scale tests

All the nine small scale tests (saturated, unsaturated and free-drainage, each with the three different flow rates) have been modelled in HYDRUS-1D.

Different parameters (regarding both water flow and solute transport) had to be inserted in the pre-processing phase. For the saturated tests, the following parameters have been set:

- geometry information, column length: $L = 24 \text{ cm}$;
- soil hydraulic parameters:
 - saturated hydraulic conductivity K_s : calculated from the Darcy's law (equation 2.4) with $i = 1$. Therefore, the K values inserted for the three different flow rates are: $1.99 \cdot 10^{-5} \text{ m/s}$, $3.73 \cdot 10^{-5} \text{ m/s}$ and $5.07 \cdot 10^{-5} \text{ m/s}$;
 - n and α have been set respectively to 1 and 0, since they refer to soil water retention curve in unsaturated conditions and they are not relevant in this case;
 - the tortuosity parameter $l = 0.5$, value suggested by Mualem (1976).
 - the saturated soil water content θ_s has been checked to be estimated.
- solute transport parameters: tracer injection duration.

The following boundary and initial conditions (BC and IC) have been then considered:

- water flow conditions:

- upper BC: constant flux.

$$q(x = 0, t) = q$$

Where, depending on the flow rate, $q = q_{min}$, $q = q_{int}$ or $q = q_{max}$;

- lower BC: constant pressure head.

$$h(x = L, t) = h_{L,0}$$

Where $h_{L,0}$ is the pressure head at the end of the column at the initial time;

- IC: pressure head profile.

$$h(x, t = 0) = h_{0,0} + x$$

Where $h_{0,0}$ is the pressure head at the initial time at the beginning of the column.

- solute transport conditions:

- upper BC: solute concentration during the injection.

$$C(x = 0, 0 < t < t_{end}) = 1$$

$$C(x = 0, t > t_{end}) = 0$$

Where t_{end} is the time of the injection's end. The concentration during the injection has been set equal to 1 in order to have the relative values for the C/C_0 curve;

- lower BC: zero concentration gradient.

$$\frac{\partial C(x = L, t)}{\partial x} = 0$$

- IC: no concentration within the column before the injection.

$$C(x, t = 0) = 0$$

In addition, the data inserted for the inverse solution are the BTCs obtained from the tests.

For the unsaturated tests, the process is more complex and it has been performed with two different iterations. The first one has been modelled as it was a saturated test in order to evaluate the volumetric soil water content θ . For the unsaturated modelling, the α and n values (now no more irrelevant) have been set to $9.83 m^{-1}$ and 4.93. These values have been obtained from the soil water retention curve of the sand used for the tests. All the other parameters have remained the same as described for the saturated modelling. While, the BCs and ICs inserted are listed below:

- water flow conditions:

- Upper BC: constant flux.

$$q(x = 0, t) = q$$

Where, depending on the flow rate, $q = q_{min}$, $q = q_{int}$ or $q = q_{max}$;

- lower BC: constant volumetric soil water content estimated from the desaturation of the column after the saturated test θ_0 . It has been calculated by measuring the quantity of water exited during the desaturation and the time for the water to arrive at the exit of the column after re-switching on the pump.

$$\theta(x = L, t) = \theta_0$$

The θ_0 values for the three different flow rates are respectively 26%, 27% and 28%.

- IC: constant profile of water content along the column length. Same values as the lower BCs.

$$\theta(x, t = 0) = \theta_0$$

- solute transport conditions: no needed in this step.

After having found the water content, the second iteration aimed to find the saturated hydraulic conductivity and dispersivity values. In this step the lower BC and the IC have been changed into the θ value found in the first iteration. In addition, the saturated water content value found in the saturated modelling has been set. All the other parameters have remained the same and the solute transport conditions and the breakthrough data have been added. The saturated hydraulic conductivity and longitudinal dispersivity have been selected to be estimated.

For the free-drainage modelling, the following parameters have been changed from the saturated model:

- saturated soil water content: values from the saturated modelling;
- water flow BC:
 - upper BC: constant flux.

$$q(x = 0, t) = q$$

Where, depending on the flow rate, $q = q_{min}$, $q = q_{int}$ or $q = q_{max}$;

- lower BC: free-drainage.

$$\frac{\partial q(x = L, t)}{\partial x} = 0$$

- IC: constant volumetric soil water content.

$$\theta(x, t = 0) = \theta_u$$

Where θ_u is the water content obtained from the previous unsaturated modelling.

All the other parameters considered have remained the same. The saturated hydraulic conductivity and longitudinal dispersivity have been selected to be estimated.

3.3.2 HYDRUS modelling for intermediate scale tests

At the intermediate scale, only the unsaturated free-drainage tests had to be modelled. Since no saturated test was performed before, the saturated soil water content had to be assumed. Even if the conditions are slightly different, for each flow rate, the values considered are the ones found from the small scale modelling. All the other parameters regarding the water flow and the solute

transport remained the same of the ones selected for the free-drainage tests in the small scale. Moreover, the geometry information about the column length has been changed to $L = 25 \text{ cm}$. The hydraulic conductivity and longitudinal dispersivity have been selected to be estimated.

The BCs and IC used for the modelling are listed below:

- water flow conditions:

- upper BC: constant flux.

$$q(x = 0, t) = q$$

Where, depending on the flow rate, $q = q_{min}$, $q = q_{int}$ or $q = q_{max}$;

- lower BC: free-drainage.

$$\frac{\partial q(x = L, t)}{\partial x} = 0$$

- IC: volumetric water content profile, values assumed equal to the water of the free-drainage simulation for the small scale.

$$\theta(x, t = 0) = \theta_u$$

- solute transport: it has been modelled with the same BCs and IC of the small scale.

In addition, the data inserted for the inverse solution inserted are the BTCs obtained from the tests.

3.3.3 HYDRUS modelling for lysimeter scale tests

The lysimeter tests to be modelled in HYDRUS-1D are three flow and three free-drainage tracer tests. The additional tracer tests at the maximum flow rate have been modelled as well.

For the lysimeter tests modelling, the length of the column has been set to 70 cm and four more nodes have been added at the four suction probes depths ($10, 25, 40$ and $55, \text{ cm}$). Since the characteristics of the sand are the same, the parameters α , n and l have been left the same as before.

The three flow tests have been modelled as follows:

- θ_s has been selected to be estimated;
- K_s has been selected to be estimated;
- water flow conditions:

- upper BC: constant flux.

$$q(x = 0, t) = q$$

Where, depending on the flow rate, $q = q_{min}$, $q = q_{int}$ or $q = q_{max}$;

- lower BC: free-drainage.

$$\frac{\partial q(x = L, t)}{\partial x} = 0$$

- IC: linear volumetric water content profile.

$$\theta(x, t = 0) = \theta_1 + \frac{x - x_1}{x_4 - x_1}(\theta_4 - \theta_1)$$

Where θ_1 and θ_4 are respectively the water contents measured by the first and fourth soil humidity sensors while, $x_1 = 10 \text{ cm}$ and $x_4 = 55 \text{ cm}$ are the related depths.

In addition, the data inserted for the inverse solution are the water boundary fluxes across the lysimeter's exit.

For the tracer test the saturated hydraulic conductivity and the dispersivity parameter has been set to be estimated. The other parameters have been inserted as follows:

- θ_s value obtained from the flow test;
- water flow: it has been modelled with the same BCs and IC of the water flow test explained above.
- solute transport: it has been modelled with the same BCs and IC of the small and intermediate scales.

Each solute tracer test has been modelled six time: one entering the data (BTCs) from every sampling point and other five different simulations, one for each sampling point by entering only the BTC of that point. The first simulation was performed to have a general value for K_s and α_L of the entire column, while the other five were done to have more specific values characterizing each layer of sand and then to evaluate a possible scale effect.

A last modelling has been performed for the estimation of K_s and α_L for the two extra tests (without suction probes). All the parameters have been set as the other solute tracer tests but, since there was no extraction from the suction probes, only the bottom node have been considered.

4 Results and discussion

4.1 Small scale results

The results obtained from the saturated tests in the small column are shown in figure 4.1. In the three graphs, there are represented both the data points obtained from the tests and the HYDRUS-1D fitting. At a first look, it is possible to observe that the BTC modelled by HYDRUS fits adequately the data points obtained from the experiments. This aspect is quantified by the *R-squared* value (R^2) that is the parameter for regression of observed versus fitted values. R^2 is an index, which lays between 0 and 1 and the closest to 1, the better the observed values are fitted by the modelled curve.

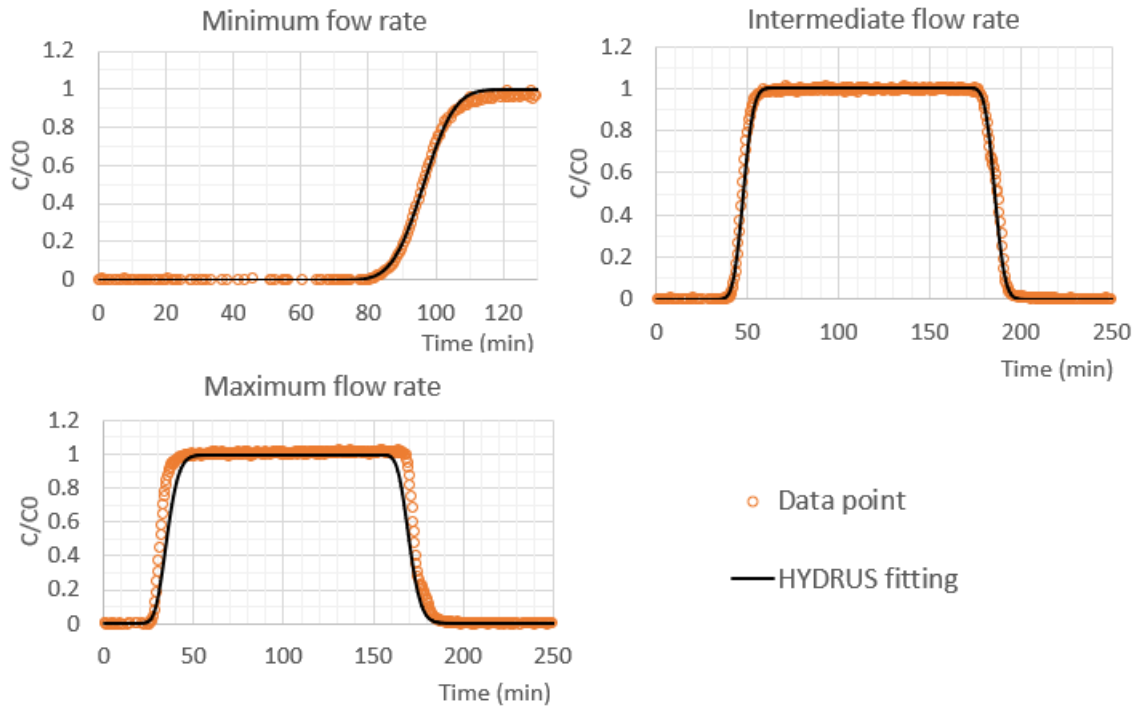


Figure 4.1. Small scale, saturated test: test data and fitting result, at the three different flow rates. Time = 0 is considered at the start of BPB injection.

By looking at figure 4.1, it is clear that, as expected, if increasing the flow rate, the arrival time of the BPB solution decreases. This aspect can be quantified by looking at the PV values (arrival time at the column exit of the advective flux):

- minimum flow rate: $\approx 96 \text{ min}$;
- intermediate flow rate: $\approx 47.5 \text{ min}$;
- maximum flow rate: $\approx 35 \text{ min}$.

A better comparison between the three flow rates can be done, by looking at figure 4.2, in which the concentration is represented as a function of the pore volume. The curves in figure represent the HYDRUS fitting curve.

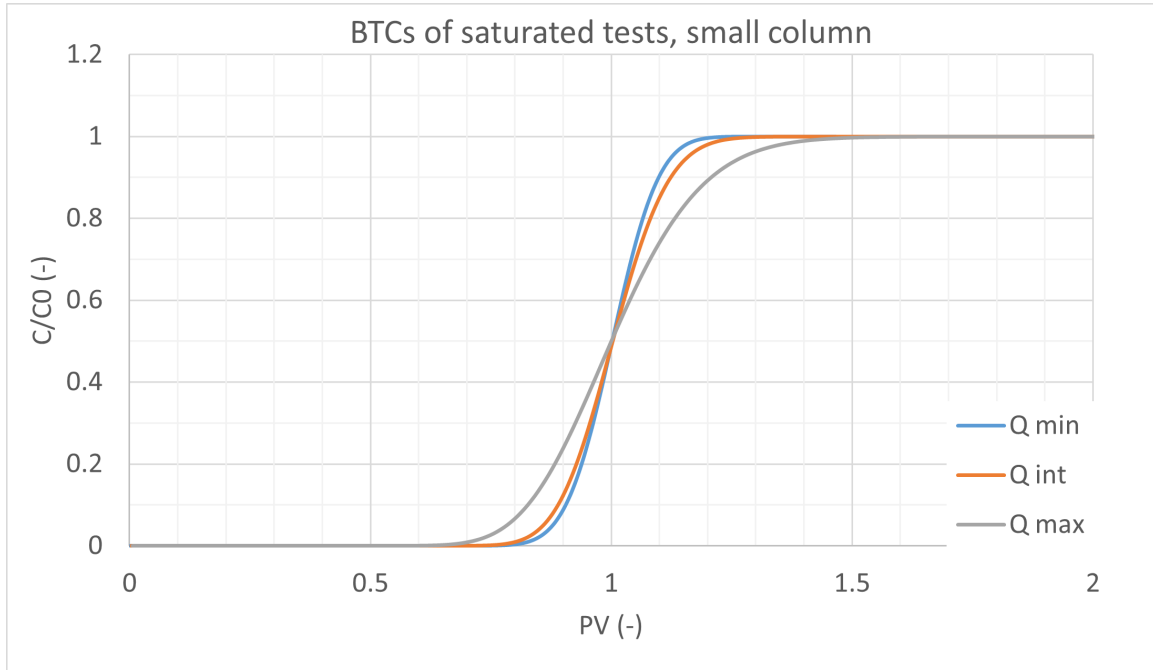


Figure 4.2. Small scale, saturated test: HYDRUS fitting curves as a function of the pore volume.

From figure 4.2, it is possible to observe that at maximum flow rate the concentration is increasing slower than at the other velocities, which means a higher dispersivity. On the other hand, for the other two curves, the shapes are very similar. For a quantitative evaluation, α and the other parameters estimated by the HYDRUS modelling are listed in table 4.1

Table 4.1. Small scale: results of HYDRUS fitting for the three saturated tracer tests, in terms of saturated water content (θ_s), longitudinal dispersivity (α_L) and R^2 .

SATURATED TRACER TEST			
	Q min	Q int	Q max
θ_s (-)	0.4847	0.4504	0.4529
α_L (m)	$6.62 \cdot 10^{-4}$	$9.79 \cdot 10^{-4}$	$2.64 \cdot 10^{-3}$
R^2 (-)	0.99915	0.99765	0.97533

From the table 4.1, it can be also observed that the dispersivity values are increasing as the flow rate increases. However, at the maximum flow rate, the fitting curve (black line) does not overlap the experimental data very well and it seems overestimating the dispersivity value. It is probably then, that the α_L value at the maximum flow rate is closer to the ones at the other velocities.

The θ_s values, representing the soil porosity are slightly different, this can be generated because the column has been unpacked and repacked every time before each test and little variations in packing can cause different porosity values, as mentioned by Bromly et al. (2007). From the R^2 value, it is possible to see that HYDRUS fits very well the observed data at the minimum and intermediate flow rate, while it is a bit lower for the maximum flow rate.

The results of the unsaturated tests (with forced bottom extraction) in small scale are displayed in figure 4.3.

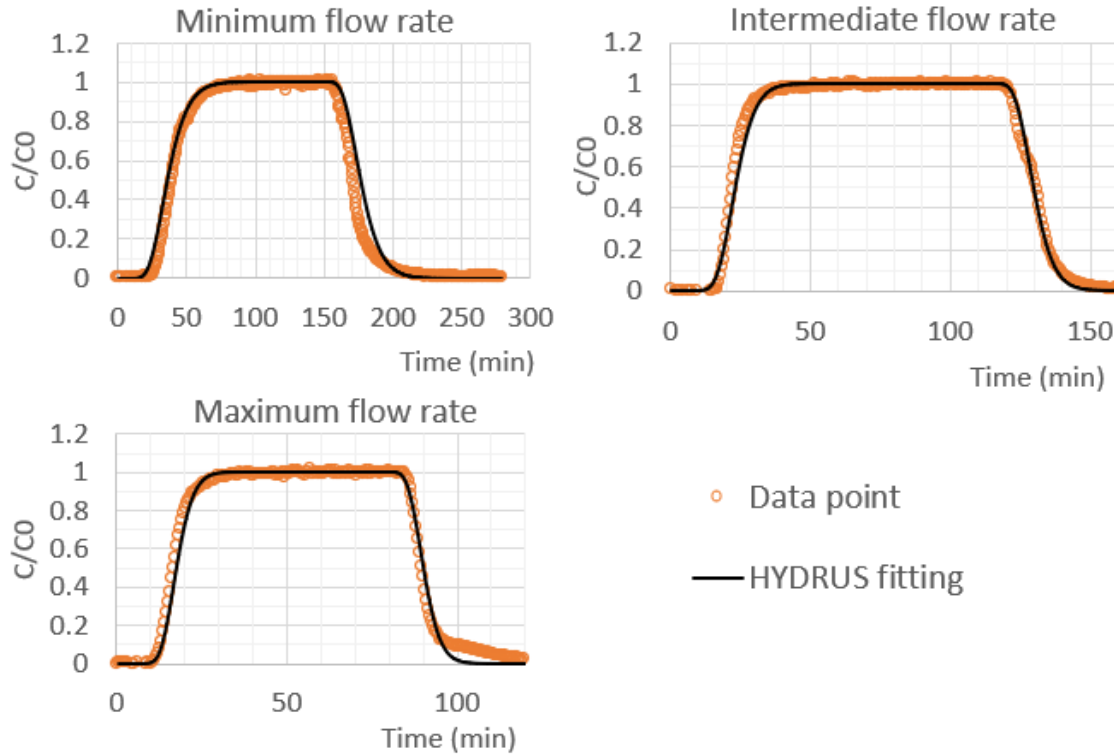


Figure 4.3. Small scale, unsaturated test: test data and fitting result, at the three different flow rates. Time = 0 is considered at the start of BPB injection.

Also from the unsaturated test results, it is possible to observe that the HYDRUS has been able to fit very well the experiment data.

The PV values of the three tests are listed here:

- minimum flow rate: $\approx 36 \text{ min}$;
- intermediate flow rate: $\approx 23.5 \text{ min}$;
- maximum flow rate: $\approx 17.5 \text{ min}$.

As it has been done for the saturated tests, in figure 4.4, the BTCs are represented as a function of the pore volume. The curves in figure represent the HYDRUS fitting curve.

In figure 4.4, it can be noticed that the intermediate and maximum flow rate are almost overlapping while, the minimum flow rate's curve is characterized by a smoother shape (higher dispersivity). This observations can be quantified in table 4.2, where there are listed all values found after the HYDRUS modelling.

The dispersivity value in this case does not follow the same trend as the saturated test: it does not increase with the increasing of the flow rate. Conversely, the water content (θ) along the column's profile increases as flow rate rises. The hydraulic conductivity average value has the same trend, as it increases with the flow rate. This value in fact, is strongly related to the water content (relation expressed in figure 2.5) and when the moisture content increases, there is an increment in hydraulic conductivity too.

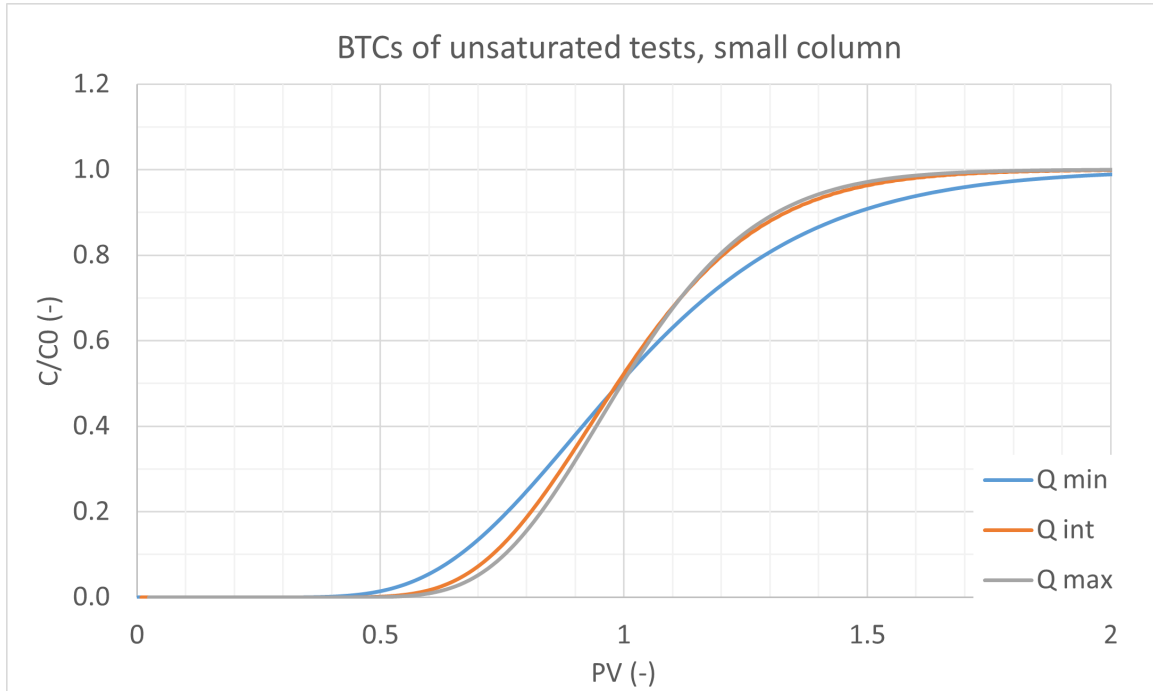


Figure 4.4. Small scale, unsaturated test (forced extraction): HYDRUS fitting curves as a function of the pore volume.

Table 4.2. Small scale: results of HYDRUS fitting for the three unsaturated tracer tests, in terms of water content (θ), saturated hydraulic conductivity (K_s), hydraulic conductivity (K), longitudinal dispersivity (α_L) and R^2 .

*Average values along the column at the end of the test.

UNSATURATED TRACER TEST			
	Q min	Q int	Q max
θ (-)*	0.187	0.225	0.230
K_s (m/s)	$7.38 \cdot 10^{-4}$	$6.25 \cdot 10^{-4}$	$7.78 \cdot 10^{-4}$
K (m/s)*	$2.5 \cdot 10^{-5}$	$3.7 \cdot 10^{-5}$	$5.4 \cdot 10^{-5}$
α_L (m)	$1.26 \cdot 10^{-2}$	$6.88 \cdot 10^{-3}$	$5.78 \cdot 10^{-3}$
R^2 (-)	0.98398	0.99615	0.9969

The last tests presented at the small scale are the ones performed in unsaturated conditions with the free-drainage exit. The result of the experiments and the HYDRUS fitting are reported in figure 4.5.

The PV values for the three tests are listed here:

- minimum flow rate: ≈ 36 min;
- intermediate flow rate: ≈ 25 min;
- maximum flow rate: ≈ 17 min.

In figure 4.6, the concentration is represented as a function of the pore volume. The curves in figure represent the HYDRUS fitting curve.

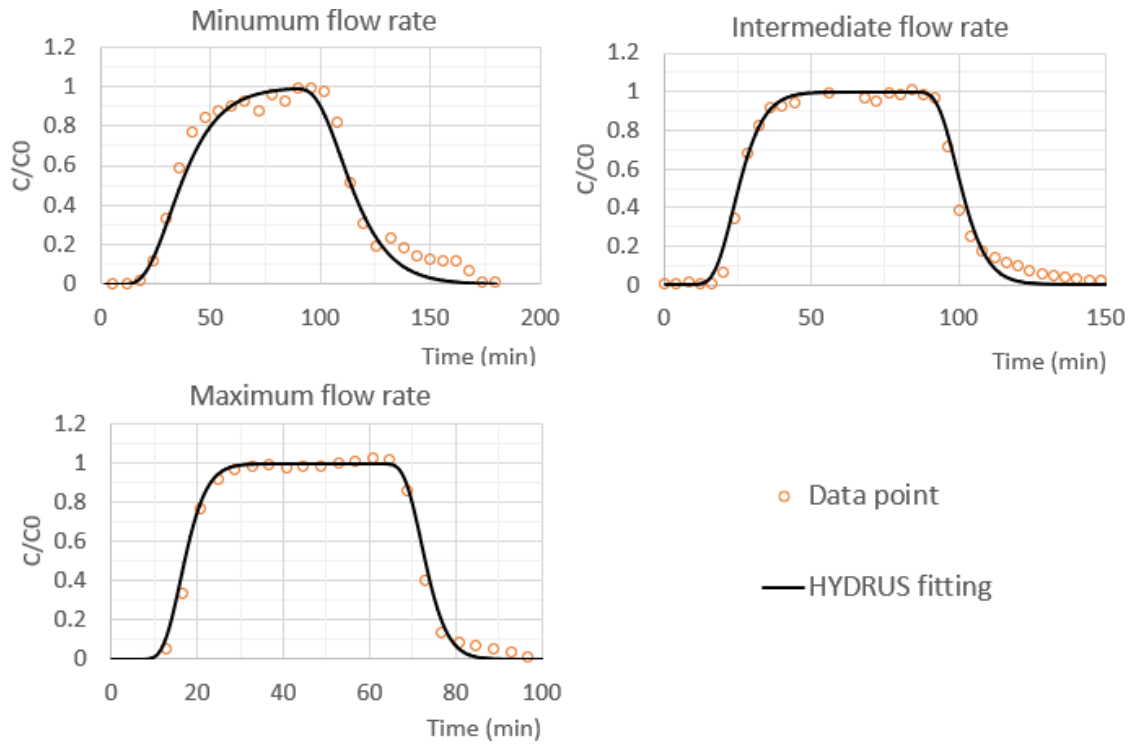


Figure 4.5. Small scale, free-drainage test: test data and fitting result, at the three different flow rates. Time = 0 is considered at the start of BPB injection.

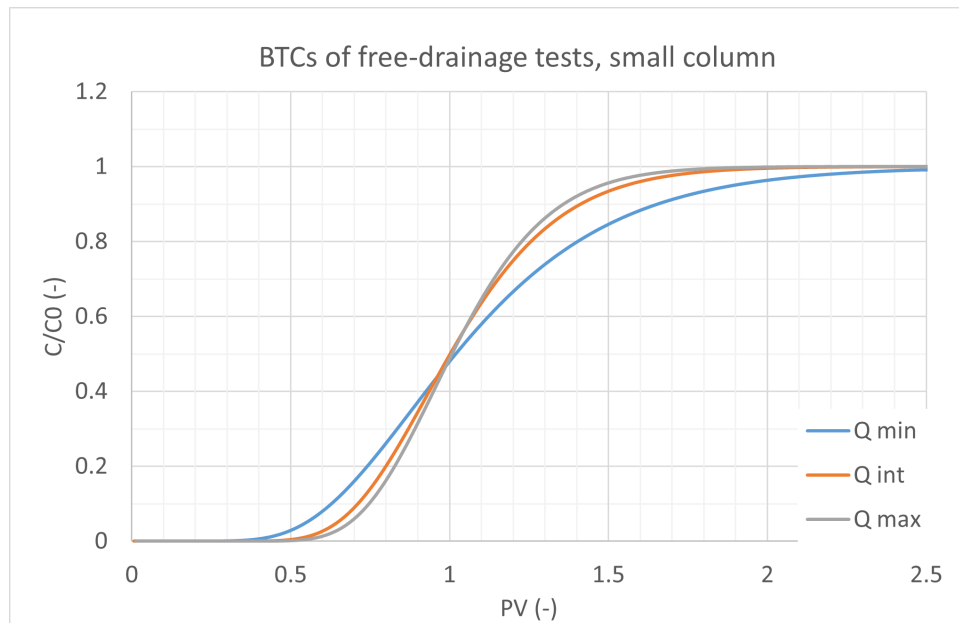


Figure 4.6. Small scale, free-drainage test: HYDRUS fitting curves as a function of the pore volume.

The results shown in figure 4.6 show a similar trend of the one observed for the other unsaturated test. At the minimum flow rate, the dispersivity value seems to be higher, while at the intermediate

and maximum velocities the two curves are almost overlapping. A quantification of the dispersivity values and the other parameters estimated from the HYDRUS fitting are listed in table 4.3.

Table 4.3. *Small scale: results of HYDRUS fitting for the three unsaturated free-drainage tracer tests, in terms of water content (θ), saturated hydraulic conductivity (K_s), hydraulic conductivity (K), longitudinal dispersivity (α_L) and R^2 .*

**Average values along the column at the end of the test.*

FREE DRAINAGE TRACER TEST			
	Q min	Q int	Q max
θ (-)*	0.196	0.245	0.227
K_s (m/s)	$6.41 \cdot 10^{-4}$	$4.53 \cdot 10^{-4}$	$1.38 \cdot 10^{-4}$
K (m/s)*	$2.00 \cdot 10^{-5}$	$4.5 \cdot 10^{-5}$	$5.1 \cdot 10^{-5}$
α_L (m)	$1.93 \cdot 10^{-2}$	$9.99 \cdot 10^{-3}$	$9.24 \cdot 10^{-3}$
R^2 (-)	0.97783	0.98640	0.99008

Also in the free-drainage test the R^2 values are above 0.97, hence the HYDRUS fitting can be considered acceptable. This can be also visible by observing the graphs in figure 4.5, the black line follows very well the experimental points. In this case, the water content does not follow the same trend as the previous results. The θ value at the intermediate flow rate is slightly higher than the one at maximum flow rate. This could have happened because the column was unpacked and repacked after every cycle of tests and so the sand's grains were not compacted in the same way for the two tests. On the other hand, the hydraulic conductivity of the tests is increasing with the flow rate increment, as presented in the previous results.

A more detailed comparison between the result previously presented can be done by plotting in the same graph (figure 4.7) the BTCs of saturated, unsaturated with forced extraction and unsaturated with free drainage test, all at the same flow rate. Since not all the tests have the same duration, only the first part has been considered.

By looking at figure 4.7, it can be easily noticed that at each flow rate, the slowest curve is the saturated one. This is a reasonable result because, in unsaturated conditions, the pathways for the water to flow are less in number and consequently the section is smaller. It can be observed also that the forced extraction and the free-drainage unsaturated tests have very similar curves. At the maximum flow rate the two lines are overlapping while at minimum and intermediate flow rates, the C/C_0 starts to increase at almost the same time but free-drainage tests have a higher dispersivity which brings the C/C_0 to arrive at the value 1 slower. This observation can be quantified also by looking at the tables 4.2 and 4.3, at every flow rate considered, the dispersivity is very similar, but slightly higher in the free-drainage tests.

It is interesting to compare the results obtained from the tests at the small scale with the ones obtained by Latrille (2013). In that research, it was highlighted the dependency of the dispersivity value on the effective velocity and the water content. In fact, it demonstrated that the dispersivity values are increasing as the pore velocity increases, with a linear dependency. In the same way, it is shown that the dispersivity value and the water content are inversely correlated, with an exponential law. In figure 4.8 and 4.9, the α_L values found by the HYDRUS modelling are plotted respectively as a function of the effective velocity ($v_e = q/\theta$) and of the water content.

The results obtained from this work are very similar to the ones of the study carried out by Latrille (2013). In figure 4.8, it is very clear increase of α_L as the velocity increases. In addition, the slope of the linear interpolation increases as the flow rate increases, as obtained from Latrille (2013). In

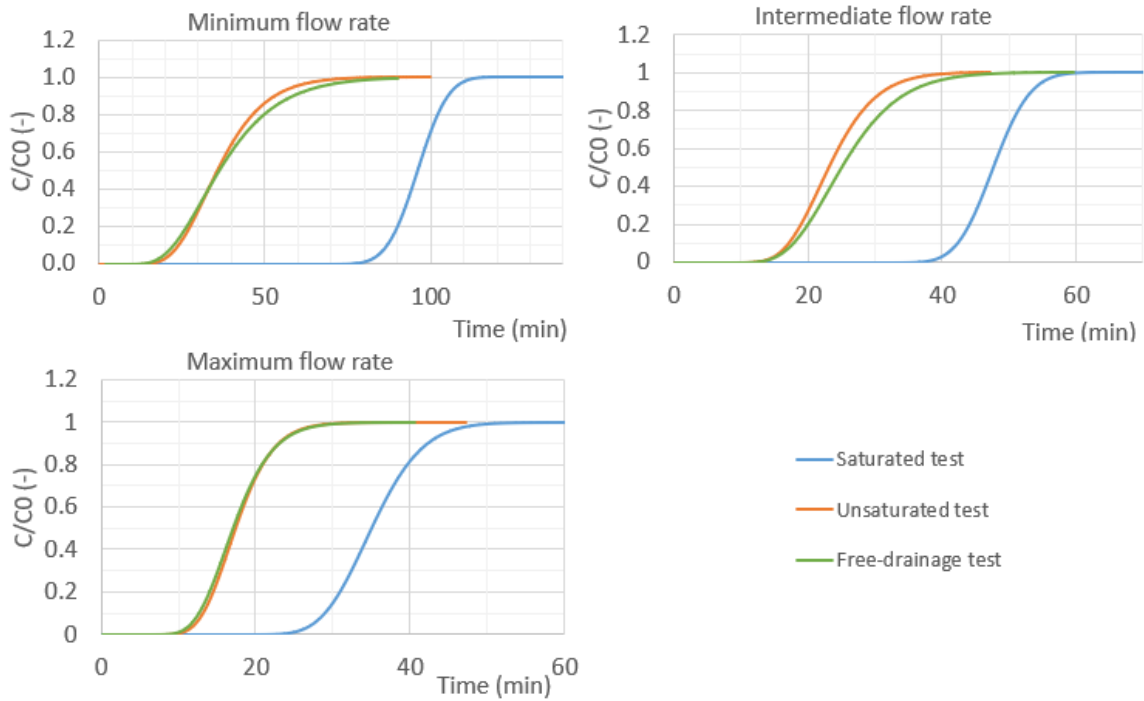


Figure 4.7. Small scale: BTCs comparison from HYDRUS fitting at the three different flow rates. In each graph the saturated, unsaturated and free-drainage results at the same flow rate are displayed. Time = 0 is considered at the start of BPB injection.

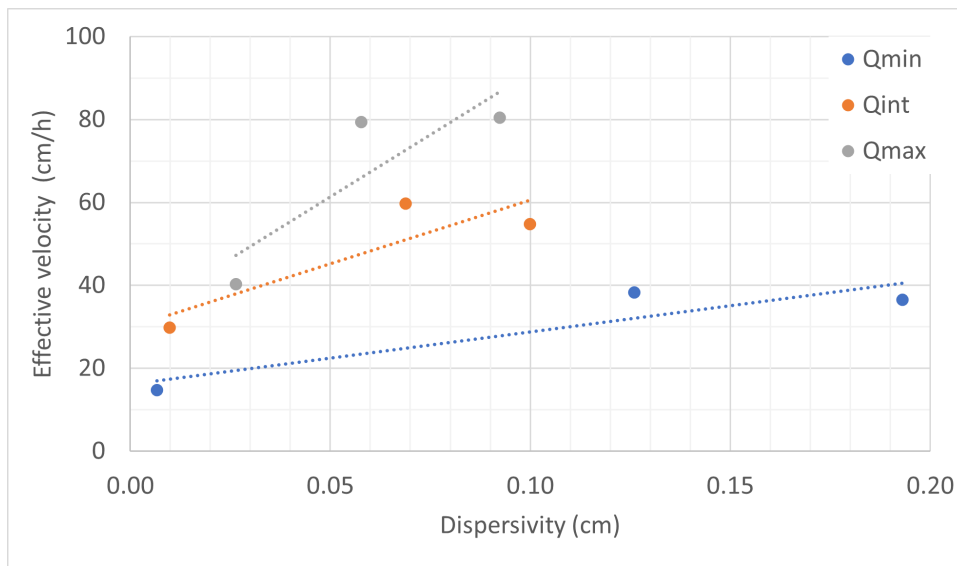


Figure 4.8. Small scale: experimental data and linear interpolations of dispersivity as a function of the effective velocity, at minimum (blue), intermediate (orange) and maximum (grey) flow rate.

figure 4.8, it is also very clear the the inverse correlation between the dispersivity and the water content. In this case, it is less clear if the interpolation curve is exponential, as mentioned by Latrille (2013). The points obtained in this thesis are very few in number, further studies should be undertaken in order to confirm and to quantify these two relationships.

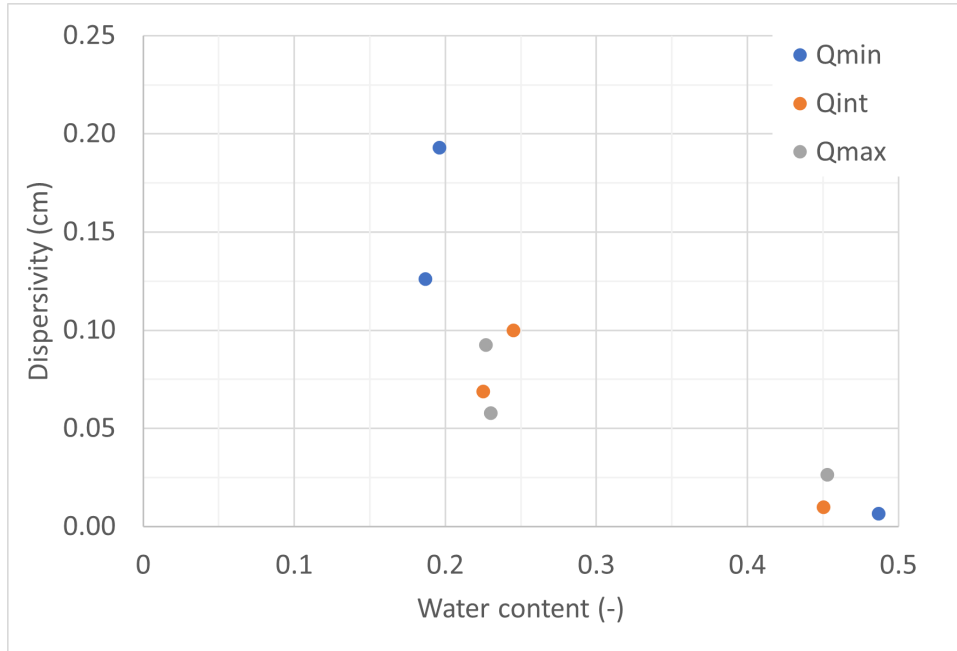


Figure 4.9. Small scale: experimental data of dispersivity as a function of the water content, at minimum (blue), intermediate (orange) and maximum (grey) flow rate.

4.2 Intermediate scale results

For the intermediate scale, the results presented are regarding the free-drainage unsaturated tests at the three flow rates. In addition, the data of the three tensiometers are presented here. From the tensiometer values and by using the soil retention water curve, theoretically it should be possible to have an estimation of the soil water content around the tensiometer depths. As already presented in the previous section, in this scale and at these depths, during the wetting curve the tensiometer does not follow always the same path (scanning curves) and therefore, there is no certain one-to-one correlation between the tensiometer's data and the water content. Therefore, the water contents presented in this section are the ones estimated by the HYDRUS modelling and not estimated by the tensiometers.

The BTCs (experimental data points and HYDRUS fitting) are shown in figure 4.10.

From the graphs in figure 4.10, it is possible to see that the shape of the curves are very similar to the ones already presented in the small scale section. As expected, by comparing the arrival times of the advective fronts (PV values), it is clear that if increasing the flow rate, the time for the solute to pass throughout the column decreases. The PVs of the three tests are:

- minimum flow rate: $\approx 78 \text{ min}$;
- intermediate flow rate: $\approx 36.5 \text{ min}$;
- maximum flow rate: $\approx 30.5 \text{ min}$.

Also in this case, it can be noticed that HYDRUS is fitting very well the experimental curves. For a better comparison of the three tests, in figure 4.11, the concentrations are represented as a function of the pore volume. In figure 4.11, the three curve's shapes are very similar, it can be noticed a

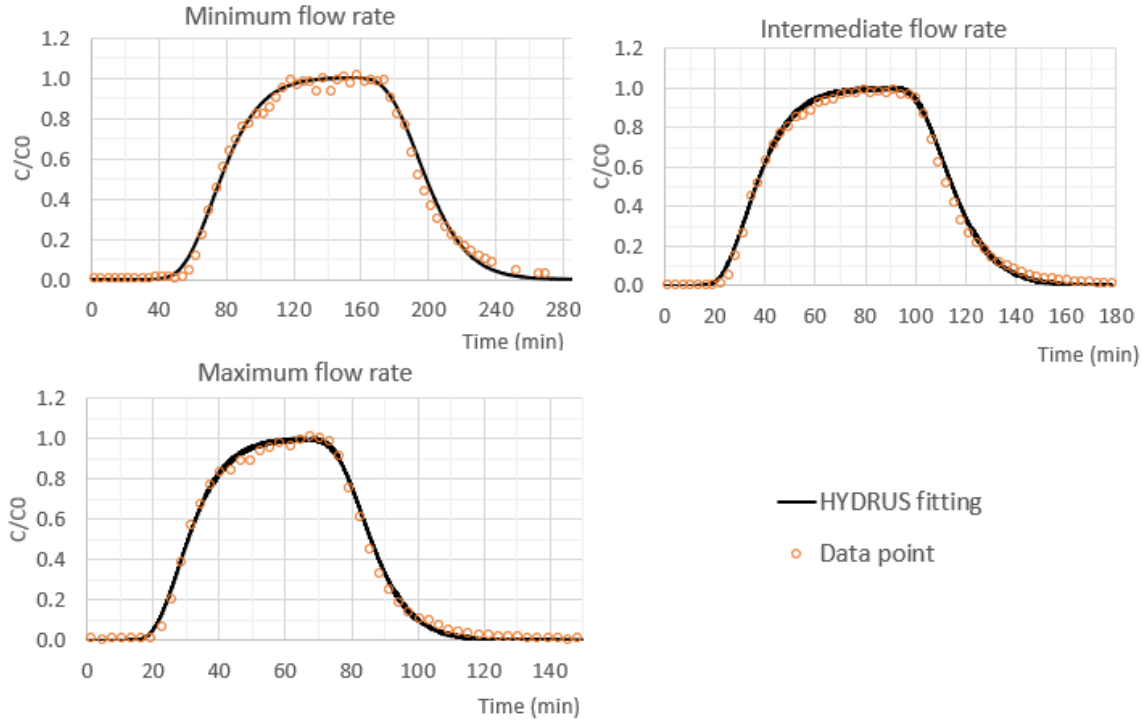


Figure 4.10. Intermediate scale, unsaturated free-drainage test: test data and fitting result, at the three different flow rates. Time = 0 is considered at the start of BPB injection.

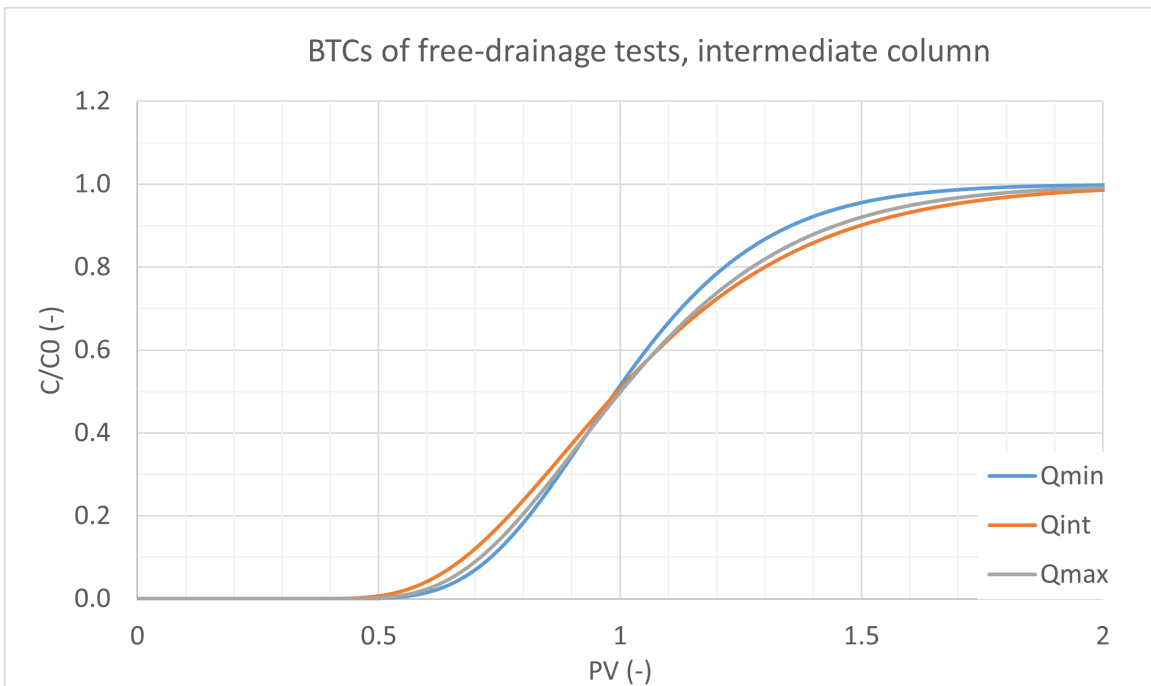


Figure 4.11. Intermediate scale, free-drainage test: HYDRUS fitting curves as a function of the pore volume.

very little difference for the minimum flow rate, where the dispersivity seems to be slightly lower.

In table 4.4, all the parameter estimated by the HYDRUS modelling are reported.

Table 4.4. *Intermediate scale: results of HYDRUS fitting for the three unsaturated free-drainage tracer tests, in terms of water content (θ), saturated hydraulic conductivity (K_s), hydraulic conductivity (K), longitudinal dispersivity (α_L) and R^2 .*

**Average values along the column at the end of the test.*

FREE DRAINAGE TRACER TEST			
	Q min	Q int	Q max
θ (-)*	0.28	0.30	0.32
K_s (m/s)	$7.89 \cdot 10^{-5}$	$1.69 \cdot 10^{-4}$	$1.94 \cdot 10^{-4}$
K (m/s)*	$1.6 \cdot 10^{-5}$	$3.3 \cdot 10^{-5}$	$4.3 \cdot 10^{-5}$
α_L (m)	$8.03 \cdot 10^{-3}$	$1.42 \cdot 10^{-2}$	$1.15 \cdot 10^{-2}$
R^2 (-)	0.9949	0.9964	0.9960

As it is possible to observe from the table 4.4, the hydraulic conductivity increases with the increment of the water content. This result is in line with the theory presented in the second chapter. The dispersivity values for the intermediate and maximum flow rate are very similar, while the same value for the minimum flow rate is smaller. In this case, it has to be kept in mind that the saturated and the initial water content have been hypothesized equal to the values obtained for the small scale. These hypotheses could have influenced the results obtained from the HYDRUS modelling. Therefore, small differences between the parameters at different scales, such as α_L , can be considered negligible. Although, the R^2 parameter is very high (> 0.99) for all the three tests.

In figure 4.12, the tensiometer's data of the three intermediate column's tests are shown, moreover the data of an additional test are presented. This test was supposed to be an unsaturated test, but the column exit was smaller than the one used for the other experiments and during the test, an increase of the water content inside the column has been visually detected. Therefore, this can be considered a failed test but here the results are reported for a comparison with the other experiments in which the water content has been approximately remained constant.

Even if it not possible to find exactly the water content from the tensiometers' data, it is possible to draw some conclusion from figure 4.12. First of all, it can be noticed that, a part little exceptions, the tension read by each tensiometer remains almost the same during the whole test. The exception is given by the second tensiometer which, at the end of the intermediate test, presents a sudden increase of the pressure read. It is likely that, at the beginning of the test, the porous cup had not the right contact with the sand. In fact, the values of the second tensiometer are expected to be in between the first and the second ones. Probably with the water passing through, the right contact between the device and the porous medium has been restored again, which have caused this sudden increase of the values at the end of the test.

However, all the other values are almost constant during each test, which can be considered a sign of the fact that the water content did not change so much during each test. On the other hand, during the failed test, it can be noticed an increase of the tensions inducted by water content increment, which has been also visually noted during the experiment. In conclusion, from these data it can be deduced that during the three tests, the stationary state had been reached and the water content did not undergo noticeable changes.

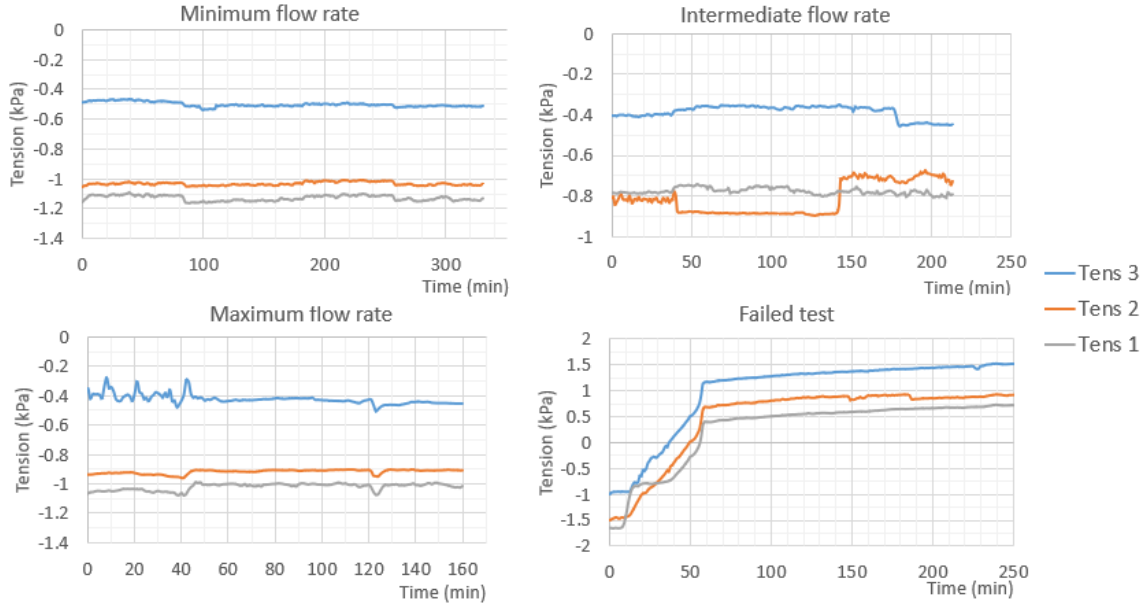


Figure 4.12. Intermediate scale, unsaturated free-drainage test: tensiometers data + the failed test. Tensiometers depths: tens1: 10cm; tens2: 15cm; tens3: 20cm.

4.3 Lysimeter results

4.3.1 Flow tests

The lysimeter test results will be presented starting from the flow tests. In figure 4.13, there is shown the water content for the three different flow rates measured by the four sensors at a depth of 10, 25, 40 and 55 cm. All the representations start from 2 hours before the tap water injection and they end 24 hours after the end of the injection. By doing this, it is possible to observe the wetting and the drying phases of the column. In the graphs the injection start is at time 0 hours and the end is at 5 hours.

From figure 4.13, it can be observed how quickly the water content increases within the column, while after stopping the water injection the moisture content takes much longer to return at the initial levels. In 24 hours of free-drainage after the injection, only with the minimum flow rate the water content returns to the level before the test. While for the intermediate and maximum flow rate, even after 24 hours the water content is still higher than the initial level. It can be also observed for the intermediate flow rate, that the θ value before the water injection is equal to zero at all the depths, while the initial value for the other two tests is higher than zero. This happened because the intermediate flow test has been the first one to be performed. The lysimeter was completely dried out, it has not been used for weeks before that test, while for the other tests the lysimeter could drainage the water only for at maximum two or three days. Moreover, at the intermediate and maximum flow rates, it is very clear the profile of the water content along the column depth. In fact, for these two tests, the water content increases the value from the top to the bottom, where it is possible to find the higher values. The first sensor is always the driest one, it goes to zero before and after the test very quickly in all the experiments. At the minimum flow rate, the sensor 4 reads lower values than the third one and so the profile is not so clear as for the other tests. Probably this can be caused by the very small flow rate which does not allow the water accumulation in the

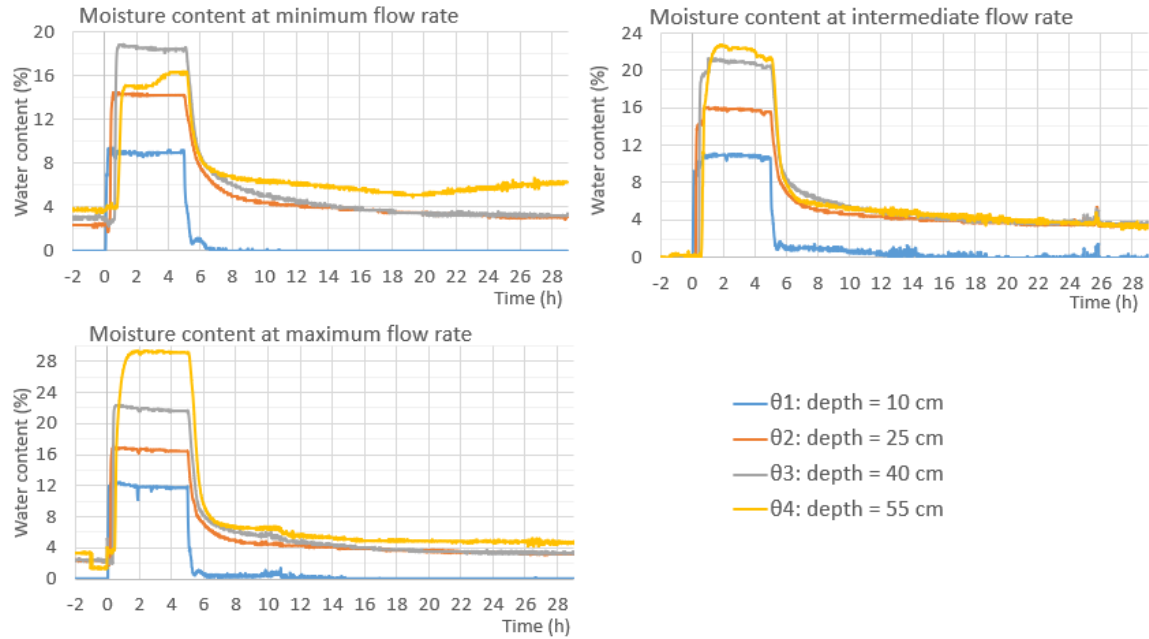


Figure 4.13. Lysimeter scale, flow test: water content data from the four sensors. Injection start at time = 0 hours; injection end at time = 5 hours.

bottom layer. In addition, if looking specifically to the θ_4 curve of the minimum flow rate test, a strange behaviour can be observed: after arriving at a certain plateau, the water content increases a bit until arriving to a second plateau which is approximately 1% higher than the first one. This phenomenon happened for other tests at the same sensor, regardless the flow rate and without any evident motivation, see water content during the tracers test in Appendix B (figures B.1, B.2 and B.3). The reason behind this behaviour is not clear, at a first sight it could be thought that it happens because the suction probe extraction stops at a certain time with a consequent increase of the water content but this "anomaly" happened also in some the tracer test in which the suction probe extraction was continuously controlled and no changes in that sense have been detected.

For an for a more quantitative evaluation, the average water content values during the tap water injection are reported in table 4.5.

Table 4.5. Lysimeter scale: average water content $\theta(-)$ read by the four sensors, during the tap water injection.

	θ_1 : depth = 10 cm	θ_2 : depth = 25 cm	θ_3 : depth = 40 cm	θ_4 : depth = 55 cm
Q min	0.088	0.142	0.185	0.155
Q int	0.108	0.158	0.207	0.222
Q max	0.119	0.166	0.219	0.292

From the table 4.5, it is even more clear the profile of increasing water content along the column for the intermediate and maximum tests. From the table, another interesting observation can be done: at each depth, the water content raises as the flow rate increases.

The results of the HYDRUS modelling of the flow test is reported in table 4.6. Since the column has not been unpacked and repacked again after each test, the saturated water content should be the same for each test. In table 4.6, it is possible to observe that the three values are slightly

Table 4.6. *Lysimeter scale, flow tests: results of HYDRUS estimation of the parameters θ_s and K_s .*

	Q min	Q int	Q max
$\theta_s (-)$	0.49	0.52	0.51
$K_s (m/s)$	$3.871 \cdot 10^{-4}$	$7.381 \cdot 10^{-4}$	$8.081 \cdot 10^{-4}$
$R^2 (-)$	0.9784	0.9615	0.9719

different but they are very similar, the differences can be caused by experimental and fitting errors. Therefore, for the lysimeter column, the θ_s value has been considered to be an average of the three values (≈ 0.505). It can be noticed that this value is a bit higher than the ones estimated in the small column (0.45 – 0.48). This is probably caused by the different methods used for packing the column. In fact, the small column was repetitively shaken while packing it, while, because of the dimension and the weight, the lysimeter was simply filled with sand without shaking it. This difference has probably resulted in a less compaction of the sand within the lysimeter vessel.

From the data in table 4.6, it can be also noted that, as for the other scales, K_s is increasing as the water flow rate increases. On the other hand, the R^2 values are slightly lower than the ones in the other tests, but they can still be considered acceptable.

4.3.2 Tracer tests

The results of the tracer tests are presented in terms of BTCs of both the experimental data and the HYDRUS fitted data. For each test, the BTCs of the five different depths are illustrated. It is important to remember that the first four sampling ports are extracting water with suction cups through a vacuum system, while the last sampling depth is placed at the column exit. In each graph, the time zero is the time in which the BPB injection starts.

In figure 4.14, the BTCs related to the minimum flow rate are displayed.

From figure 4.14, as expected, it can be observed that the BPB solution arrives at the different depths at consecutive times. The curves from 1 to 4 have a similar trend while, the fifth one has a smoother shape, it does not increase (and decrease) as quick as the others.

The PV of each depth, calculated from the experimental data of is listed below here:

- 1: $\approx 39 \text{ min}$;
- 2: $\approx 55 \text{ min}$;
- 3: $\approx 66 \text{ min}$;
- 4: $\approx 80 \text{ min}$;
- 5: $\approx 110 \text{ min}$.

In figure 4.15, the results of the tracer test at the intermediate flow rate are shown.

In figure 4.15, it can be found almost the same trend as for the minimum flow rate. The curves 2, 3 and 4 have a very similar shape and they start to increase one after the other based on the suction cup's depth. While, as it happened at the minimum flow rate, the fifth curve is characterized by a

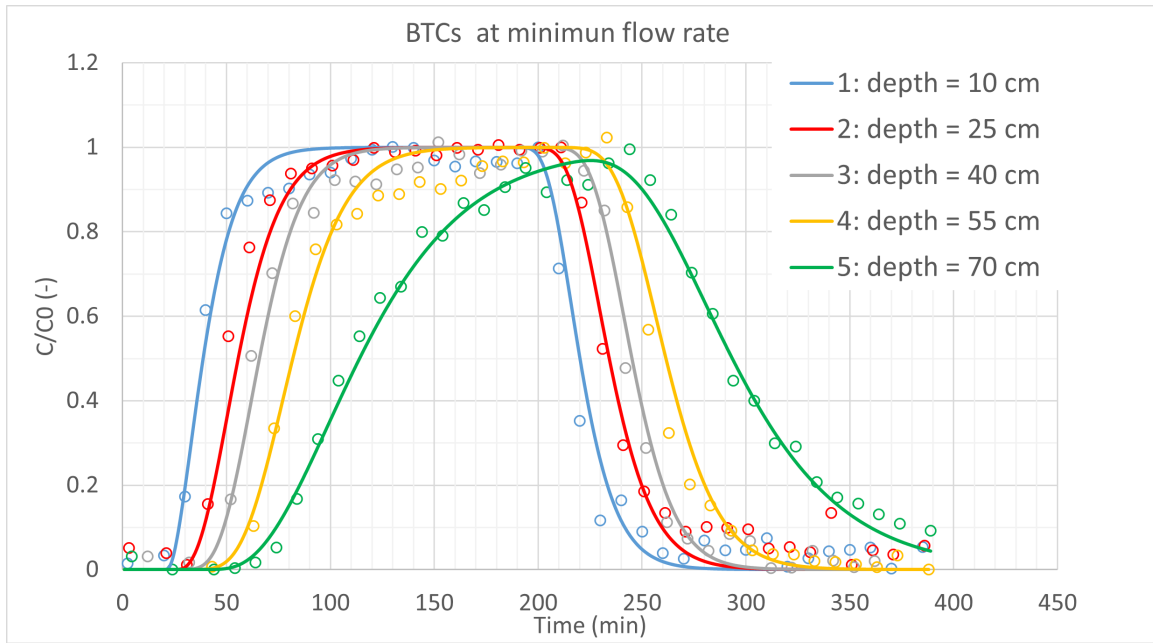


Figure 4.14. Lysimeter scale, tracer test at minimum flow rate. BTCs at the five different depths.

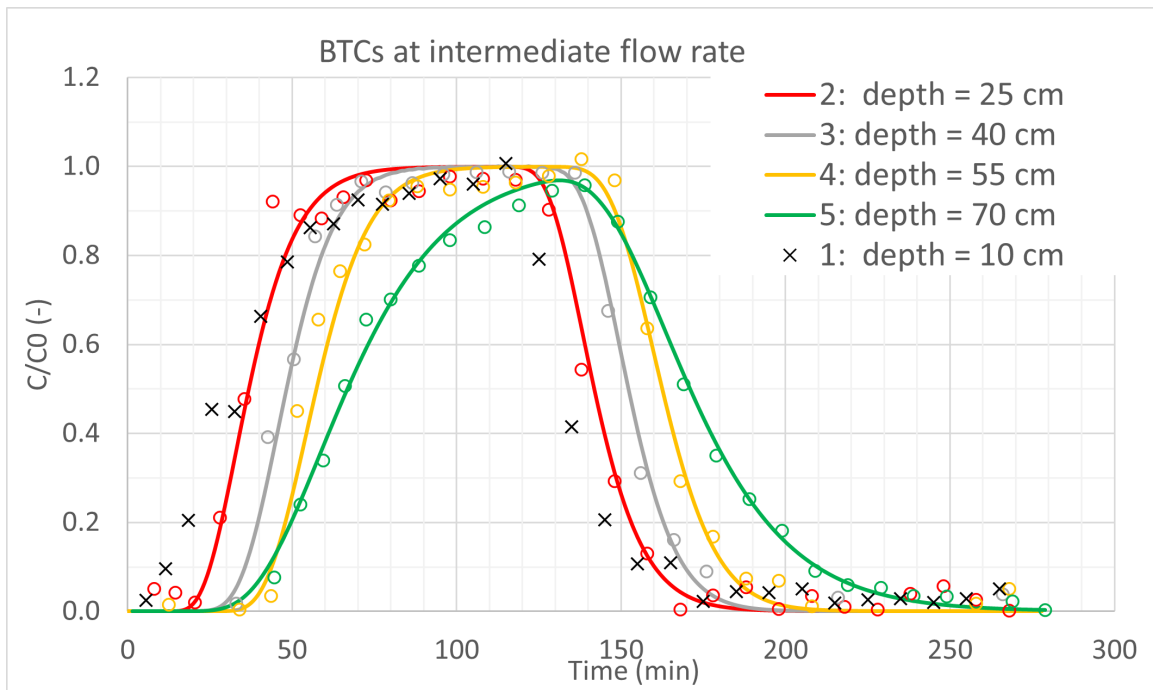


Figure 4.15. Lysimeter scale, tracer test at the intermediate flow rate. BTCs at the five different depths.

smoother shape, both in the first and in the second part of the graph. The experimental data of the depths 2, 3, 4 and 5 are very well fitted by the HYDRUS models, while something different happened for the first one. The curve 1 has an unexpected shape, it increases very slowly until arriving at the value $C/C_0 = 1$ at the very end of the BPB injection. Since it refers to the shallowest suction probe, it was expected to be the first one to arrive at the C_0 concentration. A confirmation of the unusual

behaviour is that HYDRUS was not able to fit the curve if fitted with the same procedure of the other ports. To try to explain this behaviour, some explanation can be hypothesized. First of all, it is the shallowest suction probe, only 10 cm below the soil surface, probably the incoming flow is not able to homogenize in such a short distance. If this is the reason of the "anomaly", the 1D version of HYDRUS is not enough for fitting those points, while a 2D or even 3D model would be more appropriate for this case. But the 1D modelling of the same depth at the other flow rates, had been possible, so probably this is not the only explanation to this behaviour. A second possible reason of these results could be more practical, in fact, the first suction probe is the one which extracts less water from the soil ($\approx 1 \text{ ml/min}$) and the bottle in which the extraction is temporary stored had a volume of 1 l . It can have cause a sort of dilution every time a sampling was performed, in fact not all the content of the cup could be withdrawn during the sampling but some drops always remained inside the bottle and in such a little solute volume, these drops cannot be considered negligible and they are affecting the following samples. In addition, the intermediate flow rate test was the first to be performed and for the next ones the first suction cup has been changed with a 250 ml one in order to minimize this dilution effect. As a proof that this was probably the main reason behind the anomaly, the results of the minimum and maximum flow rates (in which the bottle was changed) do not present this behaviour (see figures 4.15, 4.16).

The PV of each depth, calculated from the experimental data are the following:

- 1: $\approx 35 \text{ min}$;
- 2: $\approx 37 \text{ min}$;
- 3: $\approx 46 \text{ min}$;
- 4: $\approx 55 \text{ min}$;
- 5: $\approx 66 \text{ min}$.

The results of the tracer test at the maximum flow rate are displayed in figure 4.16.

The results in figure 4.16 show a very similar trend for curves 2, 3 and 4, and, as it happened also in the other flow rates, the fifth one is smoother than the others and this time the first one increases faster. At this flow rate, HYDRUS fits very well all the BTCs.

The PVs are the following:

- 1: $\approx 11 \text{ min}$;
- 2: $\approx 29 \text{ min}$;
- 3: $\approx 33 \text{ min}$;
- 4: $\approx 45 \text{ min}$;
- 5: $\approx 60 \text{ min}$.

The parameter α_L estimated by the HYDRUS modelling, for each depth and for the different flow rates, is presented in table 4.7.

From the table 4.7, it is possible to draw some interesting conclusions. With only three exceptions, at the depths from 1 to 4, the dispersivity value lays between 1 and 2 cm. One of the exceptions is

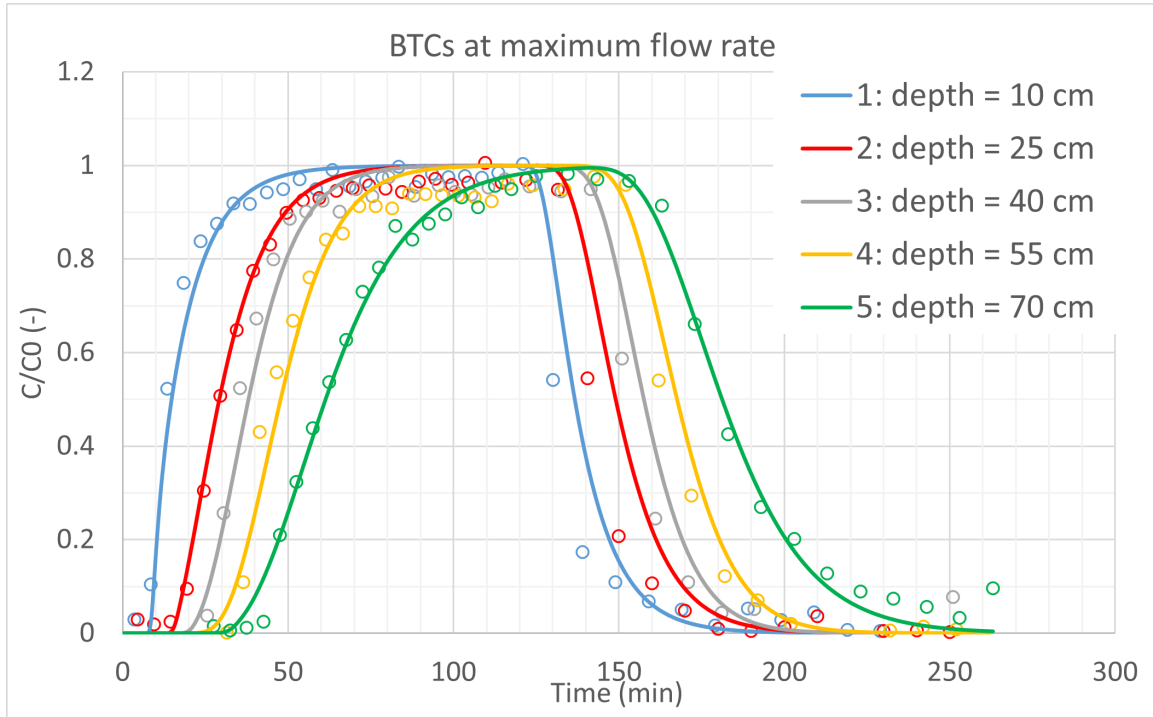


Figure 4.16. Lysimeter scale, tracer test at maximum flow rate. BTCs at the five different depths.

Table 4.7. Lysimeter scale, tracer tests: results of HYDRUS estimation of α_L .

** : the value did not converge.

	Minimum flow rate				
	Depth 1	Depth 2	Depth 3	Depth 4	Depth 5
$\alpha_L (m)$	$6.04 \cdot 10^{-3}$	$1.17 \cdot 10^{-2}$	$1.24 \cdot 10^{-2}$	$1.71 \cdot 10^{-2}$	$4.99 \cdot 10^{-2}$
$R^2 (-)$	0.99	0.99	0.99	0.99	0.99
	Intermediate flow rate				
	Depth 1	Depth 2	Depth 3	Depth 4	Depth 5
$\alpha_L (m)$	**	$1.34 \cdot 10^{-2}$	$1.18 \cdot 10^{-2}$	$1.41 \cdot 10^{-2}$	$4.91 \cdot 10^{-2}$
$R^2 (-)$	**	0.99	0.99	0.98	0.99
	Maximum flow rate				
	Depth 1	Depth 2	Depth 3	Depth 4	Depth 5
$\alpha_L (m)$	$1.88 \cdot 10^{-2}$	$2.33 \cdot 10^{-2}$	$1.55 \cdot 10^{-2}$	$1.30 \cdot 10^{-2}$	$4.05 \cdot 10^{-2}$
$R^2 (-)$	0.99	0.98	0.99	0.99	0.99

the first depth at the minimum flow, in which $\alpha_L = 0.6 \text{ cm}$. This anomaly can be caused by the fact that in such a short flow path the water/solute probably does not reach an homogeneous condition within the section and if this happens, the 1D model is probably not enough for this depth but a 2D or 3D version of HYDRUS should be used. The other exception is the second depth at the maximum flow rate, here the difference is less noticeable, the dispersivity value is in fact 2.33 cm which is slightly above the others. Probably, this has been caused by practical experimental errors caused for example by dilution during the sampling procedure.

A separate discussion deserves the last sampling depth: the column exit. Here, in all the flow rates, the dispersivity value lays between 4 and 5 cm, approximately 2/3 times the same value at the

other depths. This can be caused by different reasons. Firstly, as already presented in previous chapters, the flow path length can affect the dispersivity, it increases as the length increases. But the difference with the dispersivity at the fourth depth seems to be too pronounced. In fact, the two sampling depths are only 15 cm away each other and between the depths 2, 3 and 4 this difference does not exist, even if they are respectively at 25, 40 and 55 cm below the soil surface. The reason of the difference of the fifth depth then, has to be also re-conducted to other causes. The column exit is the only one with a different sampling method, in the suction cups 1, 2, 3 and 4, the water/solution is extracted by the suction probes while in the last one the samples are collected manually at the exit of the column. Probably, the small tank placed right below the column exit is too little for the sampling frequency used. In fact, the solution exiting the column sometimes filled the tank in a shorter period than the sampling frequency and the exceeding solute was automatically poured into the bigger tank in which the small one was placed. The consequence of this can be that the samples at the exit of the column are not referring to the average concentration during a time between two consecutive samplings, but they represent the average of only the first part of that time frame. Another possible explanation can be that, since the exit hole of vessel is a third of the lysimeter section, water/solute may accumulate in that part and it can cause a sort of dilution within the column before the liquid exits. The reasons behind this behaviour are investigated in the second extra test, whose results will be discussed.

The water content data of the tests have also been retrieved from the data logger. The average water content value at the plateau for each depth is expressed in table 4.8. As it is possible to observe, the values are very similar to the ones found during the flow tests (table 4.5). This similarity is due to the fact that the conditions are basically the same for the flow and tracer tests. For the same reason, the graphs of the water content are very similar to the ones represented in figure 4.13, they are reported in Appendix B (see figures B.1, B.2 and B.3).

Table 4.8. *Lysimeter scale: average water content θ (–) read by the four sensors, during the BPB solution injection.*

	θ_1 : depth = 10 cm	θ_2 : depth = 25 cm	θ_3 : depth = 40 cm	θ_4 : depth = 55 cm
Q min	0.088	0.141	0.183	0.156
Q int	0.108	0.156	0.204	0.202
Q max	0.117	0.162	0.215	0.277

The results of the extra test performed to understand if the suction probes influence the solute transport and water flow are displayed in figure 4.17.

From figure 4.17, it is possible to see that the shape of the curves do not change between the two tests, the only difference is that without suction from the four probes, the water arrives at column bottom slightly quicker. This test has been modelled in HYDRUS too, and the resulting values of α_L and K_s are the following:

- $\alpha_L = 4.13 \text{ cm}$ compared to 4.05 with the suction probes;
- $K_s = 9.08 \cdot 10^{-4} \text{ m/s}$ compared to $6.81 \cdot 10^{-4} \text{ m/s}$;

Also the PV of the two curves can be compared. With the suction probe the PV was around 60 minutes, while without the suction probes extraction this value drops to approximately 57 minutes. The increase in velocity happens because of the water content increase, which is around 1/2% higher in the test without suction probes extraction. The graphs of the water content during the extra test can be found in Appendix B (see figure B.4).

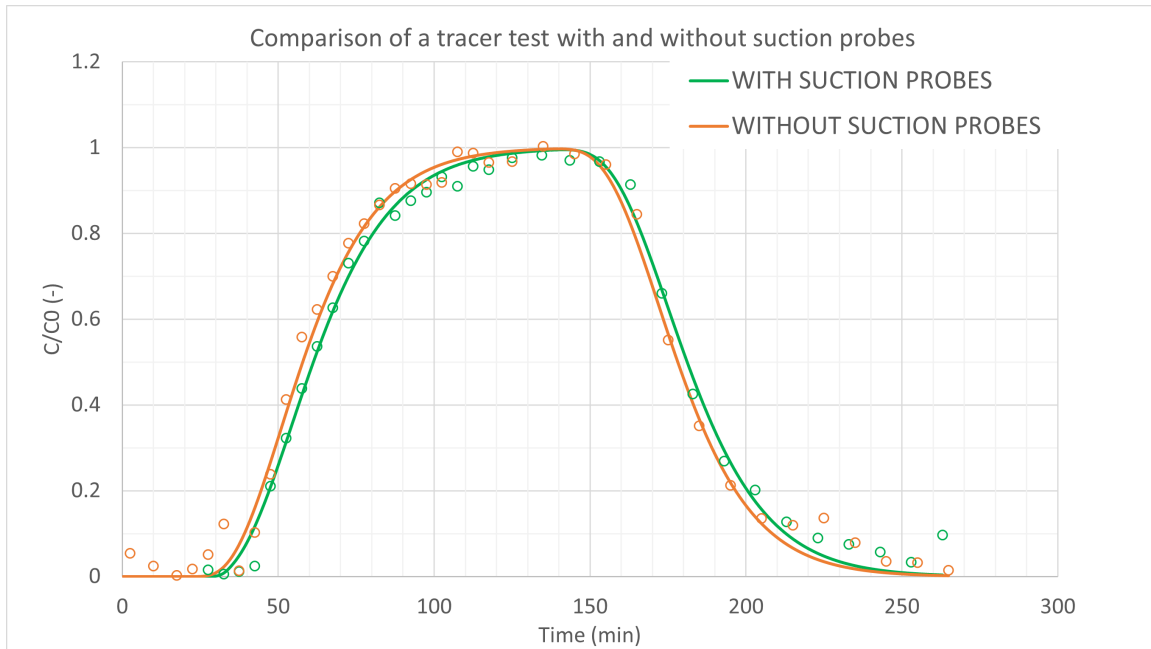


Figure 4.17. *Lysimeter scale, maximum flow rate tracer test without suction probe's extraction compared with the same test with the suction probes activated.*

From this numbers and from the graphs, it can be concluded that the extraction with the suction probes does not influence sensibly the dispersivity value but they play a not negligible role in terms of water content and water velocity, as they slow down the advective front approximately of 5% and their extraction cause a decrease of the water content of 1/2%.

Other data retrieved from the data logger are the soil-water tension measured by the four tensiometers. For each tensiometer, the data of an entire week have been plotted in the same graph. Each week includes two tests: flow and tracer tests (with the same flow rate). It has been chosen to plot the data of an entire week in order to make an evaluation of two cycles of wetting and drying. For each tensiometer, its data have been plotted vs the water content retrieved at the same depth. As already presented in the previous chapters, the graph *soil-water tensions vs water content* represents the soil water retention curve, which is a specific characteristic of each soil. The graphs obtained from the minimum, intermediate and maximum flow rate are displayed respectively in figure 4.18, 4.19 and 4.20.

From the figures 4.18, 4.19 and 4.20, it is possible to observe the tension changes as a function of the water content. The first observation that can be done by looking at the graphs is that the wetting and drying phases do not overlap. This is because of the hysteretic trend of $\psi(\theta)$, already addressed in the second chapter. At all the flow rates, each tensiometer has a curve which approximately has the same shape. The first depth data are very irregular and the wetting and drying curves are very distant from each other. In the second depth data, the two curves are closer to each other and they are more regular that the first one. The third and the fourth depth have similar shapes, probably the closest one to a hysteresis. At the intermediate flow rate, the fourth tensiometer's cycles seem shifted along the x axis. This probably happened because the first tests to be performed have been the intermediate ones and since the lysimeter was completely dried out before these tests, it is possible that at the beginning there was not the perfect contact between the sand and the porous cup, which could have generated this discrepancy. With the water passing through, it is possible

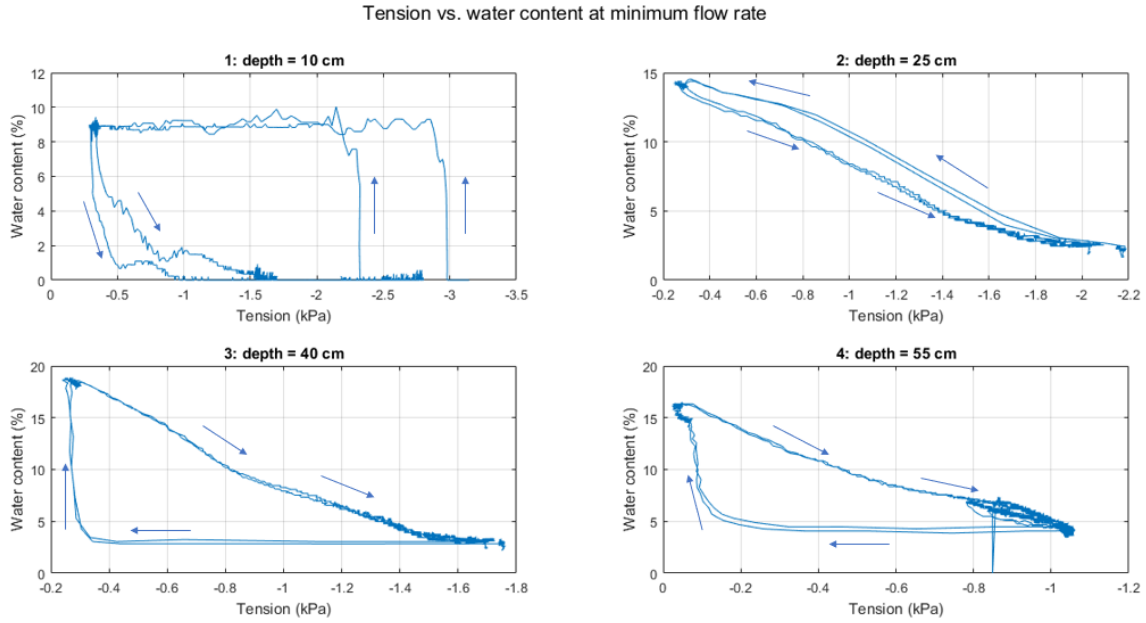


Figure 4.18. *Lysimeter scale, water content vs soil water tension data from two cycles of wetting + drying at the minimum flow rate.*

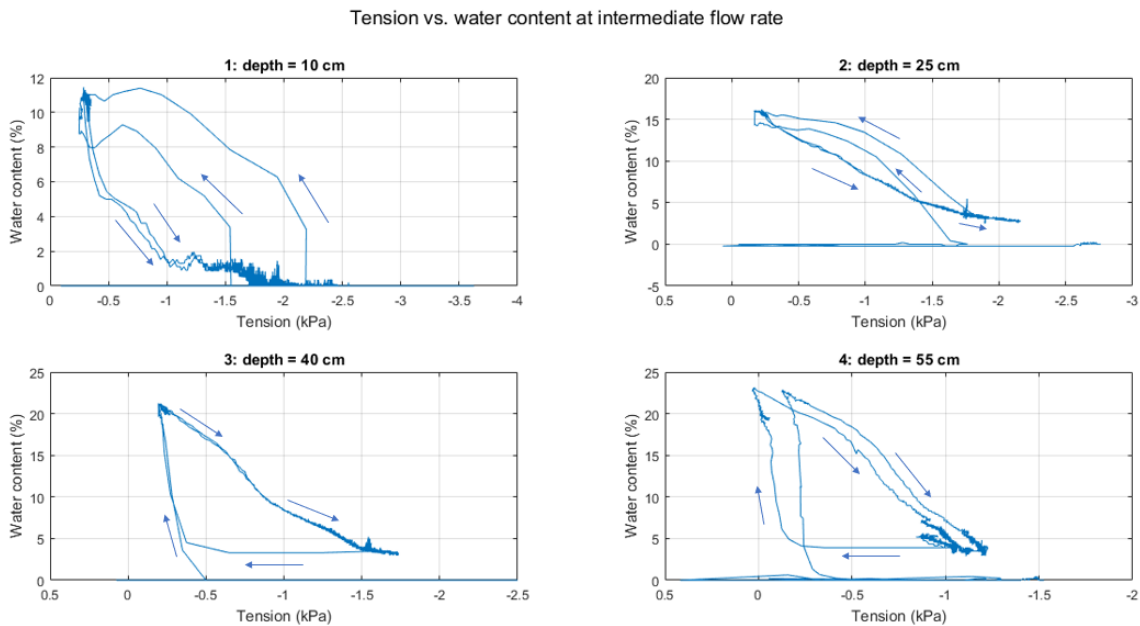


Figure 4.19. *Lysimeter scale, water content vs soil water tension data from two cycles of wetting + drying at the intermediate flow rate.*

that the sand and the tensiometer restored the right contact and therefore the device was measuring the right values again. In fact, if looking at the Appendix C (figure C.1) where all the tensiometer's data are plotted together, there is only this cycle which is shifted.

It should be noted also that at the first two depths, the wetting + drying cycles are turning counterclockwise, while at the two deepest levels the cycles are clockwise. By comparing the results

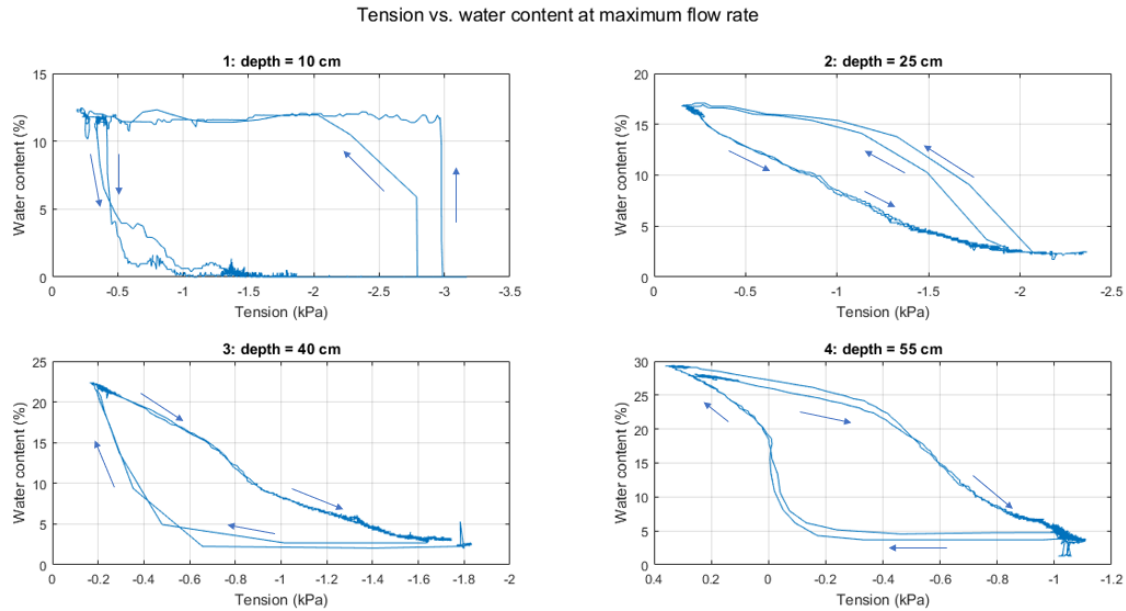


Figure 4.20. Lysimeter scale, water content vs soil water tension data from two cycles of wetting + drying at the maximum flow rate.

obtained with the ones in literature, it can be stated that the "anomalous" behaviour is the one of the first two tensiometers. Lehmann et al. (1998) clearly present that in sand, at equal soil water content, tensions are higher (considering the absolute value) during the drying phase, as it happens at the tensiometers 3 and 4. However, no explanation was found about the behaviour of the tensions at the first two depths.

The reasons why the first two curves have a different behaviour have been in part investigated with the second extra test. In this test, performed at maximum flow rate, the tensiometers 2 and 3 have been swapped to exclude a possible malfunctioning of the sensors. The results, compared with the ones previously presented in figure 4.20, are shown in figure 4.21.

From figure 4.21, it is possible to notice that the trend of the tensiometers 1 and 4 remained unaltered. The first tensiometer follows the counterclockwise movement while, the fourth one has a clockwise trend. The data of tensiometer at the second depth present a similar trend of the ones reported in figure 4.18, 4.18 and 4.18, placed at the same depth: its wetting + drying cycle is counterclockwise. Some discrepancies are visible in the wetting curve, but they are most probably caused by different starting water content (the soil water contents of the test are reported in Appendix B, see figure B.5).

The third tensiometer, which in the other tests was measuring at the second depth, has a strange behaviour. During the wetting, the curve differs noticeably from the one of the previous tests while, in the drying phase it overlaps perfectly the other curve. This phenomenon probably happened because, after the tensiometer exchange, this tensiometer may not have been perfectly in contact with the sand and therefore, the values read can be altered. With the water passing through and the increasing water content, probably the sand rearranged around the tensiometer and created the right contact again and that could be the reason why the drying phase coincides with the other drying lines.

From these considerations, it can be deduced that there was no problem in the tensiometers and

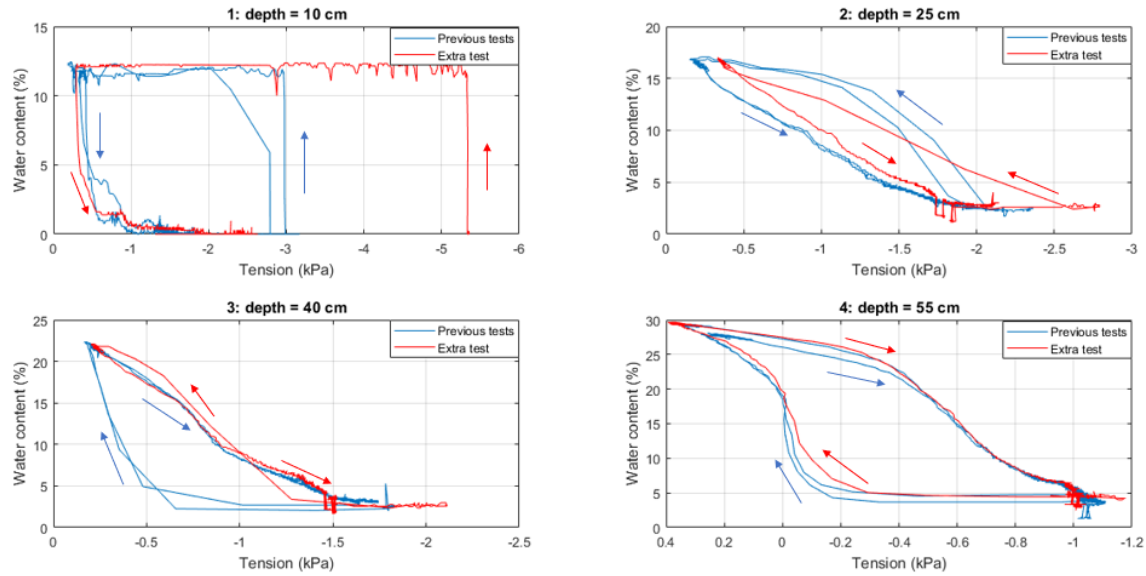


Figure 4.21. Tensiometers' data vs water content of the second extra test, compared to the ones obtained previously.

that the inversion of the cycle direction between the second and the third depth really occurs. In other words, from the data obtained from all the tests, it seems that the correlation between $\psi(\theta)$ is strongly dependent on the depth. The different trends of the first and the second two tensiometers can probably be explained with the fact that in the shallowest depth the flux is not fully homogenized within the section and somewhere between 25 and 40 cm it homogenizes. In order to evaluate the correctness of this hypothesis, further studies should be performed with different flow rates and by studying the data with a 2D or even 3D model. If this phenomenon is confirmed, also the data of the small and intermediate columns should be revised.

For a general overview of the soil-water tensions, in Appendix C (figure C.1), all the tensions vs. water content data are plotted together. These data are referring to all the water flow and tracer tests performed, hence six cycles of wetting and drying are displayed for each depth.

The second extra test has been also carried out to understand if the sampling technique had an influence on the dispersivity value. As expressed before, only the exit of the column has been sampled. The resulting BTC and the HYDRUS fitting are displayed in figure 4.22.

In figure 4.22, the two curves are very similar, they are almost overlapping but, if looking more in detail, it can be seen a very slightly discrepancy in the first part of the curve. This difference can be quantified with the result of the HYDRUS model, which estimates a longitudinal dispersivity of 3.53 cm ($R^2 = 0.99$). The previous dispersivity value was slightly higher (4.05 cm). From this data, it can be stated that with this sampling method the dispersivity value is lightly reduced, but the value is still higher than expected, it is more than twice of the dispersivities at the other depths. Therefore, from these considerations, it can be deduced that probably this anomalous dispersivity value at the end of the column is due to the dilution occurring at the bottom of the lysimeter. The column's exit is probably too little (10 cm of diameter) in comparison with the lysimeter's section.



Figure 4.22. Lysimeter scale, maximum flow rate tracer tests with the two different sampling methods. Sampling depth: column's exit (70 cm).

4.4 Comparison between scales

A comparison between the scales can be firstly done by analysing the set up and the practical conditions of the three columns.

In terms of dimensions, the small column is 24 cm long and the intermediate one is 25 cm, as well the second suction probe of the lysimeter (the one considered for the comparison) is 25 cm below the soil surface. The three diameters are respectively 1.6, 10 and 30 cm, which gives a length to diameter ratio (L/D) of 15, 2.5 and 0.8.

Another aspect to consider is the pumping rate, as explained in the previous chapters, it has been chosen in order to have the same velocity in terms of specific discharge q . In practice, the limits of the pump resulted in values not exactly the same for all the scales. The real q values used for tests are expressed in table 4.9.

Table 4.9. Values of specific discharge rate for each scale, at the three different flow rates.

	Specific discharge rate (m/s)		
	<i>Small scale</i>	<i>Intermediate scale</i>	<i>Lysimeter</i>
Q min	$1.99 \cdot 10^{-5}$	$1.71 \cdot 10^{-5}$	$2.01 \cdot 10^{-5}$
Q int	$3.73 \cdot 10^{-5}$	$3.46 \cdot 10^{-5}$	$3.54 \cdot 10^{-5}$
Q max	$5.07 \cdot 10^{-5}$	$4.31 \cdot 10^{-5}$	$4.32 \cdot 10^{-5}$

The breakthrough curves obtained from the HYDRUS fitting at different scales are represented in figure 4.23 as a function of the PV. Since the duration of injection was not the same the results are reported only in terms of first part of the curve: from $C/C_0 = 0$ to $C/C_0 = 1$.

From the graphs in figure 4.23, it is possible to evaluate qualitatively the dispersion of the tracer tests performed at the different scales. As already addressed in the second chapter, this value influences

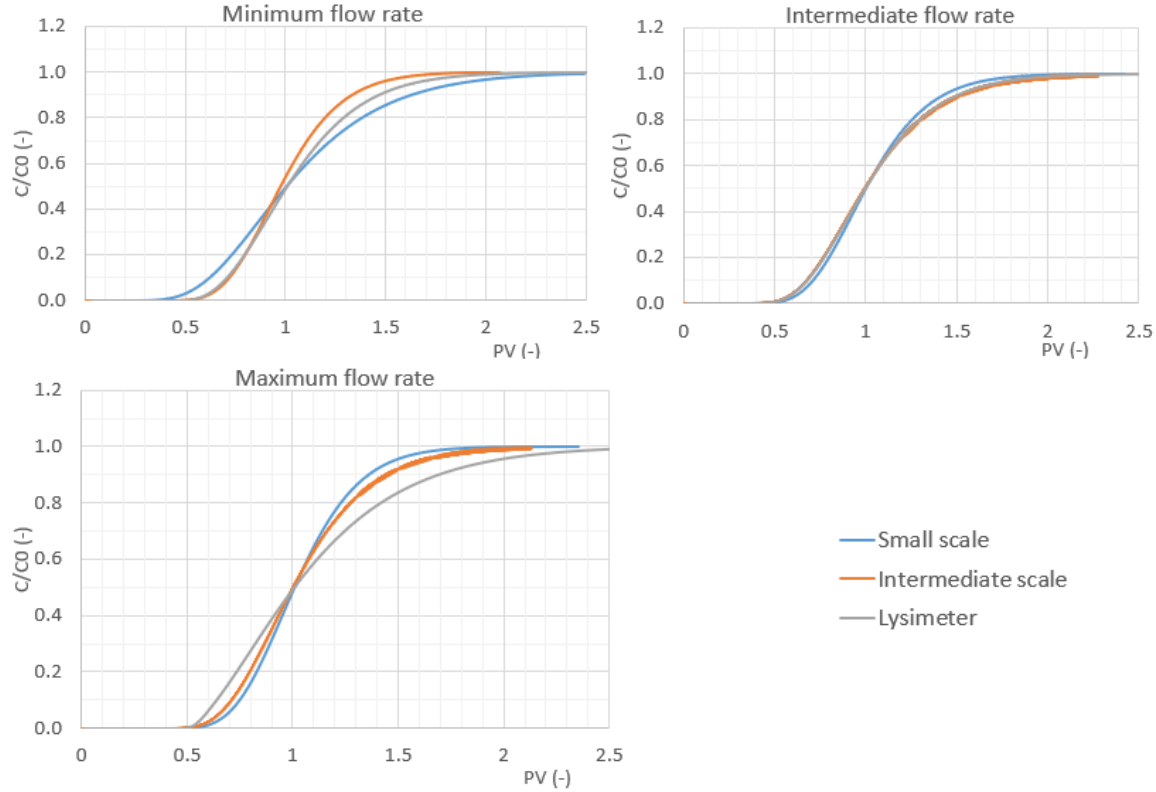


Figure 4.23. Comparison of tracer tests at the three different scales. Tests at minimum, intermediate and maximum flow rate. Lysimeter’s value referring to the second depth (25 cm).

the shape of a BTC, when the dispersivity increases the increase of C/C_0 is slower, resulting in a smoother shape of the curve. At the minimum flow rate, the curve characterized by the lower dispersivity seems to be the intermediate’s one, while the higher dispersivity can be observed at the small scale. In fact, the intermediate curve increases quicker than the others, while the small scale one is the smoothest. If analysing the intermediate flow rate, the three curves are almost overlapping, which means that they have very similar dispersivity values. At the maximum flow rate, the small scale seems to have the lower dispersivity followed by the intermediate scale and lastly by the lysimeter.

It is possible to quantify the considerations made above by looking at the dispersivity values estimated by HYDRUS-1D. Even if already reported, the dispersivity values of the test are listed all together, for a better comparison, in table 4.10. The lysimeter’s dispersivity presented in the table refers to the one estimated at the second depth, 25 cm.

Table 4.10. Values of specific discharge rate for each scale, at the three different flow rates. Lysimeter’s value referring to the second depth (25 cm).

	$\alpha_L (m)$		
	<i>Small scale</i>	<i>Intermediate scale</i>	<i>Lysimeter</i>
Q min	$1.93 \cdot 10^{-2}$	$8.03 \cdot 10^{-3}$	$1.17 \cdot 10^{-2}$
Q int	$9.99 \cdot 10^{-3}$	$1.42 \cdot 10^{-2}$	$1.34 \cdot 10^{-2}$
Q max	$9.24 \cdot 10^{-3}$	$1.15 \cdot 10^{-2}$	$2.33 \cdot 10^{-2}$

By looking at the values, it is possible to confirm and quantify the observations made before. At the minimum flow rate, the small scale and lysimeter values are very similar, while at the intermediate scale it is lower. At the intermediate flow rate, the α_L value in the small column is a bit lower than the other two, while the intermediate scale and the lysimeter present a very similar dispersivity, as already observed from the curves' overlap. As already hypothesised from figure 4.23, at the maximum flow rate, the dispersivity is increasing as the scale increases. It should be noted though, that the lysimeter dispersivity value (2.33 cm) at the maximum flow rate, represents an "outlier" between the values at the other depths of the same test. This outlier can be reconducted to errors in the sampling which caused dilution in the suction cup, as already explained in the previous chapter as a practical problem. Therefore, if taking an average α_L value of the first and third depths ($\approx 1.7 \cdot 10^{-2} m$), instead of the second one, it is closer to the one obtained at the intermediate scale. From this analysis, it is possible to conclude that the dispersivity is very similar if looking at the intermediate scale and the lysimeter, while in the small scale the dispersivity is slightly different, even though the values are comparable.

To understand better the relationship between the dispersivity and the scale, other observations can be done. Since some authors refer to the scale's influence on the dispersivity values in terms column length, while others in terms of D/L ratio, both the considerations have been done. In figure 4.24 and 4.25, it is possible to observe respectively the values of the dispersivity plotted as a function of the column's length and the L/D ratio of all the free-drainage tests performed.

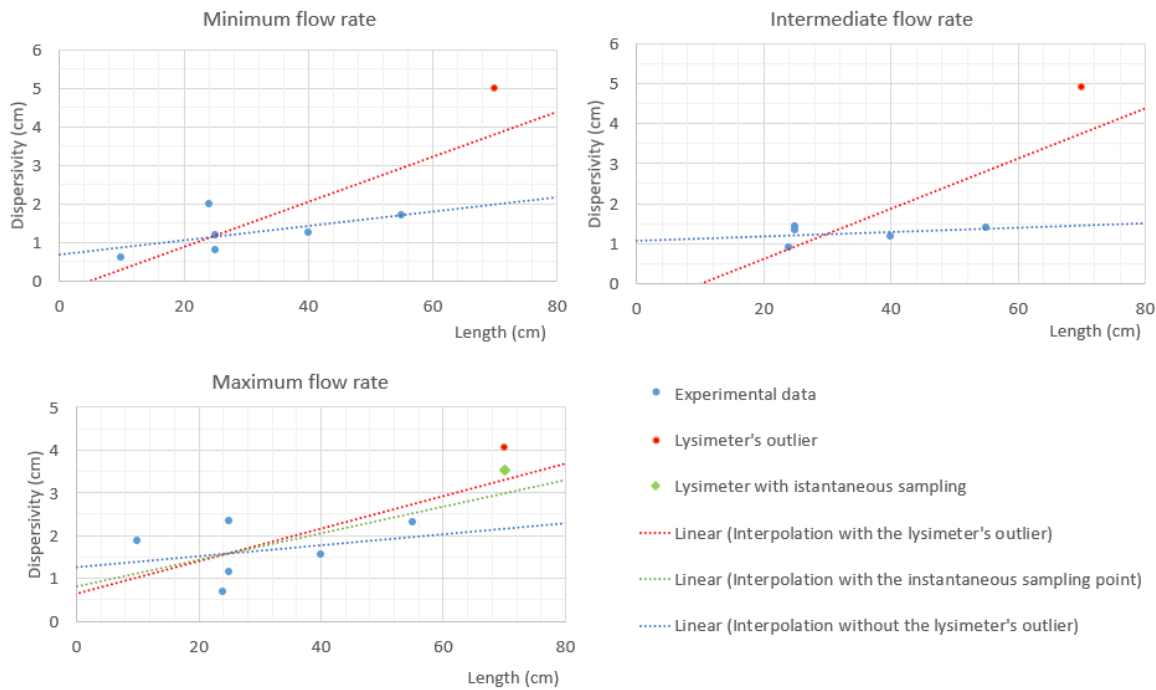


Figure 4.24. Experimental data of dispersivity as a function of the column's length. In red the outlier referred to the lysimeter's bottom.

In figure 4.24, especially at the minimum and the maximum flow rate, it can be observed an increasing trend of the dispersivity as a function of the length. Excluding the red dot and the green square, representing the lysimeter bottom exit in which the dispersivity is probably increased by a dilution effect at the bottom of the column, all the other points have very similar values of dispersivity, but it is possible to see a very slightly trend of dispersivity rising as the length

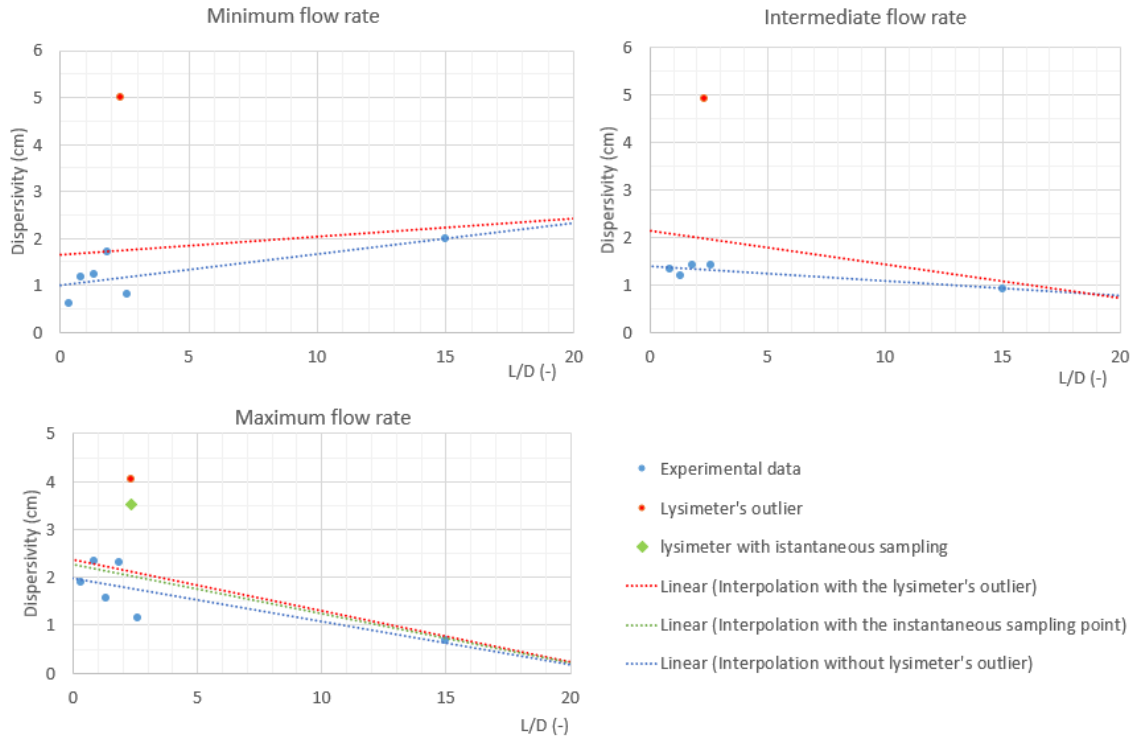


Figure 4.25. Experimental data of dispersivity as a function of the column's length to diameter ratio (D/L). In red the outlier referred to the lysimeter's bottom.

increases. It is also very clear if looking the trend lines. The red line, which includes the outlier, has an exaggerated increase, but also the blue line (without outlier) is increasing at all the flow rates. However, the experimental points are very few to draw reliable conclusions, but it can be said that these results seem to be in agreement with the ones published by Bromly et al. (2007), who states that even in laboratory columns it is possible to observe a small effect of the column's length on dispersivity.

From figure 4.25, it is possible to observe the influence of the L/D ratio on the dispersivity. At all the three flow rates, it is possible to see a cluster in the bottom-left part of the graph, and two points which can be seem outliers. The red dot, which, as before, refers to the bottom of the lysimeter, can be considered an outlier as explained above, while the other point refers to the small scale column, in which the L/D is much higher than the others. This last point has approximately the same dispersivity value of the other points, so it cannot be considered as an outlier in terms of dispersivity. In this case, the trend lines in the three graphs are going in different directions and no common behaviour can be observed. Even if the data points are not numerous enough to have a reliable statistic, from the graphs, it seems that the L/D ratio, in the range considered, does not affect the solute dispersivity. In the research carried out by Saravanan et al. (2015), it is stated that the perfect L/D ratio lays between 4 and 20, and higher or lower values can bring to a scale effect on the dispersivity value, while for values within that range the scale's influence can be considered negligible. Since almost all the L/D ratios used in this work are outside of the perfect ratio's range estimated by Saravanan et al. (2015), it is not simple to compare the results obtained from that research with the ones presented here. However, from the few data obtained, it seems that the even for values lower than 4, the L/D ratio has not a significant influence on the longitudinal dispersivity value.

From the extra test, performed with a point sampling, some considerations can be done. Some of them have been already addressed in the previous section. It is likely that the exit hole is too small, if compared with the column section, and this generates a sort of dilution because of the stagnant water present at the lysimeter's bottom. In order to avoid this dilution effect, by looking at the intermediate scale, some precautions can be taken. The intermediate column is characterized by an exit to column's section ratio even smaller than the lysimeter's one but in the intermediate column some precautions have been adopted to homogenize also the exiting flux. A *2 cm*-layer of coarse sand has been placed below the main sand layer and an additional plastic filter has been added too. The combination of these two elements in the intermediate scale is able to guarantee an homogeneous flux at the exit of the column and avoids unwanted dilution which can cause alteration of the dispersivity value. This precautions could be easily taken in the lysimeter too and, if this proves not to be enough, a slight slope can be placed at the lysimeter's bottom to guarantee the downward water flowing in order to prevent stagnant water which causes dilution.

5 Conclusions

One of the aims of the thesis was finding a suitable set-up for the lysimeter, investigating possible problems and further improvements which can be implemented to enhance the lysimeter tests. Furthermore, a large portion of this thesis focused on the comparison between three different scales (from small column to the lysimeter), in particular tracer tests with BPB solution have been used for the comparison.

Starting from this last point, the results have not highlighted a substantial difference between the three different scales in terms of water velocity and hydraulic conductivity. The differences found in the arrival times of the BTCs, at the different scales, can be reconducted to the different experimental conditions of the three columns. In fact, it is important to remember that the columns did not have all the same length (for the lysimeter the second suction probe has been considered for this comparison) and for practical issues, the pumps were not able to supply exactly the same water flux for all the scales. In addition, the different packing methods have led to different porosities which influence the water content and consequently the water velocity.

However, some interesting conclusions regarding the dispersivity values can be drawn. The influence of the scale on the longitudinal dispersivity, in laboratory columns, is something already addressed in literature with some contrasting opinions. From an accurate analysis of the dispersivities estimated from the HYDRUS-1D models, it is possible to state that there is a very slightly increase of the longitudinal dispersivity value as the column's length increases. These results have been obtained in a column's length range between 10 and 70 cm. Conversely, the length to diameter ratio seems not to influence the outcomes in terms of dispersivity. By reading these outcomes, it is important to keep in mind the errors and uncertainties present in this work. In fact, the number of tests performed is not very large and hence, the data for the comparison, are not very numerous. Further experiments should be performed in order to obtain more data to draw more reliable conclusion. Furthermore, it has to be considered the possible human errors during the experiments and data analysis, e.g. errors during the sampling, during the column packing, etc. In addition, the dispersivity values presented in the thesis have been estimated from 1-dimensional models, which in some cases, could lead to an approximation of the reality which is not so accurate.

If looking specifically at the lysimeter's results, it has been observed that the suction probes extraction does not influence sensibly the dispersivity values while it decreases the water velocity of approximately 5% and the water content of around 1 – 2%. Also these findings should be further investigated by running more tests with different flow rates.

From the lysimeter's tests, problems and possible improvements have been detected. Firstly, the method used for the sampling at the exit of the lysimeter seemed to affect the dispersivity value, so at that depth, a point measuring is suggested, but an increase of dispersivity has been also been detected with a instantaneous measurement. This anomalous dispersivity value is probably due to dilution inside the vessel caused by stagnant water at the bottom of it. To avoid that, some precautions are suggested. Firstly, a coarse sand layer which is able to drain water easily can be placed at the bottom of the main sand layer, right above the exit. In addition, if this is not enough to guarantee the wanted conditions, it can be placed a slight slope which helps the water flowing towards the exit hole, avoiding stagnant liquid which causes dilution.

Furthermore, some improvements can be implemented in the lysimeter's set-up to enhance the suction probe sampling process. A suggestion is to insert a spectrophotometer in line between the suction probe and its liquid tank. By doing this, the water/solute, before going into the waste

tank, would pass through a flow-cell in which the absorbance would be automated measured. With this set-up, it would be avoided the bottle's opening which causes a loss of vacuum, that has to be restored every time when each bottle is closed again. In addition, the spectrophotometer automated measurement would guarantee a higher sampling frequency. It means that it would be possible to estimate profiles of concentration along the column, which is not possible with the actual sampling method because there is a difference of at least 4 minutes between the first and the last sample. However, the correct set-up should be studied *ad hoc*. In fact, the flow rates in the suction probe's tubes are very low and they should be enough to guarantee a complete recirculation within the flow cell in the spectrophotometer, otherwise a dilution would be generated by stagnant water inside the cell. In addition, it should be guaranteed the tightness of the flow cell and the entire system to avoid loss of pressures which would caused loss of vacuum inside the suction bottles.

From the lysimeter's experiments, interesting results come also from the tensiometers data. It has been observed an anomalous behaviour in the first two depths (10 and 25 cm) during the wetting and drying phases. In fact, in *tensions vs water content* graphs, the cycles of wetting + drying, of the first two tensiometers, are moving counterclockwise while, the other two have an opposite behaviour, and they are more similar to the theoretical hysteresis. It is not clear why this phenomenon happens, but a hypothesis could be given. It is possible in fact, that this behaviour occurs because the water flow is not fully developed before the two depths. If this hypothesis would be confirmed, it means that the water flow homogenize within the section, only after the second tensiometer which is placed at 25 cm below the soil surface. This interesting outcomes could have some repercussions also on the results obtained in the intermediate column, which geometrically speaking, is very similar to the lysimeter. In order to better understand the reasons behind this behaviour, some further experiments should be performed. Firstly, a possible study could be done by modelling the results with a 2D or even 3D model and adopting models which consider also the hysteresis (i.e. both main and scanning curves). In addition, the soil-water tension could be studied in different conditions and different scales, for example by inserting soil water content sensors in the intermediate column.

To conclude, from the lysimeter experiments it can be stated that this device has a great potential. All the high-precision sensors, within the vessel, can help a better understanding of the water flow in soils under unsaturated conditions, as it happened with the tensiometers and water content sensors. The suction probes extraction and automated weighing system are further advantages of this device in comparison to the other scales. However, not all the lysimeter's potential has been exploited in this study. For instance, temperature, EC, pH and redox potential data have not been considered in this thesis but surely could be useful for further studies. This thesis can be considered a good starting point, from which new studies, regarding infiltration and movement of water and contaminant in the vadose zone, can be undertaken.

References

- Akhtar, M. S., Steenhuis, T. S., Richards, B. K., & McBride, M. B. (2003). Chloride and lithium transport in large arrays of undisturbed silt loam and sandy loam soil columns. *Vadose Zone Journal*, 2(4), 715-727.
- Basile, A., Ciollaro, G., & Coppola, A. (2003). Hysteresis in soil water characteristics as a key to interpreting comparisons of laboratory and field measured hydraulic properties. *Water Resources Research*, 39(12).
- Bergström, L. (2000). Leaching of agrochemicals in field lysimeters—A method to test mobility of chemicals in soil. *Pesticide/Soil Interactions; INRA: Paris, France*, 279-285.
- Bromly, M., Hinz, C., & Aylmore, L.A.G., 2007. Relation of dispersivity to properties of homogeneous saturated repacked soil columns. *European Journal of Soil Science* 58 (1), 293–301.
- Brown, C. D., Hollis, J. M., Bettinson, R. J., & Walker, A. (2000). Leaching of pesticides and a bromide tracer through lysimeters from five contrasting soils. *Pest Management Science: formerly Pesticide Science*, 56(1), 83-93.
- Bunsri, T., Sivakumar, M., & Hagare, D. (2008). Influence of dispersion on transport of tracer through unsaturated porous media.
- Burgess, P.S., (1921). The soil solution, extracted by Lipman's direct-pressure method, compared with 1: 5 water extracts. *Soil Science* 14 (3), 191–216.
- Cannon, C. G., & Butterworth, I. S. C. (1953). Beer's law and spectrophotometer linearity. *Analytical Chemistry*, 25(1), 168-170.
- Canone, D., Ferraris, S., Sander, G., & Haverkamp, R. (2008). Interpretation of water retention field measurements in relation to hysteresis phenomena. *Water resources research*, 44(4).
- Chow, T. V., Maidment, D. R., & Mays, L. W. (1988). Applied hydrology. *Water Resources Handbook; McGraw-Hill: New York, NY, USA*.
- Clapp, R. B., & Hornberger, G. M. (1978). Empirical equations for some soil hydraulic properties. *Water resources research*, 14(4), 601-604.
- Clausnitzer, V., Hopmans, J. W., & Starr, J. L. (1998). Parameter uncertainty analysis of common infiltration models. *Soil Science Society of America Journal*, 62(6), 1477-1487.
- Costanza-Robinson, M. S., & Brusseau, M. L. (2002). Gas phase advection and dispersion in unsaturated porous media. *Water Resources Research*, 38(4), 7-1.
- Cvetkovic, V., Martinet, P., Baresel, C., Lindgren, G., Nikolic, A., Molin, S., & Carstens, C. (2006). Environmental Dynamics: An introduction to modeling anthropogenic impact on natural systems. Course Compendium for Environmental Dynamics/Physical Processes. *Department of Land and Water Resources Engineering, Royal Institute of Technology (KTH), US AB Universitetservice, Stockholm*.
- Dalton, J. (1802). *Experiments and observations to determine whether the quantity of rain and dew is equal to the quantity of water carried off by the rivers and raised by evaporation: With an enquiry into the origin of springs*. R. & W. Dean.

- Davidson, J. M., Nielsen, D. R., & Biggar, J. W. (1966). The dependence of soil water uptake and release upon the applied pressure increment. *Soil Science Society of America Journal*, 30(3), 298-304.
- Dontsova, K. M., Yost, S. L., Šimunek, J., Pennington, J. C., & Williford, C. W. (2006). Dissolution and transport of TNT, RDX, and Composition B in saturated soil columns. *Journal of environmental quality*, 35(6), 2043-2054.
- Eijkelkamp, (2017). Eijkelkamp Smart Lysimeters, User Manual. [Online]. Retrieved from: `file:///D:/Downloads/M1681e_Eijkelkamp_Smart_Lysimeters_29c2.pdf` [Accessed: 02/11/2020]
- Fireman, M., (1944). Permeability measurements on disturbed soil samples. *Soil Science* 58 (5), 337-353.
- Freeze, R. A., & Cherry, J. A. (1979). *Groundwater* (No. 629.1 F7).
- Führ, F., Hance, R. J., Plimmer, J. R., & Nelson, J. O. (Eds.). (1998). *The lysimeter concept: Environmental behavior of pesticides*. American Chemical Society.
- Granetto, M., (2018). *A novel herbicide formulation to reduce the environmental impact of agrochemicals*. [Online] Available at: <https://webthesis.biblio.polito.it/view/creators/Granetto=3AMonica=3A=3A.default.html> [Accessed 12 June 2019].
- Hillel, D. (1980). Fundamentals of soil physics. *Academic press*, San Diego, CA. Academic Press, San Diego, CA.
- Hillel, D., Rosenzweig, C., Powlson, D., Scow, K., Singer, M., & Sparks, D., (2004). *Encyclopedia of soils in the environment*. Four-volume set. Volume 2.
- Howell, T. A., Schneider, A. D., & Jensen, M. E. (1991). History of lysimeter design and use for evapotranspiration measurements. In *Lysimeters for evapotranspiration and environmental measurements* (pp. 1-9). ASCE.
- Huang, K., Toride, N., & Van Genuchten, M. T. (1995). Experimental investigation of solute transport in large, homogeneous and heterogeneous, saturated soil columns. *Transport in Porous Media*, 18(3), 283-302.
- Huang, H. C., Tan, Y. C., Liu, C. W., & Chen, C. H. (2005). A novel hysteresis model in unsaturated soil. *Hydrological Processes: An International Journal*, 19(8), 1653-1665.
- Hutchison, J., Seaman, J., Aburime, S., & Radcliffe, D. (2003). Chromate transport and retention in variably saturated soil columns. *Vadose Zone journal* 2, 702-714.
- Kartha, S. A., & Srivastava, R. (2008). Effect of immobile water content on contaminant transport in unsaturated zone. *Journal of hydro-environment research*, 1(3-4), 206-215.
- Kutilek, M., & Nielsen D. R. (1994). Soil Hydrology. *Catena-Verlag: Cremlingen-Destedt, Germany*; 73.
- Landsberg, J. J., Sands, P. J., Landsberg, J., & Sands, P. (2011). Physiological ecology of forest production: principles, processes and models (Vol. 4). *Amsterdam, the Netherlands: Elsevier/Academic Press*.

- Lehmann, P., Stauffer, F., Hinz, C., Dury, O., & Flühler, H. (1998). Effect of hysteresis on water flow in a sand column with a fluctuating capillary fringe. *Journal of Contaminant Hydrology*, 33(1-2), 81-100.
- Latrille, C. (2013). Effect of water content on dispersion of transferred solute in unsaturated porous media. *Procedia Earth and Planetary Science*, 7, 463-466.
- Lawes, J., Gilbert, J., & Warington, R. (1882). On the Amount and Composition of the Rain and Drainage Water Collected at Rothamstead. *William Clowes and Sons, Ltd, London*.
- Lewis, J., & Sjöström, J. (2010). Optimizing the experimental design of soil columns in saturated and unsaturated transport experiments. *Journal of contaminant hydrology*, 115(1-4), 1-13.
- Lewis, J., & Sjöström, J. (2010). Optimizing the experimental design of unsaturated soil columns. *In WORLD CONGRESS OF SOIL SCIENCE "SOIL SOLUTIONS FOR A CHANGING WORLD" (Vol. 19, pp. 1-6)*.
- Li, X. S. (2005). Modelling of hysteresis response for arbitrary wetting/drying paths. *Computers and Geotechnics*, 32(2), 133-137.
- Mali, N., Urbanc, J., & Leis, A. (2007). Tracing of water movement through the unsaturated zone of a coarse gravel aquifer by means of dye and deuterated water. *Environmental geology*, 51(8), 1401-1412.
- Marion, A. (2008). Physical Transport Processes in Ecology: Advection, Diffusion, and Dispersion.
- Masipan, T., Chotpantarat, S., & Boonkaewwan, S. (2016). Experimental and modelling investigations of tracer transport in variably saturated agricultural soil of Thailand: Column study. *Sustainable Environment Research*, 26(2), 97-101.
- Mualem, Y., & Dagan, G., (1975). A dependent domain model of capillary hysteresis. *Water Resources Research* 11: 452-460.
- Mualem, Y., 1976. A new model for predicting the hydraulic conductivity of unsaturated porous media. *Water Resources Research*, 13(3), pp. 513-522.
- Namitha, M. R., & Ravikumar, V. (2018). Determination of Dispersivity in A Laboratory soil column. *International Journal of Trend and Scientific Research and Development (IJTSRD)*. 2(4), 2731-3735.
- Nielsen, D. R., Th. Van Genuchten, M., & Biggar, J. W. (1986). Water flow and solute transport processes in the unsaturated zone. *Water resources research*, 22(9S), 89S-108S.
- Peruski, K. M., Maloubier, M., Kaplan, D. I., Almond, P. M., & Powell, B. A. (2018). Mobility of Aqueous and Colloidal Neptunium Species in Field Lysimeter Experiments. *Environmental science & technology*, 52(4), 1963-1970.
- Quartzsande, 2020a. Quartzsande "DORSILIT nr. 8" [Online]. Retrieved from: http://www.quartzsande.at/source/kristallquartzsand_feuergetrocknet/PDB%20Dorsilit%208.pdf [Accessed: 16/09/2020]
- Quartzsande 2020b. Quartzsande, "DORSILIT nr. 7" [Online]. Retrieved from: http://www.quartzsande.at/source/kristallquartzsand_feuergetrocknet/PDB%20Dorsilit%207.pdf [Accessed: 16/09/2020]

- Rai, R. K., & Ojha, C. S. P. (2007). Estimating dispersion coefficient from soil-column test. *ISH Journal of Hydraulic Engineering*, 13(2), 1-14.
- Rawls, W. J., Brakensiek, D. L., & Miller, N. (1983). Green-Ampt infiltration parameters from soils data. *Journal of hydraulic engineering*, 109(1), 62-70.
- Richards, L. A., 1931. Capillary conduction of fluid through porous mediums. *Physics*, Volume 1, pp. 318-333.
- Russo, D., Jury, W. A., & Butters, G. L. (1989). Numerical analysis of solute transport during transient irrigation: 1. The effect of hysteresis and profile heterogeneity. *Water Resources Research*, 25(10), 2109-2118.
- Saravanan, N., Mohan, N., & Navaneetha Gopalakrishnan, A., 2015. Scale Effect on Dispersion Coefficient of Conservative Solute through Break through Curve (BTC): Experimental Study. *International Journal of Earth Sciences and Engineering*, volume 08, No.02.
- Sethi, R., & Di Molfetta, A. (2019). Groundwater Engineering. *Springer International Publishing*.
- Shokrollahi, A., & Zare, E. (2016). Determination of acidity constants of bromophenol blue and phenol red indicators by solution scanometric method and comparison with spectrophotometric results. *Journal of Molecular Liquids*, 219, 1165-1171.
- Silliman, S. E., & Simpson, E. S. (1987). Laboratory evidence of the scale effect in dispersion of solutes in porous media. *Water Resources Research*, 23(8), 1667-1673.
- Simonenko, E., Gomonov, A., Rolle, N., & Molodkina, L. (2015). Modeling of H₂O₂ and UV oxidation of organic pollutants at wastewater post-treatment. *Procedia engineering*, 117, 337-344.
- Simunek, J., Sejna, M., Saito, H., & Van Genuchten, M. T., (2013). HYDRUS-1D. The HYDRUS-1D Software Package for Simulating the One-Dimensional Movement of Water, Heat, and Multiple Solutes in Variably-Saturated Media, version, 4.17.
- Sołtysiak, M., & Rakoczy, M. (2019). An overview of the experimental research use of lysimeters. *Environmental & Socio-economic Studies*, 7(2), 49-56.
- Smiles, D. E., & Knight, J. H. (1976). A note on the use of the Philip infiltration equation. *Soil Research*, 14(1), 103-108.
- Sugita, F., & Nakane, K. (2007). Combined effects of rainfall patterns and porous media properties on nitrate leaching. *Vadose Zone Journal*, 6(3), 548-553.
- Tarboton, D. G. (2003). Rainfall-runoff processes. *Utah State University*, 1(2).
- Tindall, J. A., Kunkel, J. R., & Anderson, D. E. (1999). Unsaturated zone hydrology for scientists and engineers (Vol. 3). *Upper Saddle River, NJ: Prentice Hall*.
- Topp, G. C. (1969). Soil-water hysteresis measured in a sandy loam and compared with the hysteretic domain model. *Soil Science Society of America Journal*, 33(5), 645-651.
- Topp, G. C., Davis, J. L., & Annan, A. P. (1980). Electromagnetic determination of soil water content: Measurements in coaxial transmission lines. *Water resources research*, 16(3), 574-582.

- Toride, N., Inoue, M., & Leij, F.J., 2003. Hydrodynamic dispersion in an unsaturated dune sand. *Soil Science Society of America Journal* 67 (3), 703–712.
- UGT, (2019). Lab Lysimeter, Operating Manual. [Online]. Retrieved from: https://www.ugt-online.de/fileadmin/Public/downloads/Produkte/Lysimetertechnik/Laborlysimeter_-_Operating_Manual.pdf [Accessed: 08/10/2020]
- UGT, (2019). UPM-2, Operating Manual. UPM-2 combined soil humidity, conductivity and temperature sensor.
- United Nations, (2019). World Population Prospects 2019: Highlights, Department of Economic and Social Affairs: Population Division. [Online]. Retrieved from: <https://population.un.org/wpp/> [Accessed: 09/11/2020]
World Population Prospects 2019
- Van Genuchten, M. T., 1980. A Closed-form Equation for Predicting the Hydraulic Conductivity of Unsaturated Soils. *Soil Science Society of America Journal*, Volume 44, pp. 892-898.
- Van Genuchten, M. T., & Pachepsky, Y. A. (2011). Hydraulic properties of unsaturated soils. *Encyclopedia of agrophysics*, 368-376.
- Voegelin, A., Barmettler, K., & Kretzschmar, R. (2003). Heavy metal release from contaminated soils: Comparison of column leaching and batch extraction results. *Journal of environmental quality*, 32(3), 865-875.
- Zupanc, V., Nolz, R., Cepuder, P., Bračič-Železnik, B., & Pintar, M. (2012). Determination of water balance components with high precision weighing lysimeter in Kleče. *Acta agriculturae Slovenica*, 99(2), 165-173.

A Appendix A

DORSILIT nr. 8 sand

Table A.1. DORSILIT nr. 8 sand characteristics. Data retrieved from Quartzsande (2020a)

SAND CHARACTERISTICS	
Grain dimension (mm)	0.3-0.8
Bulk density (g/cm ³)	2.65
Apparent density (g/cm ³)	1.4-1.5
SiO ₂ % m/m	97.9
Fe ₂ O ₃ % m/m	0.02
Al ₂ O ₃ % m/m	0.47
TiO ₂ % m/m	0.03

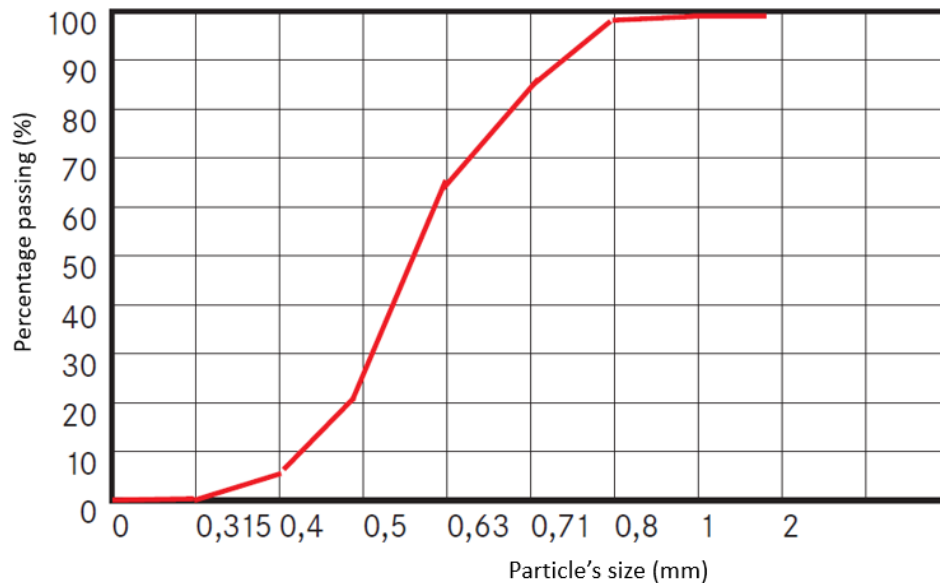


Figure A.1. Granulometric curve of DORSILIT nr. 8 sand. Source: modified image from Quartzsande (2020a)

DORSILIT nr. 7 sand

Table A.2. DORSILIT nr. 7 sand characteristics. Data retrieved from Quartsande (2020b)

SAND CHARACTERISTICS	
Grain dimension (mm)	0.6-1.2
Bulk density (g/cm ³)	2.65
Apparent density (g/cm ³)	1.4-1.5
SiO ₂ % m/m	97.9
Fe ₂ O ₃ % m/m	0.02
Al ₂ O ₃ % m/m	0.47
TiO ₂ % m/m	0.03

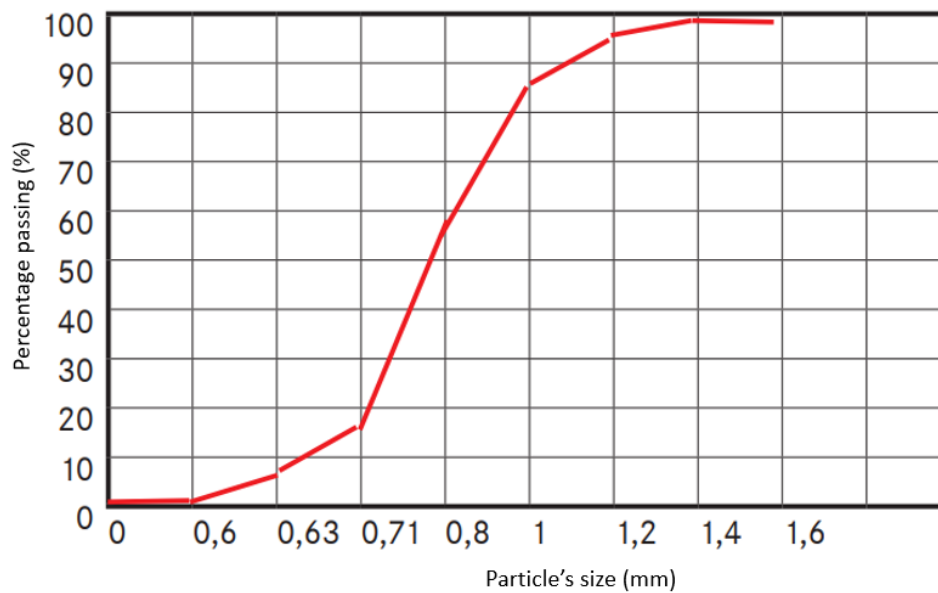


Figure A.2. Granulometric curve of DORSILIT nr. 7 sand. Source: modified image from Quartsande (2020b)

B Appendix B

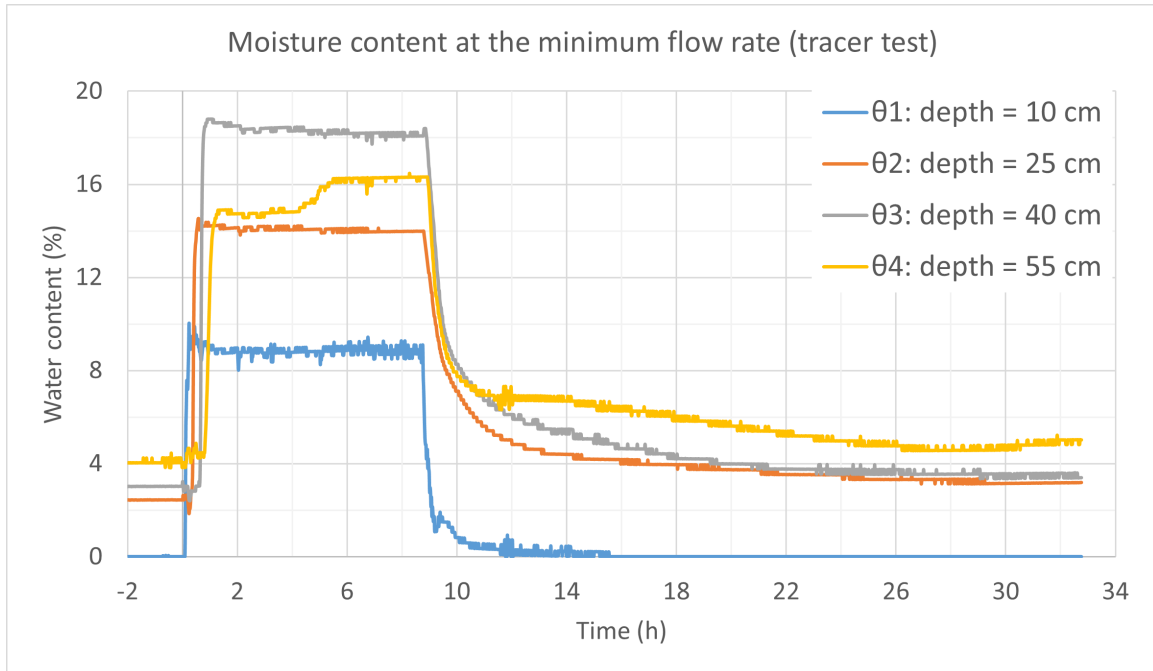


Figure B.1. Lysimeter scale, tracer test: water content data from the four sensors.

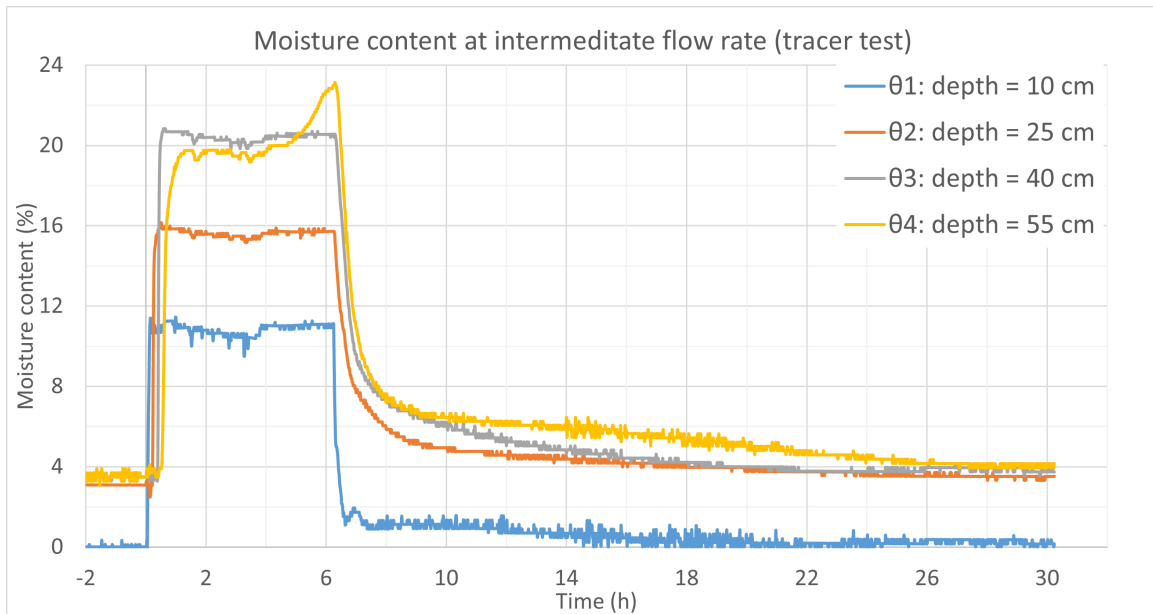


Figure B.2. Lysimeter scale, tracer test: water content data from the four sensors.

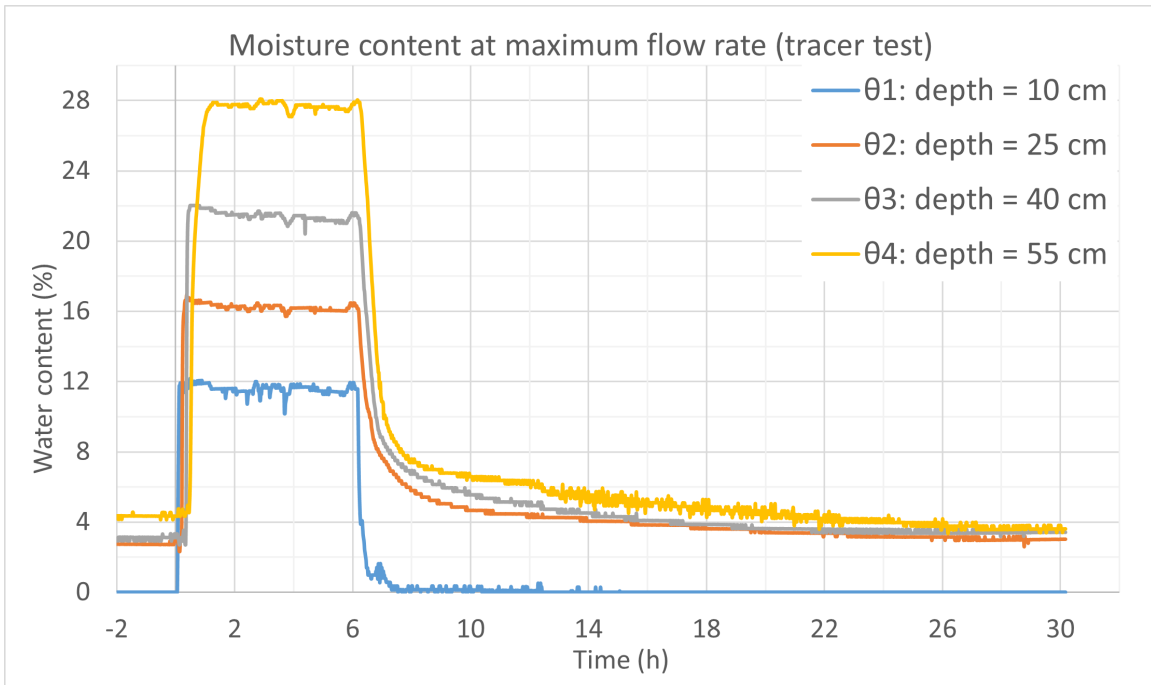


Figure B.3. Lysimeter scale, tracer test: water content data from the four sensors.

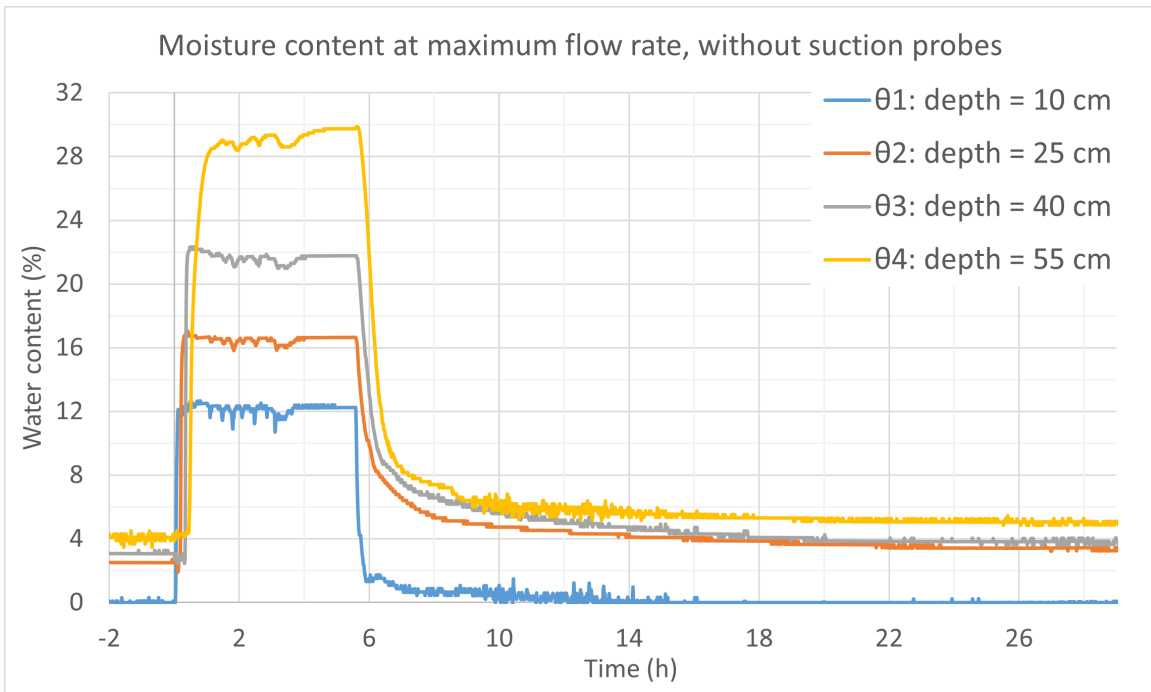


Figure B.4. Lysimeter scale, first extra tracer test (without suction probe extraction): water content data from the four sensors.

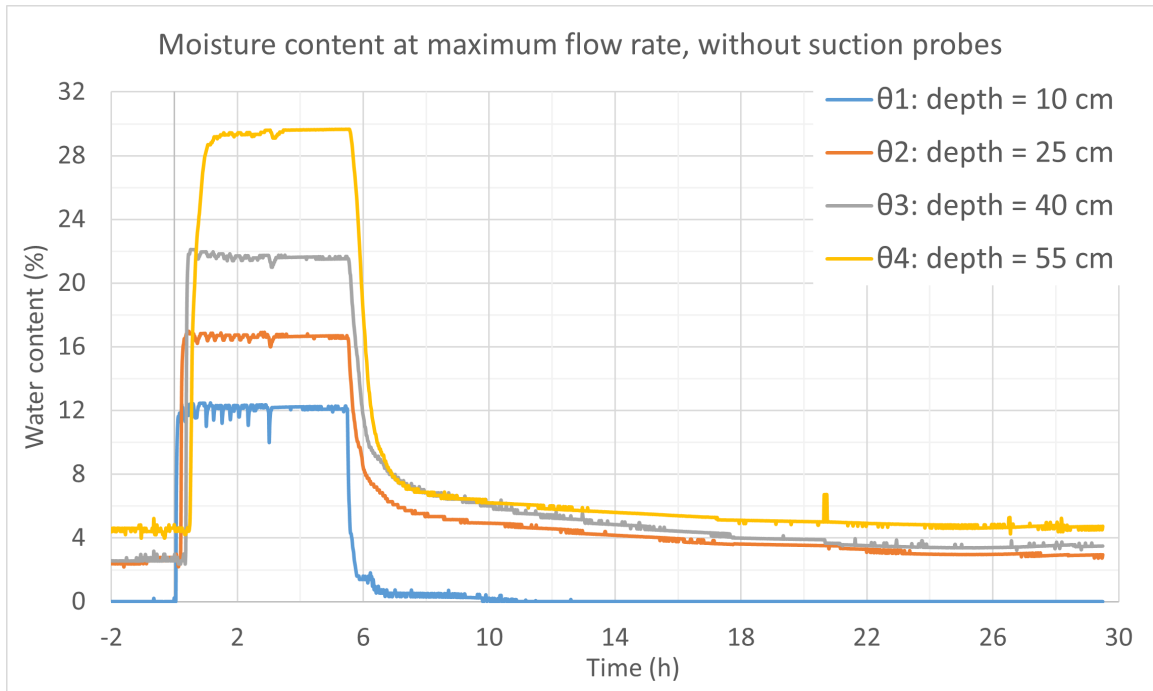


Figure B.5. *Lysimeter scale, second extra tracer test (point sampling, without suction probe extraction): water content data from the four sensors.*

C Appendix C

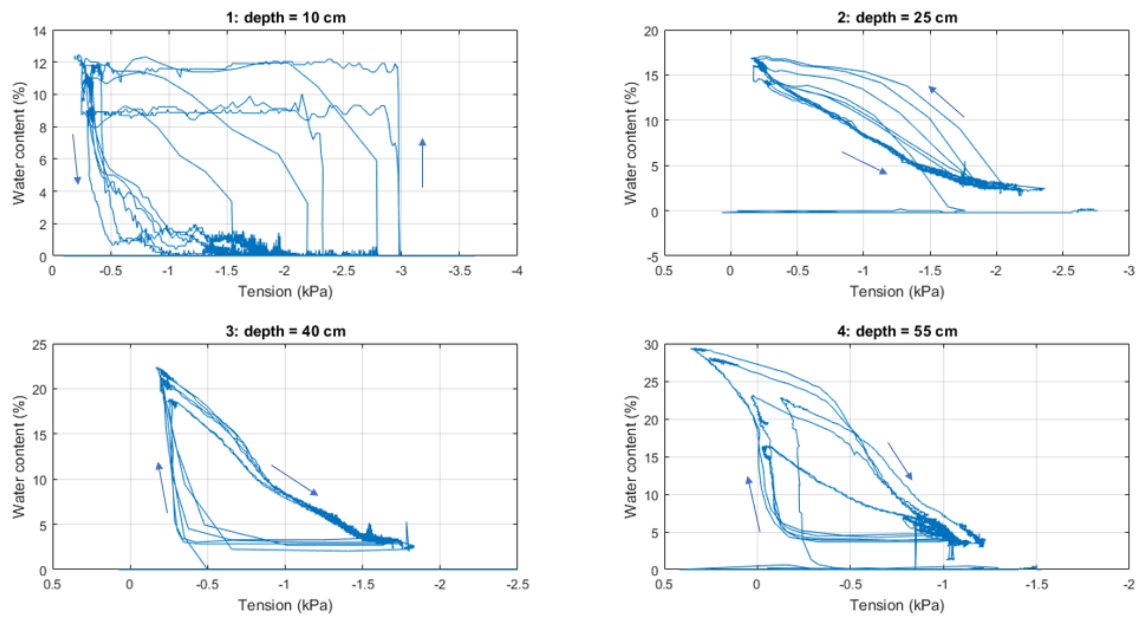


Figure C.1. Lysimeter scale, water content vs soil water tension data from six cycles of wetting + drying, with all the three different flow rates.

Acknowledgements

First of all, I would like to thank all the Groundwater research group. During the months I spent in laboratory, everyone made me feel welcomed since my very first day, everyone has been always willing to help me and the practical advices they have given to me have been very precious.

In particular, I want to thank Prof. Tiziana Tosco who has been always available for me, giving me suggestions and comments every time I needed it. I would like to deeply thank Monica. During these months, she has been always there for me, she guided me since the very first day in laboratory becoming a precious point of reference for me.

I would like to thank all my friends, who always supported me during these years. A huge thank to the old friends who have been always there for me. I wanted to thank also all the university friend group, which made the university's years enjoyable and unforgettable, from my first bachelor's year to the last year in Stockholm I have never felt alone. I always had someone by my side I could count on and this is a privilege that I would not have without them.

Lastly, the most important thank goes to my family. In these 25 years, you always gave me the opportunity to build my life and you always supported me in all my decisions. My parents, my siblings, my grandparents, each of them has a special and unique role in my life. I am proud of my family, each of you is a part of me and I will never be able to thank you enough.